AEDC-TR-67-80

ARCHIVE COPY
DO NOT LOAN

FULLY DEVELOPED MAGNETOGASDYNAMIC FLOW BETWEEN DIVERGING PLANE WALLS

William T. Snyder and James R. Maus
The University of Tennessee Space Institute

April 1967

Distribution of this document is unlimited.

AEDC TECHNICAL LIBRARY
5 0720 00036 7856

ARNOLD ENGINEERING DEVELOPMENT CENTER
AIR FORCE SYSTEMS COMMAND
ARNOLD AIR FORCE STATION, TENNESSEE

PROPERTY OF U. S. AIR FORCE
AEDC LIBRARY
AF 40(600)1200

NOTICES

When U. S. Government drawings specifications, or other data are used for any purpose other than a definitely related Government procurement operation, the Government thereby incurs no responsibility nor any obligation whatsoever, and the fact that the Government may have formulated, furnished, or in any way supplied the said drawings, specifications, or other data, is not to be regarded by implication or otherwise, or in any manner licensing the holder or any other person or corporation, or conveying any rights or permission to manufacture, use, or sell any patented invention that may in any way be related thereto.

Qualified users may obtain copies of this report from the Defense Documentation Center.

References to named commercial products in this report are not to be considered in any sense as an endorsement of the product by the United States Air Force or the Government.

FULLY DEVELOPED MAGNETOGASDYNAMIC FLOW BETWEEN DIVERGING PLANE WALLS

William T. Snyder and James R. Maus
The University of Tennessee Space Institute

Distribution of this document is unlimited.

AF - AEDC
Arnold AFS Tenn

FOREWORD

The work reported herein was sponsored by Arnold Engineering Development Center (AEDC), Air Force Systems Command (AFSC), Arnold Air Force Station, Tennessee, under Program Element 62405334, Project 8950, Task 895001.

The results of research presented were obtained by the University of Tennessee Space Institute under Contract AF 40(600)-1113. The manuscript was submitted for publication on April 13, 1967.

The reproducibles used in the reproduction of this report were supplied by the authors.

This technical report has been reviewed and is approved.

Ian F. Flemming
F/L, RCAF
Research Division
Directorate of Plans
and Technology

Edward R. Feicht
Colonel, USAF
Director of Plans and
Technology

ABSTRACT

A solution has been obtained to the magnetogasdynamic equations of motion including the effects of compressibility, viscosity, thermal conductivity and crossed electric and magnetic fields. The solution obtained is valid for an acceleration flow in which a separation of variable form of solution is utilized. The constraints under which a separable solution is valid are clearly delineated. The solution is an exact solution in the sense that no terms have been dropped from the governing equations and boundary layer approximations have not been employed.

The results of the investigation were presented in the form of velocity and temperature profiles for several values of the electromagnetic parameters Ha and Φ. Although the mathematical model used in the present investigation is too crude to be utilized for detailed design of a practical MHD accelerator, it is believed, nevertheless, that the model displays certain qualitative features of the flow which are likely to be encountered in a practical device.

TABLE OF CONTENTS

		Page
	ABSTRACT	iii
	NOMENCLATURE	xi
I.	INTRODUCTION	1
II.	PREVIOUS WORK	
	2.1 One Dimensional Studies	4
	2.2 Incompressible Studies	5
	2.3 Viscous Magnetogasdynamic Studies	6
III.	FORMULATION OF THE PROBLEM	9
IV.	TECHNIQUE OF SOLUTION	
	4.1 Solution Difficulties of the Direct Boundary Value Problem	23
	4.2 The Initial Value Problem	28
V.	DISCUSSION OF RESULTS	37
VI.	VARIABLE PROPERTIES	
	6.1 Formulation of the Equations	44
	6.2 Discussion of Results	47
VII.	SUMMARY	49
VIII.	REFERENCES	51

LIST OF ILLUSTRATIONS

Figure

1. MHD Powered Wind Tunnel

2. Channel Configuration

3. Relationship Among Parameters α, Ha and Φ

4. Relationship Among Parameters $g(\alpha)$, Ha, Φ, and α

5. Region of Acceptable Solutions for Ha = 200, Φ = 1.6

6. Velocity and Temperature Profiles for Ha = 100, Φ = 1.2

7. Velocity and Temperature Profiles for Ha = 100, Φ = 1.6

8. Velocity and Temperature Profiles for Ha = 100, Φ = 2.0

9. Velocity and Temperature Profiles for Ha = 150, Φ = 1.2

10. Velocity and Temperature Profiles for Ha = 150, Φ = 1.6

11. Velocity and Temperature Profiles for Ha = 150, Φ = 2.0

12. Velocity and Temperature Profiles for Ha = 200, Φ = 1.2

13. Velocity and Temperature Profiles for Ha = 200, Φ = 1.6

14. Velocity and Temperature Profiles for Ha = 200, Φ = 2.0

15. Variation of the Velocity Gradient at the Wall for $\alpha = 1.5°$, $g(\alpha) = 0.2$

16. Variation of the Temperature Gradient at the Wall for $\alpha = 1.5°$, $g(\alpha) = 0.2$

17. Velocity and Temperature Profiles for Ha = 100, Φ = 1.6

18. Velocity and Temperature Profiles for Ha = 150, Φ = 1.2

19. Velocity and Temperature Profiles for Ha = 150, $\Phi = 1.6$

20. Velocity and Temperature Profiles for Ha = 100, $\Phi = 1.6$, $\sigma \sim T^{3/2}$

21. Velocity and Temperature Profiles for Ha = 150, $\Phi = 1.2$, $\sigma \sim T^{3/2}$

22. Velocity and Temperature Profiles for Ha = 150, $\Phi = 1.6$, $\sigma \sim T^{3/2}$

23. Velocity and Temperature Profiles for Ha = 100, $\Phi = 1.6$, $\sigma \sim T^{3/2}$, $\mu \sim \kappa \sim T^{1/2}$

24. Velocity and Temperature Profiles for Ha = 150, $\Phi = 1.2$, $\sigma \sim T^{3/2}$, $\mu \sim \kappa \sim T^{1/2}$

25. Velocity and Temperature Profiles for Ha = 150, $\Phi = 1.6$, $\sigma \sim T^{3/2}$, $\mu \sim \kappa \sim T^{1/2}$

26. Variation of α with Re and M for Ha = 100, $\Phi = 1.2$

27. Variation of $g(\alpha)$ with Re and M for Ha = 100, $\Phi = 1.2$

28. Variation of α with Re and M for Ha = 100, $\Phi = 1.6$

29. Variation of $g(\alpha)$ with Re and M for Ha = 100, $\Phi = 1.6$

30. Variation of α with Re and M for Ha = 100, $\Phi = 2.0$

31. Variation of $g(\alpha)$ with Re and M for Ha = 100, $\Phi = 2.0$

32. Variation of α with Re and M for Ha = 150, $\Phi = 1.2$

33. Variation of $g(\alpha)$ with Re and M for Ha = 150, $\Phi = 1.2$

34. Variation of α with Re and M for Ha = 150, $\Phi = 1.6$

35. Variation of $g(\alpha)$ with Re and M for Ha = 150, $\Phi = 1.6$

36. Variation of α with Re and M for Ha = 150, $\Phi = 2.0$

37. Variation of $g(\alpha)$ with Re and M for Ha = 150, $\Phi = 2.0$

38. Variation of α with Re and M for Ha = 200, $\Phi = 1.2$

39. Variation of $g(\alpha)$ with Re and M for Ha = 200, $\Phi = 1.2$

40. Variation of α with Re and M for Ha = 200, $\Phi = 1.6$

41. Variation of $g(\alpha)$ with Re and M for Ha = 200, $\Phi = 1.6$

42. Variation of α with Re and M for Ha = 200, $\Phi = 2.0$

43. Variation of $g(\alpha)$ with Re and M for Ha = 200, $\Phi = 2.0$

44. Variation of α with Re and M for Ha = 100, $\Phi = 1.6$, $\sigma \sim T^{3/2}$

45. Variation of $g(\alpha)$ with Re, M for Ha = 100, $\Phi = 1.6$, $\sigma \sim T^{3/2}$

46. Variation of α with Re and M for Ha = 150, $\Phi = 1.2$, $\sigma \sim T^{3/2}$

47. Variation of $g(\alpha)$ with Re and M for Ha = 150, $\Phi = 1.2$, $\sigma \sim T^{3/2}$

48. Variation of α with Re and M for Ha = 150, $\Phi = 1.6$, $\sigma \sim T^{3/2}$

49. Variation of $g(\alpha)$ with Re and M for Ha = 150, $\Phi = 1.6$, $\sigma \sim T^{3/2}$

50. Variation of α with Re and M for Ha = 100, $\Phi = 1.6$, $\sigma \sim T^{3/2}$, $\mu \sim \kappa \sim T^{1/2}$

51. Variation of $g(\alpha)$ with Re and M for Ha = 100, $\Phi = 1.6$, $\sigma \sim T^{3/2}$, $\mu \sim \kappa \sim T^{1/2}$

52. Variation of α with Re and M for Ha = 150, $\Phi = 1.2$, $\sigma \sim T^{3/2}$, $\mu \sim \kappa \sim T^{1/2}$

53. Variation of $g(\alpha)$ with Re and M for Ha = 150, $\Phi = 1.2$, $\sigma \sim T^{3/2}$, $\mu \sim \kappa \sim T^{1/2}$

54. Variation of α with Re and M for Ha = 150, $\Phi = 1.6$, $\sigma \sim T^{3/2}$, $\mu \sim \kappa \sim T^{1/2}$

55. Variation of $g(\alpha)$ with Re and M for Ha = 150, $\Phi = 1.6$, $\sigma \sim T^{3/2}$, $\mu \sim \kappa \sim T^{1/2}$

LIST OF TABLES

I Limiting Values of α, M and Re

II Summary of Results for Constant Properties

III Comparison of $f'(\alpha)$ and $g'(\alpha)$ for Constant and Variable Properties

NOMENCLATURE

$\vec{B}$	Magnetic induction (B_r, B_θ, B_z)
C_p	Specific heat capacity
d	Channel height
$\vec{E}$	Electric field vector (E_r, E_θ, E_z)
$f(\theta)$	Dimensionless velocity, Eq. (42)
$g(\theta)$	Dimensionless temperature, Eq. (42)
h	Enthalpy
Ha	Hartmann number, Eq. (44)
Ha^*	Hartmann number based on d_o
$\vec{J}$	Current density vector (J_r, J_θ, J_z)
M	Mach number, Eq. (44)
p	Static pressure
Pr	Prandtl number, Eq. (44)
r	Coordinate direction
R	Gas constant
Re	Reynolds number, Eq. (44)
Re^*	Reynolds number based on d_o
R_M	Dimensionless parameter, Eq. (60)
T	Temperature
$\bar{T}(\theta)$	Dimensional temperature function
$\vec{U}$	Velocity vector (U_r, U_θ, U_z)
$\bar{U}(\theta)$	Dimensional velocity function
z	Coordinate direction
α	Divergence angle
γ	Specific heat ratio, C_p/C_v

η	Normalized coordinate, θ/α
θ	Coordinate direction
κ	Thermal conductivity
λ	Mean free path
μ	Viscosity
μ_e	Magnetic permeability
π	Dimensionless parameter, Eq. (60)
ρ	Density
σ	Electrical conductivity
Φ	Loading parameter, Eq. (44)
ω	Exponent, Eq. (110)

SUBSCRIPTS

c	Characteristic or reference values
o	Values at the channel entrance, $r = r_o$
w	Values at the wall $\theta = \alpha$

I
INTRODUCTION

For several years there has been considerable interest in the electromagnetic acceleration of ionized gases for space propulsion purposes and for application to high speed wind tunnels. Many types of devices have been proposed to accomplish this acceleration and a number of prototypes have been built that demonstrate technical feasibility. One of the more promising of these devices is the steady flow, crossed field or Faraday accelerator. There is particular interest in this type of accelerator for wind tunnel applications.

One factor that limits conventional hypervelocity flight simulation techniques is the necessity of confining a high temperature gas at high pressure prior to expanding in a supersonic nozzle. By directly adding kinetic energy to the flow, a magnetogasdynamic accelerator would, to a large extent, alleviate this containment problem. Ring (Ref. 1) has stated, "In a sense, MHD techniques offer the first promise of a quantum increase in aerodynamic test capabilities since the introduction of shock-tube, shock-tunnel techniques a number of years ago."

A schematic drawing of a crossed field accelerator to be used for the simulation of high speed flight is shown in Fig. 1. In such an arrangement air would be preheated, seeded, and ionized in an arc heater and then passed through a low Mach number supersonic nozzle into the accelerating channel. In the accelerator itself, energy would be added to the ionized gas or plasma by the crossed electric and magnetic fields. A large portion of this added energy would be in the form of directed kinetic energy, the remainder being random thermal energy increasing the enthalpy of the plasma. A post-accelerator nozzle would expand the gas to the desired static conditions and further increase the Mach number.

It is clear that the accelerator itself is the heart of such a flight simulation system and that it is important that the details of the flow in this device be well understood.

A considerable amount of theoretical work has been done on the crossed field accelerator and in the next section a brief survey of the more pertinent of these analyses is presented. The majority of these investigations have treated

an inviscid, non-heat conducting gas, the tacit assumption being made that the viscous and heat transfer effects are confined to a thin boundary layer adjacent to the channel wall. However, in wind tunnel accelerators where relatively large length to diameter ratios will be necessary to produce the required acceleration, it is likely that a significant portion of the flow will be fully developed in the sense that the boundary layers have merged. Thus, the influences of viscosity and thermal conductivity would extend throughout the flow field. This would especially be true for accelerators operating at low to moderate Reynolds number i.e. low density. It is well known (Ref. 2) that under these conditions the flow must be treated as fully viscous and that boundary layer theory is no longer applicable. Under these circumstances, the results of one-dimensional analyses cannot be expected to accurately describe the actual flow.

It would appear then that there is a need for a study of the crossed field accelerator including the effects of compressibility, viscosity, and thermal conductivity. A general study of such a problem would be a formidable undertaking indeed. In this investigation attention is focused on a special type of accelerator flow for which it is possible to obtain a solution to the governing equations including the aforementioned effects.

The flow considered is a two-dimensional gas flow between diverging plane walls, the pressure and Mach number being constant down the channel. For this model it is possible to separate the axial and cross channel dependence of velocity and temperature. Performing this separation results in a pair of coupled, non-linear, ordinary differential equations for the cross channel variations. This system of equations is extremely complex and must be integrated by numerical methods. Moreover it is shown that the problem is generally over specified and that solutions cannot be obtained for arbitrary values of the parameters. This difficulty is circumvented by converting the boundary value problem to an initial value problem and allowing the wall divergence angle and wall temperature to be determined by the integration.

In order to accomplish the separation of variables mentioned above it is necessary to assume that the viscosity, thermal conductivity, and electrical conductivity do not change down the channel. Consequently, in the main portion of this report, it is assumed that these properties are constant throughout the flow field. This assumption represents a rather severe restriction because the viscosity

and electrical conductivity are strong functions of temperature. The latter section of this report is concerned with an attempt to assess the effect of these property variations across the channel on the velocity and temperature profiles.

II
PREVIOUS WORK

2.1 ONE-DIMENSIONAL STUDIES

The one-dimensional magnetogasdynamic equations for an inviscid non-heat conducting gas were presented by Resler and Sears (Ref. 3), and many of the interesting properties of these equations were pointed out. In particular, the possibility of accelerating a gas, flowing in a channel, to very high speeds was noted. In another paper (Ref. 4) the same authors discussed in some detail constant area magnetogasdynamic channel flow listing eight possible flow situations that might occur, depending on the initial velocity and initial Mach number.

In the succeeding years, a number of authors have analyzed quasi-one-dimensional channel flow problems with crossed electric and magnetic fields. Matthews (Ref. 5), for example, has presented a number of solutions for the steady flow crossed field accelerator. Following the approach of Resler and Sears, Matthews assumes the electrical conductivity to be a constant and ignores the effect of the induced magnetic field. The latter assumption permits the gas dynamical equations to be treated independently of Maxwell's electromagnetic equations. A further consequence of this assumption is that the variation of two of the dependent variables must be specified before a solution can be obtained.

Drake (Ref. 6) studied the isothermal acceleration of a plasma with the aim of optimizing the channel design. Using a variational technique he determined the channel shape that would yield a minimum accelerator length for a given velocity change.

Krupka and Kezios (Ref. 7) analyzed a constant area accelerator for constant applied electric and magnetic fields. In their study the induced field in the direction of the applied field was not neglected and the electrical conductivity was taken to be a function of temperature. The results of Krupka and Kezios indicate that the Mach number increase during acceleration is limited and that the flow cannot be accelerated through the sonic velocity.

Two investigations of inviscid magnetogasdynamic flow are of particular interest in connection with the present work. These are the papers by Hains (Ref. 8) and Podolsky and Borman (Ref. 9). Hains examined several cases of

magnetogasdynamic source flow and obtained a particularly simple solution for the case of crossed electric and magnetic fields. The electric field was assumed constant and the magnetic field was assumed to vary inversely with radial distance from the source. The electrical conductivity was assumed constant and induced field effects and Hall effects neglected. Hains found that the flow proceeds outward from the source at constant pressure and constant Mach number, the velocity increasing linearly with radial distance and the temperature increasing as the square of the radial distance.

In a related investigation, Podolsky and Borman (Ref. 9) considered precisely the geometry that is dealt with in the present study. The governing equations for a crossed field accelerator were written in cylindrical coordinates, neglecting changes in the z and θ directions. These equations were then numerically integrated for specified entrance conditions at r_o. For large values of r they obtained a solution of the form

$$u \sim r$$

$$p = \text{constant}$$

$$T \sim r^2$$

From the solution graph presented it appears that this pattern is established fairly quickly and is valid for values of $r/r_o > 3$. In the entrance region where $1 < r/r_o < 3$ the velocity is still almost linear although the pressure drops rapidly. Podolsky and Borman also treat this problem for a lithium vapor propellant using values for the conductivity calculated from the degree of ionization at equilibrium.

Sherman (Ref. 10) has extended the work of Podolsky and Borman to include Hall currents and propellants that are mixtures of inert gas and ionized seed gas.

2.2 INCOMPRESSIBLE STUDIES

A vast number of articles have been published that deal with magnetohydrodynamic channel flows, and only a few of the more pertinent will be discussed here. No survey of the literature in this area would be complete, however, without mentioning the original paper in the field by Hartmann (Ref. 11), which deals with fully developed laminar flow

between parallel, non-conducting walls. A discussion of Hartmann's work and several other interesting magnetohydrodynamic channel flows is contained in a recent book by Sutton and Sherman (Ref. 12).

In an incompressible study somewhat similar to the present work, Axford (Ref. 13) examined the magnetohydrodynamic flow between non-parallel plane walls, an extension of the classical Jeffrey-Hamel problem. The channel shape and magnetic field distribution were the same as those considered in this investigation, but the applied electric field was taken to be zero, corresponding to a short circuited MHD generator. Writing the governing equations in cylindrical coordinates, Axford was able to separate the axial and cross channel dependence. By assuming small magnetic Reynolds number, i.e. neglecting the induced field, he was able to obtain a closed form solution for the cross channel variation. The emphasis in this study was on the mathematical analysis and only a limited number of numerical results were presented. It was reported that for divergent flow the tendency toward separation and back flow at high Reynolds number is opposed by the transverse magnetic field. Velocity profiles presented for convergent flow show the characteristic flattening for increasing magnetic field strength.

Vatazhin (Ref. 14) examined some limiting cases of the divergent channel problem treated by Axford and obtained solutions in terms of elementary functions. Vatazhin's results support the conclusions made by Axford.

Heywood (Ref. 15) investigated the magnetohydrodynamic flow between parallel plates assuming an electrical conductivity-temperature relation of the form $\sigma \sim T^{\omega}$. He found very little effect on the temperature profile due to the conductivity variation but a noticeable alteration of the velocity profile. He noted, however that for gases flowing at high speed the effect on the temperature distribution could be significant.

2.3 VISCOUS MAGNETOGASDYNAMIC STUDIES

In an early paper, Bleviss (Ref. 16) studied magnetogasdynamic Couette flow in an effort to deduce information about the magnetogasdynamic boundary layer. Hall effects were not included in this study but the variation of transport properties was taken into account. Bleviss' results show a rather severe distortion of the velocity and temperature distributions with increasing magnetic field strength. This study was directed toward aerodynamic boundary layers

on space vehicles reentering the atmosphere rather than boundary layers in channels. Consequently the effect of an applied electric field was not considered.

Martin (Ref. 17) studied the flow of a compressible, viscous fluid in a pipe of circular cross section; the fluid being accelerated by an axial body force. His work dealt with both the entrance flow and the fully developed flow which was defined as a non-accelerating parallel flow. A body force is required in order for the fully developed flow to exist. By assuming that the viscosity, thermal and electrical conductivities were constant and that the flow was unidirectional throughout, Martin was able to solve the linearized momentum equation independently of the energy equation.

Although the applicability of this study to magnetogasdynamic channel flows was stressed, it is doubtful that the body forces assumed could actually be produced by the interaction of electric and magnetic fields in circular pipes.

Some very interesting results were obtained by Hale and Kerrebrock (Ref. 18) in a study of insulator boundary layers in crossed field accelerators. Two models for the electrical conductivity variation were employed: an equilibrium model where the degree of ionization was determined by the local gas temperature and pressure, and a non-equilibrium model in which the electrical conductivity is strongly coupled to the electric field strength.

It was found that similar solutions could be obtained only for very restricted conditions and local similarity was assumed.

The boundary layer profiles for the non-equilibrium case show some very unusual characteristics and were extremely sensitive to the free stream Mach number and electromagnetic loading parameter. For certain values of the parameters, the velocity and temperature profiles show very pronounced bulges near the wall. The variation of the profiles for the equilibrium case is less pronounced.

Sonnerup (Ref. 19) investigated the fully developed flow of a compressible, electrically conducting fluid in slowly diverging channels. Sonnerup's work differs from the present study in that he was concerned with flow in a generator and the confining walls were electrode surfaces rather than insulator surfaces. The most interesting feature of this work is that a closed form solution was obtained.

Sonnerup simplified the governing equations via boundary layer type approximations in a manner similar to Williams (Ref. 2). By choice of the proper wall geometry the pressure gradient and the electromagnetic body force were made to balance each other. This, in turn, permitted the energy equation and the momentum equation to be uncoupled and analyzed separately. The velocity profiles were found to be self-similar but the temperature profiles were generally non-similar.

Although the emphasis of Sonnerup's work was on the mathematical analysis some numerical results were presented. The velocity and temperature profiles given exhibit no unusual characteristics.

III
FORMULATION OF THE PROBLEM

Consider the steady, two-dimensional, laminar flow of an electrically conducting gas between diverging plane walls as shown in Fig. 2. The problem is best described in cylindrical polar coordinates.

The flow may either be considered as emerging from a line source at $r = 0$ or as the fully developed portion of an actual channel flow. The rays $\theta = \pm \alpha$ are electrically insulated walls and the magnetic field is applied in the θ direction. An electric field is applied in the negative z direction, i.e. into the paper.

The governing equations of motion for a single fluid plasma are expressed in cylindrical polar coordinates in Eqs. (1) through (5).

Continuity equation:

$$\frac{\partial \rho}{\partial t} + \frac{1}{r}\frac{\partial(\rho U_r r)}{\partial r} + \frac{1}{r}\frac{\partial(\rho U_\theta)}{\partial \theta} + \frac{\partial(\rho U_z)}{\partial z} = 0 \tag{1}$$

r momentum equation:

$$\rho\left[\frac{DU_r}{Dt} - \frac{U_\theta^2}{r}\right] = (\vec{J}x\vec{B})_r - \frac{\partial p}{\partial r} + \frac{\partial}{\partial r}\left[\mu\left(2\frac{\partial U_r}{\partial r} - \frac{2}{3}\nabla \cdot \vec{U}\right)\right]$$

$$+ \frac{1}{r}\frac{\partial}{\partial \theta}\left[\mu\left(\frac{1}{r}\frac{\partial U_r}{\partial \theta} + \frac{\partial U_\theta}{\partial r} - \frac{U_\theta}{r}\right)\right] + \frac{\partial}{\partial z}\left[\mu\left(\frac{\partial U_r}{\partial z} + \frac{\partial U_z}{\partial r}\right)\right]$$

$$+ \frac{2\mu}{r}\left(\frac{\partial U_r}{\partial r} - \frac{1}{r}\frac{\partial U_\theta}{\partial \theta} - \frac{U_r}{r}\right) \tag{2}$$

θ momentum equation:

$$\rho\left[\frac{DU_\theta}{Dt} + \frac{U_r U_\theta}{r}\right] = (\vec{J}\times\vec{B})_\theta - \frac{1}{r}\frac{\partial p}{\partial\theta} + \frac{1}{r}\frac{\partial}{\partial\theta}\left[\mu\left(\frac{2}{r}\frac{\partial U_\theta}{\partial\theta}\right.\right.$$

$$\left.\left. + \frac{2U_r}{r} - \frac{2}{3}\nabla\cdot\vec{U}\right)\right] + \frac{\partial}{\partial z}\left[\mu\left(\frac{\partial U_\theta}{\partial z} + \frac{1}{r}\frac{\partial U_z}{\partial\theta}\right)\right] + \frac{\partial}{\partial r}\left[\mu\left(\frac{1}{r}\frac{\partial U_r}{\partial\theta}\right.\right.$$

$$\left.\left. + \frac{\partial U_\theta}{\partial r} - \frac{U_\theta}{r}\right)\right] + \frac{2\mu}{r}\left(\frac{1}{r}\frac{\partial U_r}{\partial\theta} + \frac{\partial U_\theta}{\partial r} - \frac{U_\theta}{r}\right) \tag{3}$$

z momentum equation:

$$\rho\frac{DU_z}{Dt} = (\vec{J}\times\vec{B})_z - \frac{\partial p}{\partial z} + \frac{\partial}{\partial z}\left[\mu\left(2\frac{\partial U_z}{\partial z} - \frac{2}{3}\nabla\cdot\vec{U}\right)\right.$$

$$\left. + \frac{1}{r}\frac{\partial}{\partial r}\left[\mu r\left(\frac{\partial U_r}{\partial z} + \frac{\partial U_z}{\partial r}\right)\right] + \frac{1}{r}\frac{\partial}{\partial\theta}\left[\mu\left(\frac{1}{r}\frac{\partial U_z}{\partial\theta} + \frac{\partial U_\theta}{\partial z}\right)\right]\right. \tag{4}$$

Energy equation:

$$\rho\frac{Dh}{Dt} = \frac{Dp}{Dt} + \frac{J^2}{\sigma} + \frac{1}{r}\frac{\partial}{\partial r}\left(r\kappa\frac{\partial T}{\partial r}\right) + \frac{1}{r^2}\frac{\partial}{\partial\theta}\left(\kappa\frac{\partial T}{\partial\theta}\right) + \frac{\partial}{\partial z}\left(\kappa\frac{\partial T}{\partial z}\right)$$

$$+ \mu\left[2\left(\frac{\partial U_r}{\partial r}\right)^2 + 2\left(\frac{1}{r}\frac{\partial U_\theta}{\partial\theta} + \frac{U_r}{r}\right)^2 + 2\left(\frac{\partial U_z}{\partial z}\right)^2 + \left(\frac{1}{r}\frac{\partial U_z}{\partial\theta} + \frac{\partial U_\theta}{\partial z}\right)^2\right.$$

$$\left. + \left(\frac{\partial U_r}{\partial z} + \frac{\partial U_z}{\partial r}\right)^2 + \left(\frac{1}{r}\frac{\partial U_r}{\partial\theta} + \frac{\partial U_\theta}{\partial r} + \frac{U_\theta}{r}\right)^2\right] - \frac{2}{3}\mu(\nabla\cdot\vec{U})^2 \tag{5}$$

where

$$\frac{D}{Dt} = \frac{\partial}{\partial t} + U_r \frac{\partial}{\partial r} + \frac{U_\theta}{r} \frac{\partial}{\partial \theta} + U_z \frac{\partial}{\partial z}$$

$$\nabla \cdot \vec{U} = \frac{1}{r} \frac{\partial (rU_r)}{\partial r} + \frac{1}{r} \frac{\partial U_\theta}{\partial \theta} + \frac{\partial U_z}{\partial z}$$

The necessary equations for the electromagnetic variables are:

Ampere's law:

$$\nabla \times \vec{B} = \mu_e \vec{J} \tag{6}$$

Faraday's law:

$$\nabla \times \vec{E} = - \frac{\partial \vec{B}}{\partial t} \tag{7}$$

Ohm's law:

$$\vec{J} = \sigma(\vec{E} + \vec{U} \times \vec{B}) \tag{8}$$

The equations as written incorporate the so-called magnetohydrodynamic approximations, i.e. the dielectric displacement current is neglected in Eq. (6) and the gas is assumed to be electrically neutral. The latter assumption permits deletion of the convection current term in Ohm's law and a body force term due to the electric field. These approximations are discussed by Sutton and Sherman (Ref. 12) and are standard magnetofluiddynamic assumptions.

Ohm's law is written in its simplified form neglecting Hall currents and ion slip effects.

In addition to the equations listed above we have an equation of state:

$$p = p(\rho, T) \tag{9}$$

a caloric equation of state:

$$h = h(\rho, T) \tag{10}$$

and relations for the transport properties:

$$\mu = \mu(\rho, T) \quad , \quad \sigma = \sigma(\rho, T) \quad , \quad \kappa = \kappa(\rho, T) \tag{11}$$

Eqs. (1) through (10) are sixteen equations for the sixteen unknowns p, ρ, T, h, $\vec{U}$, $\vec{B}$, $\vec{E}$, and $\vec{J}$. With appropriate boundary conditions they represent, theoretically, a determinate set. These equations will now be reduced to a form suitable for the particular problem being investigated.

As was stated previously, the flow is assumed to be steady and two dimensional, i.e. $\partial/\partial t = \partial/\partial z = 0$. Also, the transverse velocity components U_θ and U_z are assumed to be zero. It is further assumed that the induced magnetic field is negligibly small compared to the applied magnetic field. This last assumption permits the gas dynamical equations to be uncoupled from and solved independently of Ampere's law. The assumption has been used extensively in magnetogasdynamic studies and is equivalent to requiring that the magnetic Reynolds number, $R_\sigma = \sigma\mu_e UL$, be small compared to unity.

With these assumptions the equations of motion reduce to the following form:

Continuity Equation:

$$\frac{\partial}{\partial r}(\rho U_r r) = 0 \tag{12}$$

r momentum equation:

$$\rho U_r \frac{\partial U_r}{\partial r} = - \frac{\partial p}{\partial r} + \mu[\frac{4}{3} \frac{\partial^2 U_r}{\partial r^2} + \frac{4}{3r} \frac{\partial U_r}{\partial r} - \frac{4}{3r^2} U_r + \frac{1}{r^2} \frac{\partial^2 U_r}{\partial \theta^2}]$$

$$+ (\frac{4}{3} \frac{\partial U_r}{\partial r} - \frac{2}{3r} U_r) \frac{\partial \mu}{\partial r} + \frac{1}{r^2} \frac{\partial U_r}{\partial \theta} \frac{\partial \mu}{\partial \theta} - J_z B_\theta \tag{13}$$

θ Momentum Equation:

$$0 = - \frac{1}{r} \frac{\partial p}{\partial \theta} + \frac{\mu}{3} (\frac{1}{r} \frac{\partial^2 U_r}{\partial r \partial \theta} + \frac{7}{r^2} \frac{\partial U_r}{\partial \theta})$$

$$- \frac{2}{3} (\frac{1}{r} \frac{\partial U_r}{\partial r} - 2 \frac{U_r}{r^2}) \frac{\partial \mu}{\partial \theta} + \frac{1}{r} \frac{\partial U_r}{\partial \theta} \frac{\partial \mu}{\partial r} \tag{14}$$

Energy Equation:

$$\rho U_r \frac{\partial h}{\partial r} = U_r \frac{\partial p}{\partial r} + \frac{1}{r} \frac{\partial}{\partial r} (r\kappa \frac{\partial T}{\partial r}) + \frac{1}{r^2} \frac{\partial}{\partial \theta} (\kappa \frac{\partial T}{\partial \theta})$$

$$+ \mu \left[2(\frac{\partial U_r}{\partial r})^2 + 2(\frac{U_r}{r})^2 + (\frac{1}{r} \frac{\partial U_r}{\partial \theta})^2 \right]$$

$$- \frac{2}{3} \mu (\frac{\partial U_r}{\partial r} + \frac{U_r}{r})^2 + \frac{J_z^2}{\sigma} \tag{15}$$

Ohm's Law:

$$J_z = \sigma(E_z + U_r B_\theta) \tag{16}$$

The fluid medium is assumed to behave as a perfect

gas, both thermally and calorically so that:

$$p = \rho RT \tag{17}$$

$$h = C_p T \tag{18}$$

where Cp is a constant.

To complete the specification of the problem, boundary conditions must be imposed on the independent variables U_r, T, and p. Along the channel centerline, $\theta = 0$, a condition of symmetry is imposed.

$$\frac{\partial U_r(r,0)}{\partial \theta} = 0 \quad , \quad \frac{\partial T(r,0)}{\partial \theta} = 0 \quad , \quad \frac{\partial p(r,0)}{\partial \theta} = 0 \tag{19}$$

At the wall, the no slip condition is applied and the pressure and temperature variations are specified.

$$U_r(r,\alpha) = 0 \quad , \quad T(r,\alpha) = T_w(r) \quad , \quad p(r,\alpha) = p_w(r) \tag{20}$$

Rather than specifying the additional boundary conditions necessary at a particular value of r, a separable form of solution is assumed. It is then assumed that the dependent variables, transport properties, and applied fields can be expressed in the following form:

$$U_r(r,\theta) = \bar{U}(\theta) r^a$$

$$\rho(r,\theta) = \bar{\rho}(\theta) r^b$$

(Equation continued)

$$p(r,\theta) = \bar{p}(\theta)r^c$$

$$T(r,\theta) = \bar{T}(\theta)r^d$$

$$E_z(r) = -\bar{E}r^e$$

$$B_\theta(r) = \bar{B}r^f$$

$$\mu(r,\theta) = \bar{\mu}(\theta)r^g$$

$$\sigma(r,\theta) = \bar{\sigma}(\theta)r^h$$

$$\kappa(r,\theta) = \bar{\kappa}(\theta)r^j \tag{21}$$

where the exponents a, b, c, etc. are constants to be determined. Substitution of Eqs. (21) into Eqs. (12) through (15) and eliminating J_z and h gives:

$$(a + b + 1)\bar{\rho}\bar{U}r^{a+b} = 0 \tag{22}$$

$$a\bar{\rho}\bar{U}^2r^{2a+b-1} = -c\bar{p}r^{c-1} + \frac{4}{3}\bar{\mu}[a(a-1)\bar{U}$$

$$+ a\bar{U} - \bar{U}]r^{a+g-2} + \bar{\mu}\bar{U}''r^{a+g-2} + (\frac{4}{3}a\bar{U} - \frac{2}{3}\bar{U})g\bar{\mu}r^{a+g-2}$$

$$+ \bar{U}'\bar{\mu}'r^{a+g-2} + \bar{\sigma}\bar{E}\bar{B}r^{e+f+h} - \bar{\sigma}\bar{U}\bar{B}^2r^{a+2f+h} \tag{23}$$

$$0 = -\bar{p}'r^{c-1} + \frac{\bar{\mu}}{3}(a\bar{U}' + 7\bar{U}')r^{a+g-2}$$

$$- \frac{2}{3}(a\bar{U} - 2\bar{U})\bar{\mu}'r^{a+g-2} + g\bar{U}'\bar{\mu}r^{a+g-2} \tag{24}$$

$$d\bar{\rho}\bar{U}C_p\bar{T}r^{a+b+d-1} = c\bar{U}\bar{p}r^{a+c-1} + \bar{\sigma}(\bar{E} - \bar{U}\bar{B})^2 r^{h+2e}$$

$$+ d(d + j)\bar{\kappa}\bar{T}r^{d+j-2} + (\bar{\kappa}\bar{T}'' + \bar{\kappa}'\bar{T}')r^{j+d-2}$$

$$+ \bar{\mu}\ [2a^2\bar{U}^2 + 2\bar{U}^2 + (\bar{U}')^2]r^{2a+g-2}$$

$$- \frac{2}{3}\bar{\mu}\ (a + 1)^2\bar{U}^2 r^{2a+g-2} \tag{25}$$

$$\bar{p}r^c = \bar{\rho}R\bar{T}r^{b+d} \tag{26}$$

where the prime refers to differentiation with respect to θ.

If $\bar{U}$, $\bar{T}$, etc, are to be functions of θ only, as assumed, then Eqs. (22) through (26) may not involve the variable r. Therefore the following equations must be satisfied by the exponents:

$$a + b + 1 = 0$$

$$2a + b - 1 = c - 1 = a + g - 2$$

$$= e + f + h = a + 2f + h$$

$$a + b + d - 1 = a + c - 1 = h + 2e$$

$$= d + j - 2 = 2a + g - 2$$

$$c = b + d \tag{27}$$

Eqs. (27) represent only seven independent equations for the nine exponents which can be solved in terms of the electric and magnetic field exponents e and f.

$$
\begin{aligned}
a &= e - f & U_r &= \bar{U}(\theta) r^{e-f} \\
b &= f - e - 1 & \rho &= \bar{\rho}(\theta) r^{f-e-1} \\
c &= e - f - 1 & p &= \bar{p}(\theta) r^{e-f-1} \\
d &= 2(e - f) & T &= \bar{T}(\theta) r^{2(e-f)} \\
g &= 0 & \mu &= \bar{\mu}(\theta) \\
h &= -2(f + 1) & \sigma &= \bar{\sigma}(\theta) r^{-2(f+1)} \\
j &= 0 & \kappa &= \bar{\kappa}(\theta)
\end{aligned}
\tag{28}
$$

Since the fluid transport properties cannot vary with r, they are assumed independent of θ as well, i.e. μ = constant and κ = constant will be assumed.

From Eqs. (28) it is clear that the radial variations of the quantities U_r, ρ, p, and T are determined by electric and magnetic field distributions. These distributions will be chosen so as to be consistent with Maxwell's electromagnetic equations.

The r and θ components of Faraday's law for steady state are:

$$
\begin{aligned}
\frac{\partial E_z}{\partial \theta} - \frac{\partial (r E_\theta)}{\partial z} &= 0 \\
\frac{\partial E_r}{\partial z} - \frac{\partial E_z}{\partial r} &= 0
\end{aligned}
\tag{29}
$$

Then since $\partial/\partial z = 0$ by assumption

$$
\frac{\partial E_z}{\partial r} = \frac{\partial E_z}{\partial \theta} = 0
$$

or

$$E_z = \text{constant}, \quad e = 0 \tag{30}$$

Such an electric field could be produced by using parallel equipotential electrode surfaces for the channel sidewalls.

A solution to Ampere's law, Eq. (6) is

$$\vec{B} = \vec{B}_H + \vec{b} \tag{31}$$

where

$$\nabla \times \vec{B}_H = 0$$

$$\nabla \times \vec{b} = \mu_e \vec{J}$$

It is clear that $\vec{B}_H$, the solution to the homogeneous equation, is the applied field B_θ and that $\vec{b}$ is the induced field. By assumption $|\vec{b}| << B_\theta$. Thus the applied magnetic field B_θ should satisfy the z component of Ampere's law with $J_z = 0$.

$$\frac{\partial(rB_\theta)}{\partial r} = 0$$

or

$$B_\theta \sim \frac{1}{r} \quad , \quad f = -1 \tag{32}$$

Such a magnetic field could be produced by a current carrying wire coincident with Z axis and could doubtless be closely approximated by a magnet with diverging pole faces.

It should be pointed out that while Eqs. (30) and (32) define the only electric and magnetic field distributions rigorously consistent with the geometry and assumptions of this model, in an actual three-dimensional channel other distributions are not only possible but may be desirable.

By using finely segmented, individually powered electrodes almost any reasonable electric field distribution can be closely approximated. Although the magnetic field is not so easily modified, this distribution too can be tailored to some extent.

Introducing the values of e and f into Eqs. (28) gives:

$$
\begin{aligned}
a &= 1 & U_r &= \bar{U}(\theta)r \\
b &= -2 & \rho &= \rho(\theta)r^{-2} \\
c &= 0 & p &= \bar{p}(\theta) \\
d &= 2 & T &= \bar{T}(\theta)r^2 \\
h &= 0 & \sigma &= \sigma(\theta) = \text{constant}
\end{aligned}
\tag{33}
$$

Since the electrical conductivity cannot vary with r, it will be taken to be a constant.

Eqs. (33) show that the gas is accelerated down the channel, the pressure and Mach number being constant along radial lines. It is not surprising that these radial variations are of the same form as found by Hains (Ref. 8) and Podolsky and Borman (Ref. 9) on the basis of inviscid models.

Substituting the values of the exponents into Eqs. (22) through (26) gives:

$$\bar{\rho}\bar{U}^2 = \mu\bar{U}'' + \sigma(\bar{E} - \bar{U}\bar{B})\bar{B} \tag{34}$$

$$\bar{p}' = \frac{8}{3}\mu\bar{U}' \tag{35}$$

$$
\begin{aligned}
2\bar{\rho}\bar{U}C_p\bar{T} &= \sigma(\bar{E} - \bar{U}\bar{B})^2 + \kappa\bar{T}'' + 4\kappa\bar{T} \\
&\quad + \mu[(\bar{U}')^2 + \frac{4}{3}\bar{U}^2]
\end{aligned}
\tag{36}
$$

$$\bar{p} = \bar{\rho} R \bar{T} \tag{37}$$

Eq. (22) is identically satisfied.

In summary the additional restrictions that have been forced by the separation of variables are:

1. The variations of velocity, density, temperature and pressure down the channel have been specified.

2. It has been shown that the viscosity, thermal conductivity, and electrical conductivity cannot change with r. These properties have been taken to be constant.

3. The variation of temperature and the constancy of pressure have been specified along the channel wall.

$$T(r,\alpha) = T_w(r) = \bar{T}_w r^2$$

$$p(r,\alpha) = p_w(r) = p_w$$

Eq. (35), the θ momentum equation, can be integrated immediately to give

$$\bar{p} = \frac{8}{3} \mu \bar{U} + p_w \tag{38}$$

Using Eq. (38) and the equation of state given by Eq. (22) the density $\bar{\rho}$ can be eliminated from Eqs. (34) and (36) giving:

$$\frac{\bar{U}^2}{R\bar{T}} \left(\frac{8}{3} \mu \bar{U} + p_w\right) = \mu \bar{U}'' + \sigma(E - \bar{U}\bar{B})\bar{B} \tag{39}$$

$$\frac{2C_p \, p_w}{R} \bar{U} = \sigma(\bar{E} - \bar{U}\bar{B})^2 + \kappa \bar{T}'' + 4\kappa \bar{T}$$

(Equation continued)

$$+ \mu[(\bar{U}')^2 + \frac{4}{3}(1 - \frac{4Cp}{R})\bar{U}^2] \tag{40}$$

Eqs. (39) and (40) are two coupled, non-linear differential equations for $\bar{U}$ and $\bar{T}$. The boundary conditions for these two quantities are:

$$\bar{U}'(0) = 0 \qquad \bar{U}(\alpha) = 0$$

$$\bar{T}'(0) = 0 \qquad \bar{T}(\alpha) = \bar{T}_w \tag{41}$$

Eqs. (39) and (40) can be put into dimensionless form by defining new variables

$$f(\theta) = \frac{\bar{U}r_o}{U_c} \quad , \quad g(\theta) = \frac{\bar{T}r_o^{\,2}}{T_c} \tag{42}$$

where r_o is the radial distance to the channel "entrance", U_c and T_c are characteristic values of velocity and temperature to be specified. Also define

$$B_o = \frac{\bar{B}}{r_o} \quad , \quad E_o = \bar{E} \tag{43}$$

where B_o is the magnetic induction at r_o. Define the dimensionless parameters

$$Ha = (\frac{\sigma}{\mu})^{\frac{1}{2}} B_o r_o \qquad \text{(Hartmann number)}$$

$$Re = \frac{\rho_c U_c r_o}{\mu} \qquad \text{(Reynolds number)}$$

where

$$\rho_c \equiv \frac{p_w}{RT_c} \tag{44}$$

$$\Phi = \frac{E_o}{U_c B_o}$$

$$M = \frac{U_c}{(\gamma R T_c)^{\frac{1}{2}}} \quad \text{(Mach number)}$$

$$Pr = \frac{C_p \mu}{\kappa} \quad \text{(Prandtl number)}$$

Then Eqs. (39) and (40) can be rewritten in terms of the dimensionless variables and parameters as

$$\frac{d^2 f}{d\theta^2} = \frac{8}{3} \gamma M^2 \frac{f^3}{g} + Re \frac{f^2}{g} - (Ha)^2 (\Phi - f) \tag{45}$$

$$\frac{d^2 g}{d\theta^2} + 4g = 2RePrf - (\gamma - 1) M^2 Pr (Ha)^2 (\Phi - f)^2$$

$$- (\gamma - 1) M^2 Pr \left(\frac{df}{d\theta}\right)^2 + \frac{4}{3} (3\gamma + 1) M^2 Prf^2 \tag{46}$$

with boundary conditions

$$f'(0) = 0 \qquad f(\alpha) = 0$$

$$g'(0) = 0 \qquad g(\alpha) = \frac{\bar{T}_w r_o}{T_c} \tag{47}$$

Eqs. (45) and (46) with boundary conditions given by Eq. (47) represent the analytical model for the present investigation.

IV
TECHNIQUE OF SOLUTION

4.1 SOLUTION DIFFICULTIES OF THE DIRECT BOUNDARY VALUE PROBLEM

Eqs. (45) through (47) appear to define a straight forward but complicated non-linear boundary value problem. The following method of solution would seem applicable.

1. Assign values for the divergence angle α and the wall temperature $g(\alpha)$.

2. Specify values for the six dimensionless parameters γ, Pr, Ha, Re, M, Φ.

3. Guess initial values for the dimensionless velocity and temperature $f(0)$ and $g(0)$.

4. Numerically integrate Eqs. (45) and (46) using the Runge-Kutta method from $\theta = 0$ to $\theta = \alpha$ hoping to satisfy the boundary conditions at the wall.

5. Adjust the values of $f(0)$ and $g(0)$ as necessary and integrate the equations again. Repeat until the boundary conditions at α are met.

6. Assign new values for the parameters γ, Pr, Ha, Re, M, Φ and repeat steps 3 through 5.

The iterative procedure outlined above would obviously involve considerable computation time with no a priori guarantee of convergence. There is also, however, another somewhat more subtle difficulty with this method.

In order that the dimensionless variables and parameters be well defined, the characteristic velocity U_c and the characteristic temperature T_c must be specified. A convenient value for the characteristic temperature is the wall temperature at r_o, $T_c = \bar{T}_w r_o^2$, so that the temperature boundary condition becomes $g(\alpha) = 1$. For the characteristic velocity, a logical choice would be the average velocity at r_o, defined as

$$U_c = \frac{r_o}{2\alpha} \int_{-\alpha}^{\alpha} \bar{U}(\theta) d\theta \tag{48}$$

Introducing

$$f(\theta) = \frac{U(\theta)r_o}{U_c} \qquad \text{gives}$$

$$\int_{-\alpha}^{\alpha} f(\theta)d\theta = 2\alpha \tag{49}$$

Defining $\eta = \theta/\alpha$ and using the fact that $f(\theta)$ is an even function gives

$$\int_{0}^{1} f(\eta)d\eta = 1 \tag{50}$$

an extra condition of f that generally would not be satisfied. For problems that can be solved explicitly in closed form, this extra condition usually defines a relationship between the parameters. For example, in ordinary hydrodynamic flow between parallel plates a condition similar to Eq. (50) gives a relation between the mean velocity and the pressure gradient.

Thus in the present problem one would expect some relationship among the parameters γ, Pr, Ha, Re, M, and Φ that must be satisfied before a solution can be obtained. This conclusion can be illustrated by considering the corresponding one-dimensional, inviscid problem.

The governing equations for the inviscid problem can be obtained from Eqs. (12) through (18) by setting $\mu = \kappa = 0$. The resulting equations are

$$\frac{\partial(\rho U_r r)}{\partial r} = 0 \tag{51}$$

$$\rho U_r \frac{\partial U_r}{\partial r} = -\frac{\partial p}{\partial r} + \sigma(E - U_r B)B \tag{52}$$

$$\rho U_r C_p \frac{\partial T}{\partial r} = U_r \frac{\partial p}{\partial r} + \sigma(E - U_r B)^2 \tag{53}$$

$$p = \rho R T \tag{54}$$

Define new dimensionless variables as

$$U^* = \frac{U_r}{U_o} \qquad \rho^* = \frac{\rho}{\rho_o} \qquad T^* = \frac{T}{T_o}$$

$$p^* = \frac{p}{p_o} \qquad r^* = \frac{r}{r_o} \tag{55}$$

where the subscript zero denotes the value of the quantity at r_o. The applied magnetic field distribution is the same as previously derived in Eq. (32), i.e. $B = B_o/r^*$.

In terms of the dimensionless variables the equations become

$$\rho^* U^* \frac{\partial U^*}{\partial r^*} = \pi \frac{\partial p^*}{\partial r^*} + R_M(\Phi - \frac{U^*}{r^*}) \frac{1}{r^*} \tag{56}$$

$$\rho^* U^* r^* = 1 \tag{57}$$

$$\frac{\rho^* U^*}{(\gamma-1)M^2} \frac{\partial T^*}{\partial r^*} = \pi U^* \frac{\partial p^*}{\partial r^*} + R_M(\Phi - \frac{U^*}{r^*})^2 \tag{58}$$

$$p^* = \rho^* T^* \tag{59}$$

where

$$\Phi = \frac{E}{U_o B_o}$$

$$R_M = \frac{\sigma r_o B_o^2}{\rho_o U_o}$$

$$\pi = \frac{p_o}{\rho_o U_o^2}$$

$$M = \frac{U_o}{(\gamma R T_o)^{\frac{1}{2}}} \tag{60}$$

The initial conditions on the dependent variables are

$$U^*(1) = 1$$

$$T^*(1) = 1$$

$$\rho^*(1) = 1$$

$$p^*(1) = 1 \tag{61}$$

Following a procedure similar to that used for the two dimensional problem assume a solution of the form

$$U^* = C_1 (r^*)^a$$

$$\rho^* = C_2 (r^*)^b$$

$$p^* = C_3 (r^*)^c$$

$$T^* = C_4 (r^*)^d \tag{62}$$

which leads to

$$U^* = \frac{R_M \Phi}{1 + R_M} r^* \tag{63}$$

$$\rho^* = \frac{1 + R_M}{R_M \Phi} (r^*)^{-2} \tag{64}$$

$$p^* = \frac{(\gamma-1)M^2\Phi}{2(1 + R_M)} \tag{65}$$

$$T^* = \frac{(\gamma-1)M^2 R_M \Phi^2}{2(1 + R_M)^2} r^{*2} \tag{66}$$

This solution will satisfy the initial conditions if and only if,

$$\frac{R_M \Phi}{1 + R_M} = 1$$

$$\frac{(\gamma - 1)M^2 R_M \Phi^2}{2(1 + R_M)^2} = 1$$

or

$$\Phi = \frac{1 + R_M}{R_M} \tag{67}$$

$$M^2 = \frac{2R_M}{\gamma - 1} \tag{68}$$

If Eqs. (67) and (68) are satisfied the solution is given by

$$U^* = r^*$$

$$\rho^* = (r^*)^{-2}$$

$$p^* = 1$$

$$T^* = (r^*)^2 \tag{69}$$

If Eqs. (67) and (68) are not satisfied the solution is entirely different, but according to Podolsky and Borman (Ref. 9) approaches the values given by Eqs. (63) through (66) for large values of r^*. The solution given above is a special case of the problem investigated by these authors although it was not specifically pointed out by them.

In view of the above considerations one is forced to conclude that the direct boundary value problem is indeed overspecified and that a solution cannot be obtained for an arbitrary choice of the parameters. This overspecification would make solution by the iterative procedure outlined previously extremely difficult. Fortunately, there is an alternate approach to the problem that alleviates this difficulty.

4.2 THE INITIAL VALUE PROBLEM

An approach which will circumvent the difficulty of overspecification of the problem mentioned above is to leave the wall divergence angle as a dependent variable of the problem. The problem also becomes an initial value problem in contrast to the two point boundary value problem specified by Eqs. (47).

For this approach the characteristic velocity and characteristic temperature of the problem are defined to be values of velocity and temperature at $r = r_o$ and $\theta = 0$, i.e.

$$U_c = U_o = U(r_o, 0)$$

$$T_c = T_o = T(r_o, 0) \tag{70}$$

With this choice the dimensionless equations and boundary conditions become

$$\frac{d^2f}{d\theta^2} = \frac{8}{3}\gamma M^2 \frac{f^3}{g} + Re\frac{f^2}{g} - (Ha)^2(\Phi - f) \tag{71}$$

$$\frac{d^2g}{d\theta^2} + 4g = 2RePrf - (\gamma - 1)M^2Pr(Ha)^2(\Phi - f)^2$$

$$- (\gamma - 1)M^2Pr\left(\frac{df}{d\theta}\right)^2 + \frac{4}{3}(3\gamma + 1)M^2Prf^2 \tag{72}$$

$$f(0) = 1 \qquad f'(0) = 0$$

$$g(0) = 1 \qquad g'(0) = 0 \tag{73}$$

Eqs. (71), (72) and (73) constitute an initial value problem that can be integrated directly by numerical methods. The divergence angle and the wall temperature are then determined by the integration. The no slip condition $f(\alpha) = 0$ is used to specify the wall divergence angle, α, and the corresponding value $g(\alpha)$ gives the ratio of wall to centerline temperatures.

Thus, in approaching the problem by the method described above, two new parameters have been introduced, giving a total of eight, namely γ, Pr, Ha, Φ, Re, M, α, $g(\alpha)$. In order to keep the number of computations required within reason, it was decided to fix and hold constant the ratio of specific heats, γ, and the Prandtl number at values typical for diatomic gases. Thus the values $\gamma = 1.4$ and $Pr = 1$ are used in all numerical calculations.

Eqs. (71) and (72) with initial conditions given by Eqs. (73) were programmed for solution using a standard fourth order Runge-Kutta scheme.

Consider now the interrelation among the remaining parameters Ha, Φ, Re, M, α, $g(\alpha)$. It is to be expected that a change in any one of the parameters Ha, Φ, Re, or M will cause a change in both α and $g(\alpha)$. Extensive computer calculations reveal that this is true. More generally it

may be said that only three of the six parameters may be held constant at once or that a change in any one of these must result in a change in two of the remaining five. Figs. 3 and 4 illustrate this behavior showing the relation between Ha, Φ, α, and $g(\alpha)$ for Re and M fixed. Lines of constant α have been cross plotted on Fig. 4.

Thus it is not possible in this problem to directly assess the effect of the change of a single parameter. Other solutions for viscous, compressible, channel flows both with and without electromagnetic effects exhibit a similar behavior (Ref. 2, 19, 20).

In view of these considerations, solutions will be compared on the following basis

1. The electromagnetic parameters Ha and Φ will be taken as the independent parameters.

2. The values α and $g(\alpha)$ will be considered as fixed.

3. The gas dynamic parameters Re and M will be considered dependent parameters.

This technique will permit a comparison of velocity and temperature profiles for flows with $Ha = Ha)_1$ and $Ha = Ha)_2$ at the same values of Φ, α, and $g(\alpha)$. Corresponding to the change in Ha there will be a change in both Re and M. It is felt that this method will yield the most information about the effect of a change in one of the electromagnetic parameters on the flow.

From the numerical calculations, graphs were constructed showing α as a function of Re and M and $g(\alpha)$ as a function of Re and M for fixed values of Ha and Φ.

Range of Parameters

It was quickly discovered through numerical computations that there are well defined limits on the values that some of the parameters can be assigned. For example, reference to Fig. 26 shows that there is a minimum value of the divergence angle which occurs at Re = 0. Moreover, it is clear that $(\partial\alpha/\partial M)_{Re = 0} = 0$. From these observations an expression can be obtained for the minimum divergence angle as a function of Ha and Φ. Putting Re = 0 and M = 0 in Eq. (45) gives

$$\frac{d^2f}{d\theta^2} + (Ha)^2(\Phi - f) = 0 \tag{74}$$

with initial conditions

$$f(0) = 1 \qquad f'(0) = 0 \tag{75}$$

which yields

$$f = \Phi + (1 - \Phi)\cosh(Ha\theta) \tag{76}$$

Using the condition $f(\alpha) = 0$ gives

$$\alpha_{min} = \frac{1}{Ha} \cosh^{-1} \frac{\Phi}{\Phi - 1} \tag{77}$$

For Ha = 100, $\Phi = 1.6$, Eq. (77) gives $\alpha_{min} = .0164$ rad = .94° which agrees with Fig. 28. Also the general behavior predicted by Eq. (77) is the same as shown by Fig. 3 for non-zero values of Re and M.

Note that as Φ approaches unity α_{min} approaches infinity and that for Φ less than one, no real values of α_{min} exist. This would suggest that meaningful solutions to Eqs. (45) and (46) are only possible for $\Phi > 1$. This conclusion has been verified by numerical calculations.

The quantity $\Phi = E_o/U_oB_o$ is an electromagnetic loading parameter and $0 \leq \Phi \leq 1$ corresponds to a generator mode of operation of the channel where energy is extracted from the fluid. The accelerator mode of operation corresponds to $\Phi > 1$. Since the solution form assumed in Eqs. (33) clearly indicates that energy is being added to the fluid by the applied fields, it is not surprising that solutions cannot be obtained for $\Phi \leq 1$.

Having obtained an expression for the minimum value of the divergence angle, it is logical to inquire whether or not this parameter has an upper limiting value. Rewriting the differential equations for $f(\theta)$ and $g(\theta)$ and the initial conditions on these variables gives

$$\frac{d^2f}{d\theta^2} = \frac{8}{3} \gamma M^2 \frac{f^3}{g} + Re \frac{f^2}{g} - (Ha)^2(\Phi - f) \tag{78}$$

$$\frac{d^2g}{d\theta^2} + 4g = 2RePrf - (\gamma - 1)M^2Pr(Ha)^2(\Phi - f)^2$$

$$- (\gamma - 1)M^2Pr(\frac{df}{d\theta})^2 + \frac{4}{3}(3\gamma + 1)M^2Prf^2 \tag{79}$$

$$f(0) = 1 \qquad f'(0) = 0$$

$$g(0) = 1 \qquad g'(0) = 0 \tag{80}$$

Then at $\theta = 0$

$$f''(0) = \frac{8}{3}\gamma M^2 + Re - (Ha)^2(\Phi - 1) \tag{81}$$

$$g''(0) = 2RePr - 4 - (\gamma - 1)M^2Pr(Ha)^2(\Phi - 1)^2$$

$$+ \frac{4}{3}(3\gamma + 1)M^2Pr \tag{82}$$

If Re, M, Ha, and Φ are chosen such that $f''(0) = 0$ and $g''(0) = 0$, it is seen by continued differentiation of Eqs. (78) and (79) and setting $\theta = 0$ that

$$f^n(0) = 0 \qquad g^n(0) = 0 \qquad n=3,4... \tag{83}$$

Thus

$$f(\theta) \equiv 1 \qquad g(\theta) \equiv 1$$

for all values of θ and $\alpha = \infty$. Obviously then there is no upper limit on the values that α can attain. Nonetheless,

a very interesting result has been obtained. Considering Ha and Φ as being fixed, the equations corresponding to $f''(0) = 0$ and $g''(0) = 0$, namely

$$\frac{8}{3}\gamma M^2 + Re - (Ha)^2(\Phi - 1) = 0 \tag{84}$$

$$2RePr - 4 - (\gamma - 1)M^2Pr(Ha)^2(\Phi - 1)^2$$

$$+ \frac{4}{3}(3\gamma + 1)M^2Pr = 0 \tag{85}$$

define a limiting point in the Re, M plane.

It is expected that for fixed values of Ha and Φ as values of Re and M are chosen approaching the limiting values, defined by Eqs. (84) and (85), larger values of α will be obtained.

It is particularly interesting to note the close relationship between Eqs. (84) and (85) and Eqs. (67) and (68), the conditions that must be satisfied in order that the inviscid solution be given by Eqs. (69). If the terms $\frac{8}{3}\gamma M^2$, 4, and $\frac{4}{3}(3\gamma + 1)M^2Pr$ are ignored, Eqs. (84) and (85) become

$$Re - (Ha)^2(\Phi - 1) = 0 \tag{86}$$

$$2RePr - (\gamma - 1)M^2Pr(Ha)^2(\Phi - 1)^2 = 0 \tag{87}$$

But

$$(Ha)^2 = \frac{\sigma}{\mu} B_o^2 r_o^2 = \left(\frac{\sigma r_o B_o^2}{\rho_o U_o}\right)\left(\frac{\rho_o U_o r_o}{\mu}\right) = R_M Re$$

so that Eqs. (86) and (87) become

$$\Phi = \frac{1 + R_M}{R_M} \tag{88}$$

$$M^2 = \frac{2R_M}{\gamma - 1} \tag{89}$$

Eqs. (88) and (89) are identical to Eqs. (67) and (68).

The terms $\frac{8}{3}\gamma M^2$, 4, and $\frac{4}{3}(3\gamma + 1)M^2Pr$ arise due to the cross channel pressure variation, axial heat conduction, and viscous dissipation due to axial velocity gradients. If the problem had been formulated not including these effects, i.e. using boundary layer type approximations to simplify the equations, then the inviscid solution given by Eqs. (69) would represent truly the limiting solution for the viscous problem. With the aforementioned effects excluded the dimensionless equations for $f(\theta)$ and $g(\theta)$ are:

$$\frac{d^2f}{d\theta^2} = Re\,\frac{f^2}{g} - (Ha)^2(\Phi - f) \tag{90}$$

$$\frac{d^2g}{d\theta^2} = 2RePrf - (\gamma - 1)M^2Pr(Ha)^2(\Phi - f)^2$$

$$- (\gamma - 1)M^2Pr\left(\frac{df}{d\theta}\right)^2 \tag{91}$$

with initial conditions

$$f(0) = 1 \qquad f'(0) = 0$$

$$g(0) = 1 \qquad g'(0) = 0 \tag{92}$$

Setting $\theta = 0$ gives

$$\frac{1}{Re} f''(0) = 1 - R_M(\Phi - 1) \tag{93}$$

$$\frac{1}{RePr} g''(0) = 2 - (\gamma - 1)M^2 R_M(\Phi - 1)^2 \tag{94}$$

so that for

$$\Phi = \frac{1 + R_M}{R_M}$$

$$M^2 = \frac{2R_M}{\gamma - 1} \tag{95}$$

$$f^n(0) = g^n(0) = 0 \quad n = 2,3,\ldots \tag{96}$$

$$f(\theta) = g(\theta) = 1 \tag{97}$$

for all θ and for all values of Re and Pr. Then the solution is

$$U_r(r,\theta) = U_o\left(\frac{r}{r_o}\right) \tag{98}$$

$$T(r,\theta) = T_o\left(\frac{r}{r_o}\right)^2 \tag{99}$$

This is, of course, the same solution obtained for the inviscid problem and is valid only when Eqs. (67) and (68) are satisfied.

Returning to a consideration of the limits on the

various parameters, it was decided to concentrate on values of $g(\alpha)$ between 0.1 and 0.5. It is unlikely that the ratio of wall temperature to centerline temperature would be outside these limits in a practical device. Fig. 5 shows the region in the Re, M plane where acceptable solutions can be obtained for Ha = 200 and $\Phi = 1.6$. As was anticipated, as values of Re and M are chosen, in this region, approaching the limit point, larger values of divergence angle are obtained. Note that the region of acceptable solutions becomes increasingly narrow as the limiting point is approached.

If values of Re and M are used that lie to the left of the region shown in Fig. 5, negative values of $g(\alpha)$ are obtained. Such a result is physically meaningless. If values are used to the right of the region shown, large values of $g(\alpha)$ are obtained and ultimately the dimensionless velocity, $f(\theta)$, grows without limit.

Finally, there are practical upper limits on the values of Ha, Φ, and α. As is shown in Fig. 3 and by Eq. (77), α tends to decrease with increasing values of Ha and Φ. Thus, for large values of these parameters, it is necessary to closely approach the limiting values of Re and M in order to hold α constant. But, as was pointed out, the region of acceptable solutions becomes very narrow in the neighborhood of the limiting point. Thus, it is very difficult to obtain solutions for large values of Ha, Φ, and α simultaneously.

In view of these considerations it was decided to concentrate on values of α between 1.0° and 1.6°, to use values of Ha = 100, 150, 200, and to use values of $\Phi = 1.2$, 1.6, 2.0. For these selections it is possible to carry out the proposed solution and comparison scheme with a reasonable amount of numerical calculations.

In summary, it has been ascertained that there are well defined limitations on the range of each of the parameters involved in the present study, Ha, Φ, Re, M, α, and $g(\alpha)$. These restrictions are either mathematical, physical, or practical, depending on the parameter but in all cases they are quite real and meaningful solutions can be obtained only within these limitations. Table 1 gives the numerical values of α_{min}, M_{limit}, Re_{limit} for the values of Ha and Φ used in this study.

V
DISCUSSION OF RESULTS

The results of this portion of the investigation are presented graphically in Figs. 6 through 18. Figs. 6 through 14 give velocity and temperature profiles for the nine combinations of Ha and Φ considered in the study. The dimensionless variables f and g are plotted against the normalized space coordinate $\eta = \theta/\alpha$. For each of these graphs the divergence angle is approximately 1.5° and the ratio of wall temperature to centerline temperature is approximately 0.2. The values of Re and M required to maintain these values α and $g(\alpha)$ were obtained from Figs. 26 through 43. Figs. 15 and 16 show the variation of viscous drag and wall heat transfer with Ha and Φ. Figs. 17 and 18 are velocity and temperature profiles for $\alpha = 1.25°$ and $g(\alpha) = 0.2$. These figures show the effect of a change in the divergence angle and will be used for comparison with the results for variable properties.

The velocity profiles can also be interpreted to give the cross channel pressure variation. Writing Eq. (38) in terms of dimensionless variables and parameters and letting

$$p^*(\theta) = \frac{p(\theta) - p_w}{p_w} \tag{100}$$

gives

$$p^*(\theta) = \frac{8}{3}\frac{\gamma M^2}{Re} f(\theta) \tag{101}$$

Table II summarizes the results giving the values of Re, M, $f'(\alpha)$, $g'(\alpha)$, and $p^*(0)$ in terms of Ha and Φ for $\alpha = 1.5°$ and $g(\alpha) = 0.2$.

It must be pointed out again that the changes in the velocity and temperature profiles exhibited in Figs. 6 through 14 cannot be solely attributed to changes in the electromagnetic parameters Ha and Φ. As has been discussed, associated with a change in one or both of these parameters, there is a change in the gas dynamic parameters Re and M. This interdependence of electromagnetic and gas dynamic parameters will be shown in the following discussion to be an important feature of the problem.

Perhaps the most salient feature of the results is the prominent bulge in the temperature profiles. Physically this is due, of course, to the concentration of joule heating and viscous heating in the vicinity of the cool wall. In this region the reversed electromotive force due to the fluid motion is small and a large current density results. This effect, however, is somewhat more pronounced than had been anticipated.

The trend exhibited by the temperature bulge as Φ changes is very interesting. If g_{max} denotes the maximum value of $g(\eta)$, for certain values of Ha, g_{max} increases monotonically with Φ. At a larger value of Ha, g_{max} increases to a maximum value and then decreases with increasing Φ, and for a still larger value of Ha, g_{max} may monotonically decrease with Φ. In particular for Ha = 100, g_{max} increases monotonically with Φ, for Ha = 150, g_{max} increases to a maximum and then decreases with Φ, and for Ha = 200, g_{max} decreases monotonically with Φ. This behavior is also reflected in Fig. 16 which shows the temperature gradient at the wall as a function of Φ for the above three values of Ha.

In order to explain this phenomenon, the behavior of the temperature profile for constant values of Ha and Φ along a line of constant $g(\alpha)$ in the Re, M plane must be examined. Now for $g(\alpha)$ fixed there is a correlation between the bulge in the temperature profile and $g''(0)$.

$$g''(0) = 2RePr - 4 - (\gamma - 1)M^2Pr(Ha)^2(\Phi - 1)^2$$

$$+ \frac{4}{3}(3\gamma + 1)M^2Pr \tag{102}$$

From Eq. (102), considering the dominant first and third terms on the right side, it is clear that $g''(0)$ increases with increasing Re and decreases with increasing values of M. Thus, referring to Fig. 5, one would expect upon moving along a line of constant $g(\alpha)$ toward the limit point that the bulge in the temperature profile would first increase, reach a maximum and then decrease. The temperature profile must flatten as the limit point is approached.

Next consider a three-dimensional Φ, Re, M space for fixed Ha. In such a space there are surfaces of constant

α and surfaces of constant $g(\alpha)$. Corresponding to the limiting point in the Re, M plane, there is a limiting curve in Φ, Re, M space. In obtaining solutions for Ha, α, and $g(\alpha)$ fixed and for various values of Φ, one obtains solutions corresponding to points in this space that lie on the line of intersection of a constant $g(\alpha)$ surface and a constant α surface. Now it was stated in Section IV that for larger values of Φ it is necessary to closely approach the limiting values of Re and M in order to hold α constant. In other words as the Φ coordinate increases the line of intersection approaches the limiting curve. Thus in obtaining solutions on the line of intersection for increasing Φ, i.e. approaching the limiting curve, one expects a behavior similar to that observed in moving along a line of constant $g(\alpha)$ in the Re, M plane, that is an increase in the temperature bulge followed by a decrease.

Mathematically, then, the reason for the aforementioned behavior becomes clear. For Ha = 100 increasing Φ from 1.2 to 2.0 along the line of intersection of the surfaces $\alpha = 1.5°$ and $g(\alpha) = 0.2$ occurs on a section of this line removed far enough from the limiting curve such that the temperature bulge becomes more pronounced. For Ha = 200 the change in Φ occurs on a section of the corresponding line close enough to the limiting curve so that the temperature bulge becomes less pronounced.

While the explanation given above is perhaps satisfactory from a mathematical point of view it yields little insight into the physical mechanisms involved.

The dimensionless parameter Φ can be interpreted as a measure of the total energy input divided by the accelerating work.

Total energy input/(unit vol)(unit time) = $\vec{J} \cdot \vec{E}$

Accelerating work/(unit vol)(unit time) = $(\vec{J} \times \vec{B}) \cdot \vec{U}$

Forming the ratio of these quantities gives

$$\frac{\vec{J} \cdot \vec{E}}{(\vec{J} \times \vec{B}) \cdot \vec{U}} = \frac{J_z E_z}{J_z B_\theta U_r} = \frac{\Phi}{f(\theta)} \tag{103}$$

where

$$\Phi = \frac{E_o}{B_o U_o}$$

But

$$\vec{J} \cdot \vec{E} = \frac{J^2}{\sigma} + (\vec{J} \times \vec{B}) \cdot \vec{U}$$

so that Eq. (103) can be written as

$$\frac{\Phi}{f(\theta)} = \frac{J^2/\sigma}{(\vec{J} \times \vec{B}) \cdot \vec{U}} + 1 \tag{104}$$

Eq. (104) indicates that for larger values of Φ a greater portion of the total energy input is dissipated in Joule heating. It has been noted that this dissipation is largest in the vicinity of the wall where the reversed electromotive force due to the fluid motion approaches zero. Then as expected, for low values of Ha this increased dissipation for larger values of Φ is exhibited as a more pronounced temperature bulge.

Evidently, however, another mechanism is involved that counteracts this effect and dominates it for large values of the Hartmann number. Examination of the velocity profiles shows that there is, as expected, a flattening of these profiles with increasing Ha and to a lesser degree with increasing Φ. It is suggested that this flattening of the velocity profiles for large values of the Hartmann number tends to depress the temperature bulge by distributing the Joule dissipation more evenly over the channel.

Obviously, the physical explanation given above is not the complete story; the effects of viscous dissipation and heat transfer to the wall certainly play an important role in the behavior of the temperature profiles. It is felt, however, that the dissipation of energy in Joule heating is the most important mechanism affecting the temperature distribution in the channel.

Another interesting feature of the results is the slight bulge in the velocity profiles that occurs at the large values of Ha and Φ. This behavior is no doubt due to the fluid density variation across the channel. Table II shows that the pressure change across the channel is very small so that the density is very nearly inversely proportional to the temperature. Thus regions of high temperature correspond to regions of low fluid density. Now the $\vec{J} \times \vec{B}$ body force is a volumetric force and therefore strongly affects the

fluid in regions of low density. It is concluded then that the bulge in the velocity profiles is caused by the density variation across the channel coupled with the electromagnetic body force. The fact that the velocity and temperature profiles do not peak at the same location is due to the growing influence of the viscous forces as the wall is approached.

The above argument can be strengthened somewhat by appealing again to the equations. Consider the differential equation and initial conditions for the dimensionless velocity function $f(\theta)$.

$$\frac{d^2f}{d\theta^2} = \frac{8}{3}\gamma M^2 \frac{f^3}{g} + Re\,\frac{f^2}{g} - (Ha)^2(\Phi - f) \tag{105}$$

$$f(0) = 1 \quad , \quad f'(0) = 0 \quad , \quad g(0) = 1$$

Then at $\theta = 0$

$$f''(0) = \frac{8}{3}\gamma M^2 + Re - (Ha)^2(\Phi - 1) \tag{106}$$

For the moment assume that the temperature function $g(\theta)$ either remains constant or decreases with θ. In this case if the parameters Ha, Φ, Re and M are so chosen that

$$f''(0) > 0$$

i.e. if

$$\frac{8}{3}\gamma M^2 + Re > (Ha)^2(\Phi - 1) \tag{107}$$

then the function $f(\theta)$ has a local minimum at $\theta = 0$. Then as θ increases from zero, f increases and all terms on the right side of Eq. (105) become more positive, the last term becoming less negative. Thus, in this case, the velocity function $f(\theta)$ increases monotonically with θ, growing without

limit, and no meaningful solution can be obtained. Then if $f''(0) > 0$ meaningful solutions can be obtained only if the temperature function $g(\theta)$ initially increases with θ and increases faster than f^2. Thus in order to have a bulge in the velocity profile there must also be a bulge in the temperature profile. This conclusion supports the argument given previously.

Fig. 15 shows the velocity gradient at the wall plotted against Φ for the three values of Ha used in this study and reflects the flattening of the velocity profiles with increasing Ha and Φ. This flattening of the velocity profile and the corresponding flattening of the temperature profile would be a desirable characteristic for wind tunnel accelerators. For aerodynamic testing purposes it is mandatory that the flow approaching the model be quite uniform.

In the present investigation the flattening of the profiles is due not only to the increasing ratio of magnetic forces to viscous forces as represented by the Hartmann number but also to the corresponding change in the ratio of inertia forces to viscous forces as represented by the Reynolds number. As has been discussed it is not possible to assess the influence of each of these effects separately. It is reasonable to suppose, however, that with larger values of the Hartmann number than used in this study both the velocity and temperature profiles would become more uniform.

Finally a comment is in order on the magnitudes of the values of Ha and Re. In the formulation of this problem these parameters were defined based on r_o, the radial distance to the channel entrance, i.e.

$$Ha = \left(\frac{\sigma}{\mu}\right)^{\frac{1}{2}} B_o r_o$$

$$Re = \frac{\rho_o U_o r_o}{\mu}$$

A more conventional procedure would be to define these quantities based on the channel height at r_o, say d_o, i.e.

$$Ha^* = \left(\frac{\sigma}{\mu}\right)^{\frac{1}{2}} B_o d_o$$

$$Re^* = \frac{\rho_o U_o d_o}{\mu}$$

These are not convenient definitions for this problem. For small values of the divergence angle α

$$d_o \approx 2\alpha r_o$$

so that

$$Ha^* = 2\alpha Ha$$

$$Re^* = 2\alpha Re$$

Then for $\alpha = 1.5° = .02618$ radians

$$Ha^* = .05236\ Ha$$

$$Re^* = .05236\ Re$$

Thus the values of the Hartmann number and Reynolds number based on the initial channel height are much smaller than the values based on the radius to the channel entrance. For small values of Re^*, one must check the validity of a continuum analysis in terms of the Knudsen number

$$\frac{\lambda}{d_o} \sim \frac{M}{Re^*}$$

In particular for $Ha = 100$ and $\Phi = 1.2$, the maximum value of M and minimum value of Re^* used in this investigation give a Knudsen number of 0.11. This value suggests that under these conditions, the continuum analysis is perhaps being pushed to the limit of validity.

VI
VARIABLE PROPERTIES

6.1 FORMULATION OF THE EQUATIONS

It was shown in Section III that, as a consequence of the separation of variables technique employed in this study, the electrical conductivity σ, the viscosity μ, and the thermal conductivity κ cannot vary down the channel. Equations have been formulated and solved assuming that these transport properties are constant throughout the flow field. Such an assumption is not realistic since the values of these properties are strongly dependent on the local temperature. The results of the investigation for constant properties indicate, however, that the temperature variation across the channel is much more pronounced than the temperature variation down the channel, i.e. $|\partial T/\partial \theta| >> |\partial T/\partial r|$. It was felt, then, that useful information about the effect of the variation of the transport properties on the velocity and temperature profiles could be obtained by allowing these properties to vary as a function of temperature across the channel while ignoring their variation down the channel.

It should be pointed out that although generally $|\partial T/\partial \theta| >> |\partial T/\partial r|$, the total temperature change between the entrance and the exit of the channel may be quite large. For example, if L is the channel length and d_o is the channel height at the entrance, then the ratio of centerline temperature at exit to the centerline temperature at entrance is

$$\frac{T_e}{T_o} = \left(\frac{r_e}{r_o}\right)^2 = \left(\frac{r_o + d_o L/d_o}{r_o}\right)^2 \tag{108}$$

and since $d_o \approx 2\alpha r_o$

$$\frac{T_e}{T_o} = \left(1 + 2\alpha \frac{L}{d_o}\right)^2 \tag{109}$$

Then for $\alpha = 1^\circ = .01745$ radians and $L/d_o = 10$,

$$\frac{T_e}{T_o} = 1.82$$

a temperature change that could not be neglected in evaluating the transport properties. Thus the equations that will be developed in this section should perhaps be considered valid only for a short section of the channel $\Delta r < d_o$.

The governing differential equations will first be formulated taking into account only the variation of the electrical conductivity. Assume a σ - T relation of the form

$$\frac{\sigma}{\sigma_c} = \left(\frac{T}{T_c}\right)^{\omega} \tag{110}$$

where σ_c and T_c are reference values of the conductivity and temperature, say values along the channel centerline. σ_c is assumed to be constant. Introducing Eq. (110) into Eqs. (34) and (36) and non-dimensionalizing yields

$$\frac{d^2f}{d\theta^2} = \frac{8}{3}\gamma M^2 \frac{f^3}{g} + Re\,\frac{f^2}{g} - (Ha)^2 g^{\omega}(\Phi - f) \tag{111}$$

$$\frac{d^2g}{d\theta^2} + 4g = 2PrRef - (\gamma - 1)M^2Pr(Ha)^2g^{\omega}(\Phi - f)^2$$

$$- (\gamma - 1)M^2Pr\left(\frac{df}{d\theta}\right)^2 + \frac{4}{3}(3\gamma + 1)M^2Prf \tag{112}$$

where now

$$Ha = \left(\frac{\sigma_c}{\mu}\right)^{\frac{1}{2}} B_o r_o$$

The initial conditions for f and g are

$$f(0) = 1, \qquad f'(0) = 0$$

$$g(0) = 1, \qquad g'(0) = 0 \tag{113}$$

Eqs. (111) and (112) together with initial conditions of Eq. (113) are amenable to solution by the same technique as used for the constant conductivity model. Figs. 44 through 49 show the divergence angle α and the ratio of wall temperature to centerline temperature $g(\alpha)$ plotted as functions of the Reynolds number and Mach number for $\omega = 3/2$ and $(Ha, \Phi) = (100, 1.6), (150, 1.2), (150, 1.6)$.

Equations will next be formulated including the cross channel variations of viscosity and thermal conductivity according to a square root law, i.e.

$$\frac{\mu}{\mu_c} = \frac{\kappa}{\kappa_c} = \left[\frac{\bar{T}(\theta)}{\bar{T}(0)}\right]^{\frac{1}{2}} \tag{114}$$

One additional assumption is made that

$$\frac{\partial p}{\partial \theta} = 0 \tag{115}$$

This assumption is convenient since the θ momentum equation can no longer be directly integrated and is justified by the results for the constant property model. Then introducing Eqs. (110), (114), and (115) into Eqs. (34) and (36) and non-dimensionalizing gives

$$\frac{d^2f}{d\theta^2} = Re\,\frac{f^2}{g^{3/2}} - \frac{1}{2g}\left(\frac{df}{d\theta}\right)\left(\frac{dg}{d\theta}\right) - (Ha)^2 g^{\omega-\frac{1}{2}}(\Phi - f) \tag{116}$$

$$\frac{d^2g}{d\theta^2} + 4g = 2RePr\,\frac{f}{g^{\frac{1}{2}}} - \frac{1}{2g}\left(\frac{dg}{d\theta}\right)^2$$

(Equation continued)

$$- (\gamma - 1)M^2 Pr(Ha)^2 g^{\omega-\frac{1}{2}}(\Phi - f)^2$$

$$- (\gamma - 1)M^2 Pr \left[\left(\frac{df}{d\theta}\right)^2 + \frac{4}{3} f^2 \right] \tag{117}$$

where

$$Ha = \left(\frac{\sigma_c}{\mu_c}\right)^{\frac{1}{2}} B_o r_o$$

$$Re = \frac{\rho_o U_o r_o}{\mu_c}$$

$$Pr = \frac{C_p \mu_c}{\kappa_c}$$

The initial conditions on f and g are

$$f(0) = 1, \qquad f'(0) = 0$$

$$g(0) = 1, \qquad g'(0) = 0 \tag{118}$$

Again Eqs. (116) and (117) with initial conditions of Eq. (118) can be treated by the technique described in Section IV. Figs. 50 through 55 show α and $g(\alpha)$ plotted as functions of Re and M.

6.2 DISCUSSION OF RESULTS

The results of this portion of the investigation are presented in Figs. 20 through 25. Figs. 20 through 22 show velocity and temperature profiles for $\sigma \sim T^{3/2}$, and Figs. 23 through 25 show velocity and temperature profiles for $\sigma \sim T^{3/2}$, $\mu \sim \kappa \sim T^{1/2}$. In both cases the divergence angle is approximately 1.25° and the ratio of wall temperature to centerline temperature is approximately 0.2. Figs. 17 through 19 show the corresponding velocity and temperature profiles for constant properties. Table III gives the

comparative values of the temperature and velocity gradients at the wall.

The most conspicuous feature of the results for the variable conductivity model is the accentuation of the bulges in both the velocity and temperature profiles. A comparison of Figs. 19 and 22 best illustrates this behavior.

The accentuation of the temperature bulge can be attributed to the increased Joule heating in the high temperature region. Using Ohm's law, the expression for the Joule heating can be written as

$$\frac{J^2}{\sigma} = \sigma U_o{}^2 B_o{}^2 (\Phi - f)^2 \tag{119}$$

Since $\sigma \sim T^{3/2}$ it is clear that this term will be large in regions of high temperatures.

With regard to the velocity bulge, in addition to the density change across the channel, which is more pronounced in this case, there is also an increase in the $\vec{J} \times \vec{B}$ force in the high temperature region as a result of the conductivity variation.

It is expected that for larger values of Ha and Φ, where it would be necessary to approach the limiting values of Re and M in order to maintain α constant, both the velocity and temperature profiles would become more uniform.

The main effects of the variation of viscosity and thermal conductivity are to depress the bulges in the velocity and temperature profiles and to steepen the velocity and temperature gradients at the wall. This can be seen by comparing Figs. 25 and 26.

In the region of high temperature the corresponding high value of thermal conductivity tends to promote the diffusion of heat to the adjacent low temperature regions. Near the cool wall the lower thermal conductivity opposes the transfer of heat.

The influence of the viscosity variation is analagous.

VII
SUMMARY

A solution has been obtained to the magnetogasdynamic equations of motion including the effects of compressibility, viscosity, thermal conductivity and crossed electric and magnetic fields. The solution obtained is an exact solution in the sense that no terms have been dropped from the governing equations and boundary layer approximations have not been employed.

The particular flow model considered was the two-dimensional, fully developed flow between diverging plane walls. Self-similar solutions to the governing equations were sought. It was determined that such solutions could be obtained under certain conditions; the resulting flow being an accelerating flow, the velocity increasing linearly with distance down the channel, in which the pressure and Mach number are constant along streamlines. For this special type of flow, with the assumption of constant transport properties, the partial differential equations of motion reduce to a pair of coupled, non-linear, ordinary differential equations, Eqs. (45) and (46) with boundary conditions given by Eq. (47).

It was shown that the boundary value problem defined by Eqs. (45) through (47) is generally overspecified. That is, if the divergence angle α and the ratio of wall temperature $g(\alpha)$ are considered fixed, and two of the four parameters Ha, Φ, Re and M are specified, then the remaining two parameters are uniquely determined. Thus, in a broad sense, Eqs. (45) through (47) constitute an eigenvalue problem. If the required relationship among the parameters is not satisfied then a self-similar solution to the governing equations does not exist. The technique used for the solution of this problem has been amply discussed in Section IV.

The results of the investigation were presented in the form of velocity and temperature profiles for several values of the electromagnetic parameters Ha and Φ. The values of the gas dynamic parameters, the eigenvalues, were selected so as to maintain the divergence angle and the ratio of wall temperature to centerline temperature constant. The most conspicuous feature of the results is the prominent bulge that occurs in the temperature distribution for certain values of the parameters. This behavior becomes less pronounced for large values of Ha and Φ where, incidentally, practical devices would be likely to operate.

Although it was not possible, in this study, to include the variation of the transport properties σ, μ and κ along the channel, it was shown that the effect of the variation of these properties across the channel is to accentuate the bulges in both the velocity and temperature profiles.

Finally, a few comments are in order on the significance of the present study with regard to wind tunnel accelerators. Certainly the mathematical model used in this investigation is too crude to be utilized for detailed design of a practical accelerator. Nonetheless there are certain qualitative features of the results, such as the bulge in the temperature profiles, which are likely to be encountered in a practical device. Also there are several characteristics of the flow situation considered in this study which might be desirable for wind tunnel accelerators. For example, although a large portion of the energy added to the plasma is dissipated in Joule heating thereby increasing the enthalpy of the gas, this enthalpy would be recoverable as directed kinetic energy in the post accelerator nozzle. In particular this expansion should pose no difficulty since no pressure drop occurs in the accelerator itself. Furthermore, despite the fact that the flow is considered fully viscous, for large values of Ha and Φ a rather well defined core region does exist where the velocity and temperature profiles are relatively flat.

From these considerations, it would appear desirable to extend the present investigation, using a more realistic model. One might, for example, relax the constraint of separation of variables technique employed here. This technique, despite its undeniable virtue of simplifying the problem, imposes rather severe restrictions on the solution obtained. Then, rather than assuming a particular form for the solution as was done in Section III, one would specify initial conditions at the channel entrance r_o. This procedure would require solution of a pair of coupled, nonlinear, partial differential equations with boundary conditions, a very difficult but not impossible task. It is likely that some of the well known techniques developed in boundary layer theory could be extended to this type of channel flow problem. Such a solution would give detailed information for a realistic MHD channel flow to a degree not presently available in the open literature.

VIII
REFERENCES

1. Ring, Leon E. "General Considerations of MHD Acceleration for Aerodynamic Testing." AEDC-TDR-64-256 (AD 453419), December 1964.

2. Williams, J. C. "Viscous Compressible and Incompressible Flow in Slender Channels." AIAA J. 1:186-195, 1963.

3. Resler E. L., Jr. and W. R. Sears. "The Prospects for Magneto-Aerodynamics." J. Aero. Sci. 25: 235-245, 1958.

4. Resler E. L., Jr. and W. R. Sears. "Magnetogasdynamic Channel Flow." ZAMP 96:509-518, 1958.

5. Matthews, C. W. "Theoretical Analysis of Several Linear Steady-Flow Plasma Accelerators with Crossed Electric and Magnetic Fields." NASA TR R212, 1964.

6. Drake, J. H. "Optimum Isothermal Acceleration of a Plasma with Constant Magnetic Field." AIAA J. 1:2053-2057, 1963.

7. Krupka, R. M. and S. P. Kezios. "The Performance of a Crossed Field Magneto-Aerodynamic Accelerator." J. App. Mech. 31:409-418, 1964.

8. Hains, F. D. "The Magnetogasdynamic Source." Flight Sciences Laboratory Report No. 58. Boeing Scientific Research Laboratories, 1962.

9. Podolsky, B. and G. Borman. "The Electromagnetic Acceleration of a Continuously Flowing Plasma." Fourth Lockheed Symposium on Magnetohydrodynamics, S. W. Kash (editor), Stanford University Press, 1960.

10. Sherman, A. "Theoretical Performance of a Crossed Field MHD Accelerator." ARS J. 32:414-420, 1962.

11. Hartmann, J. "Theory of Laminar Flow of an Electrically Conducting Liquid in a Homogeneous Magnetic Field." Kgl. Danoke Videnskabernes Selskab, Math.-Fys. Med, 15(6), 1937.

12. Sutton, G. W. and A. Sherman. Engineering Magnetohydrodynamics. McGraw Hill Book Company, New York, 1965.

13. Axford, W. I. "The Magnetohydrodynamic Jeffrey-Hamel Problem for a Weakly Conducting Fluid." Quart. J. Mech. and Applied Math. 14:335-351, 1961.

14. Vatazhin, A. B. "On the Flow in a Diffusor in the Presence of a Magnetic Field." PMM 24:524-529, 1960.

15. Heywood, J. B. "An MHD Channel Flow with Temperature Dependent Electrical Conductivity." AIAA J. 3:1752-1754, 1965.

16. Blevins, Z. O. "Magnetogasdynamics of Hypersonic Couette Flow." J. Aero-Space Sci. 25:601-615, 1958.

17. Martin, E. D. "A Study of Laminar Compressible Viscous Pipe Flow Accelerated by an Axial Body Force, with Application to Magnetogasdynamics." National Aeronautics and Space Administration Technical Note D-855, 1961.

18. Hale, F. J. and Kerrebrock, J. L. "Insulator Boundary Layers in Magnetohydrodynamic Channels." AIAA J. 2:461-469, 1964.

19. Sonnerup, B. O. U. "Theory of Viscous Magnetogasdynamic Flow in Slowly Diverging Two-Dimensional Channels." AFOSR 1332, Armed Services Technical Information Agency, Arlington, Virginia, 1961.

20. Adams, J. C., Jr. "Similar Solutions for Viscous Compressible Laminar Flow in Slender Axisymmetric Channels." Ph.D. Dissertation, North Carolina State University at Raleigh, 1966.

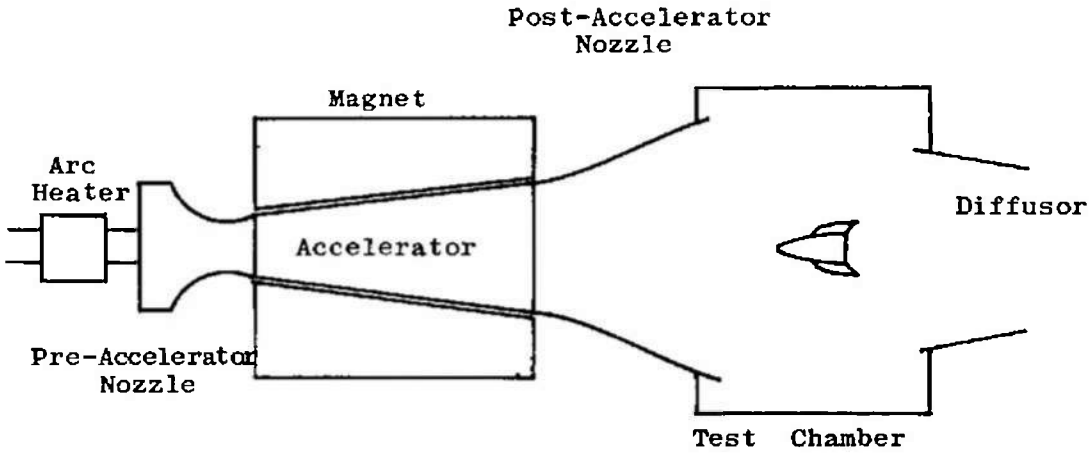

Fig. 1 MHD Powered Wind Tunnel

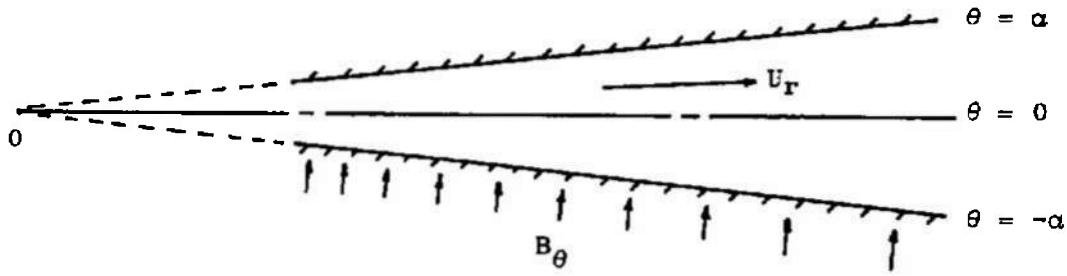

Fig. 2 Channel Configuration

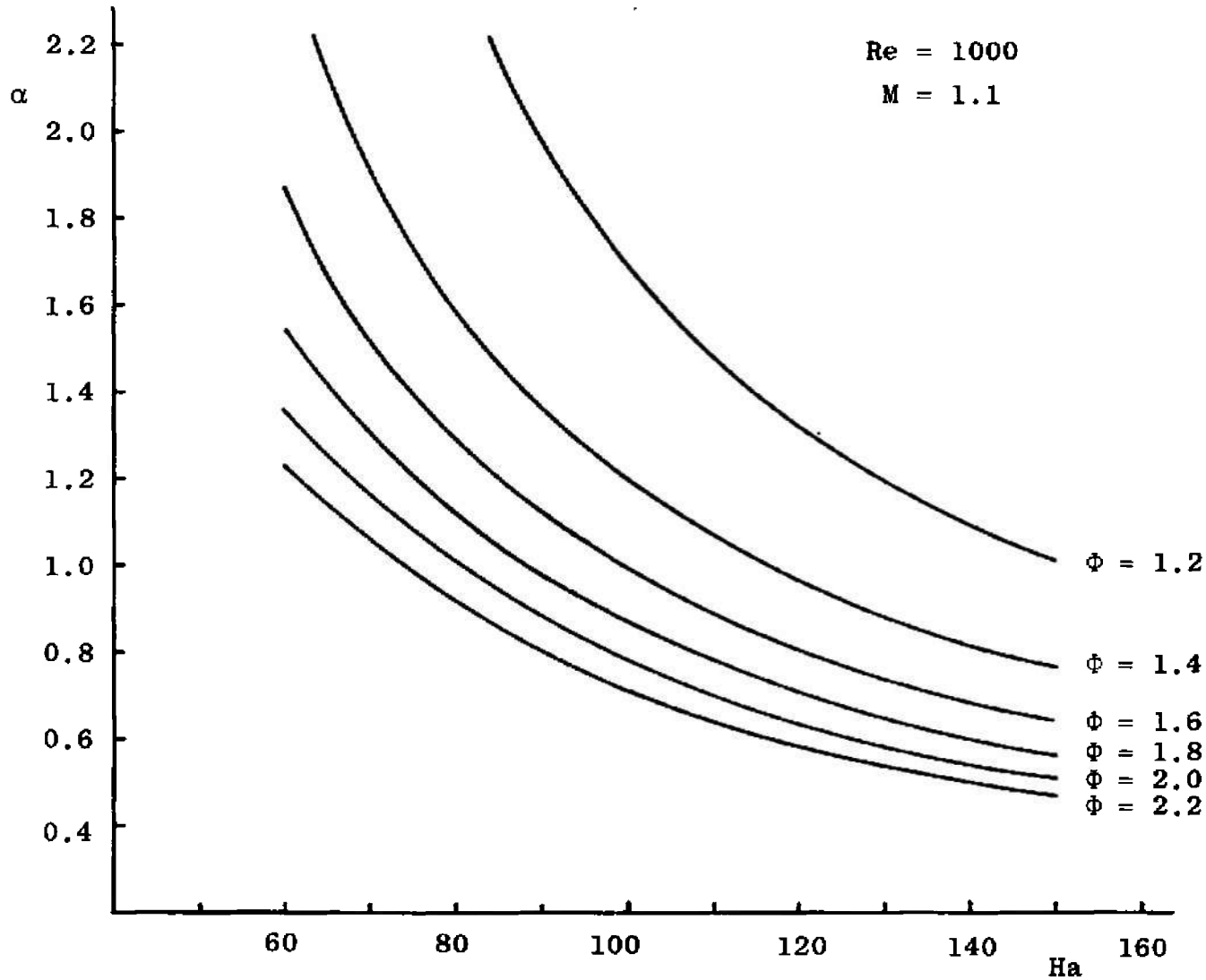

Fig. 3 Relationship Among Parameters α, Ha and Φ

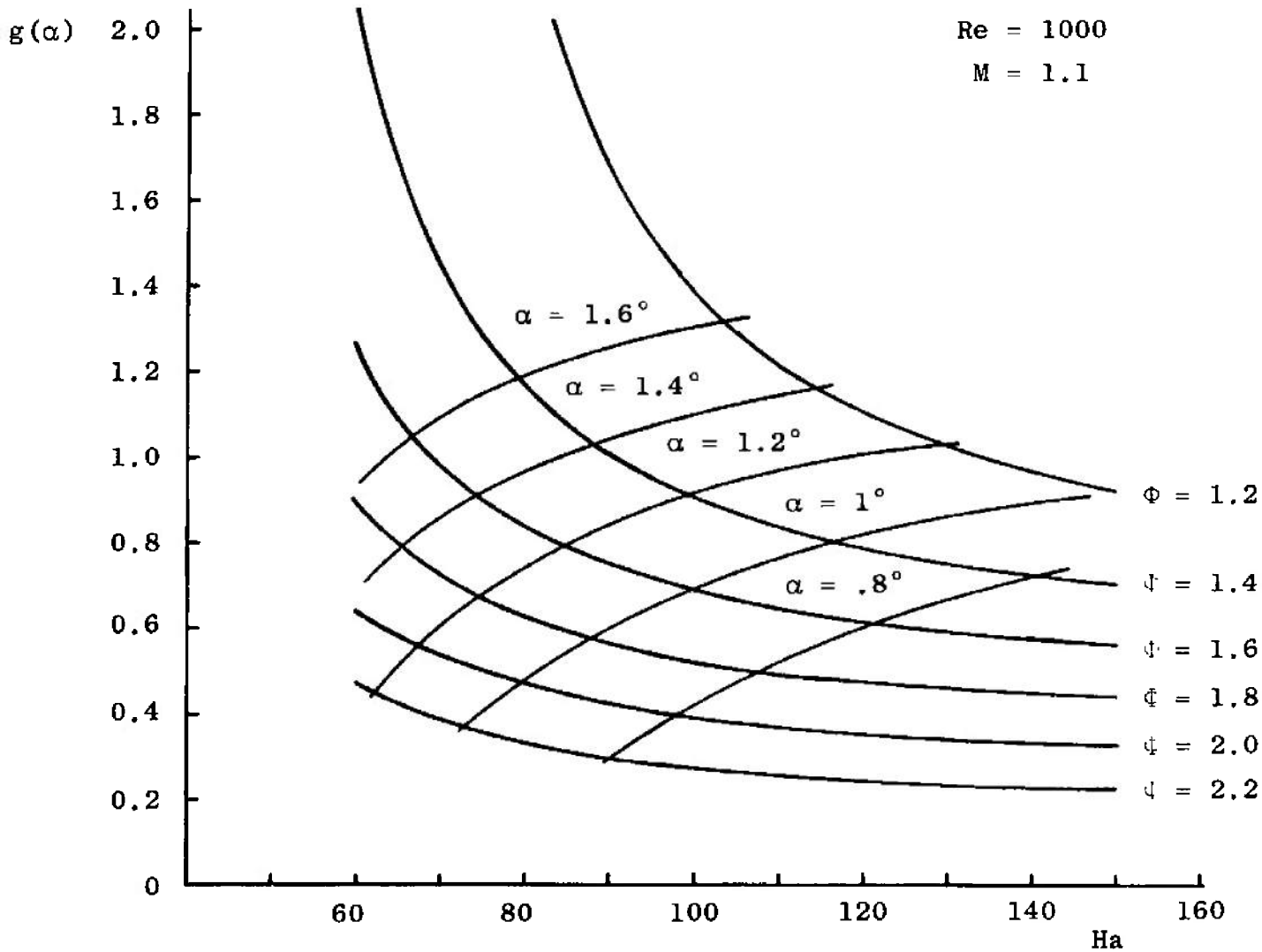

Fig. 4 Relationship Among Parameters g(α), Ha, Φ, and α

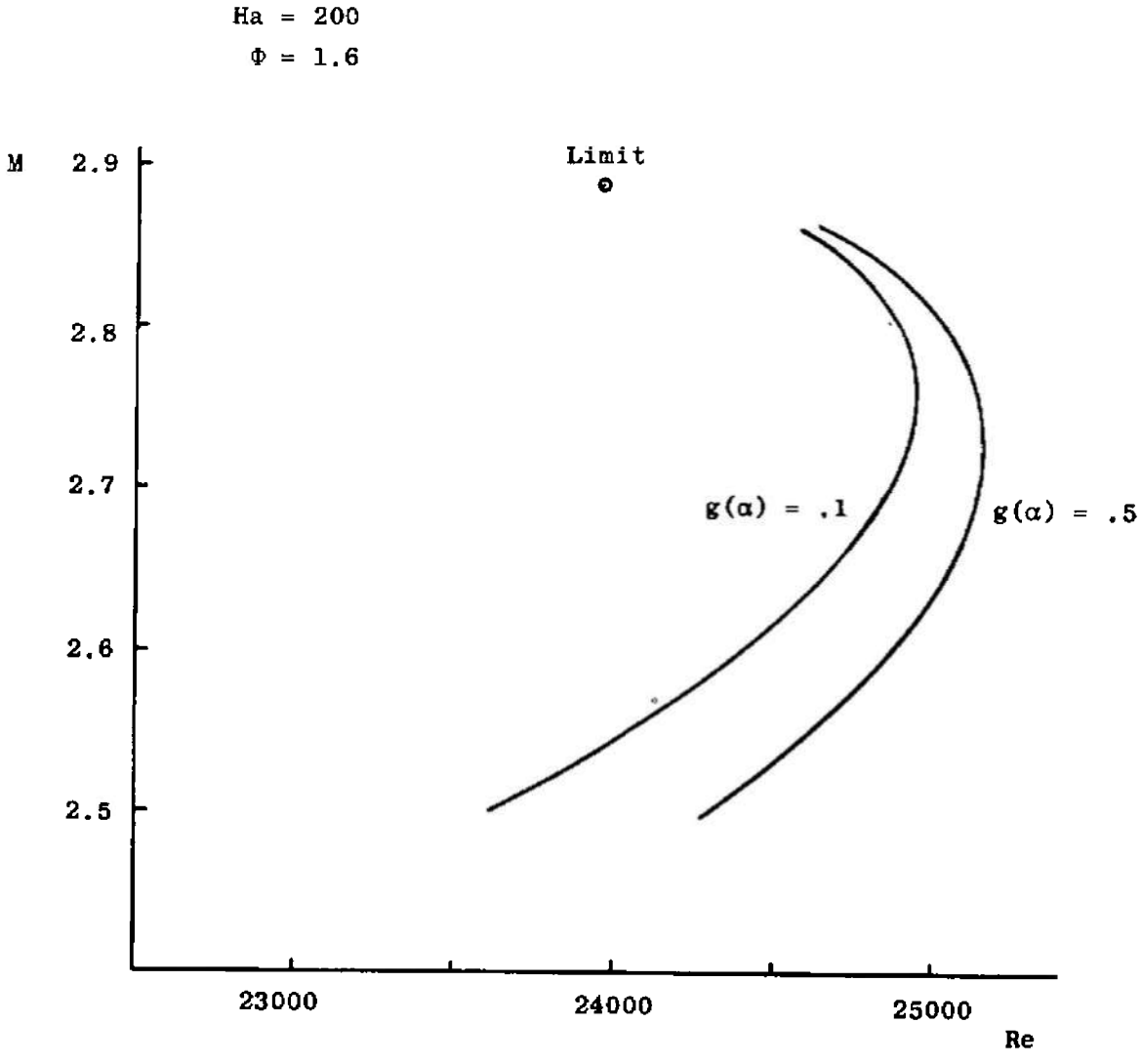

Fig. 5 Region of Acceptable Solutions for Ha = 200, Φ = 1.6

Ha = 100 α = 1.503°

Φ = 1.2 g(α) = .200

M = 1.87

Re = 350

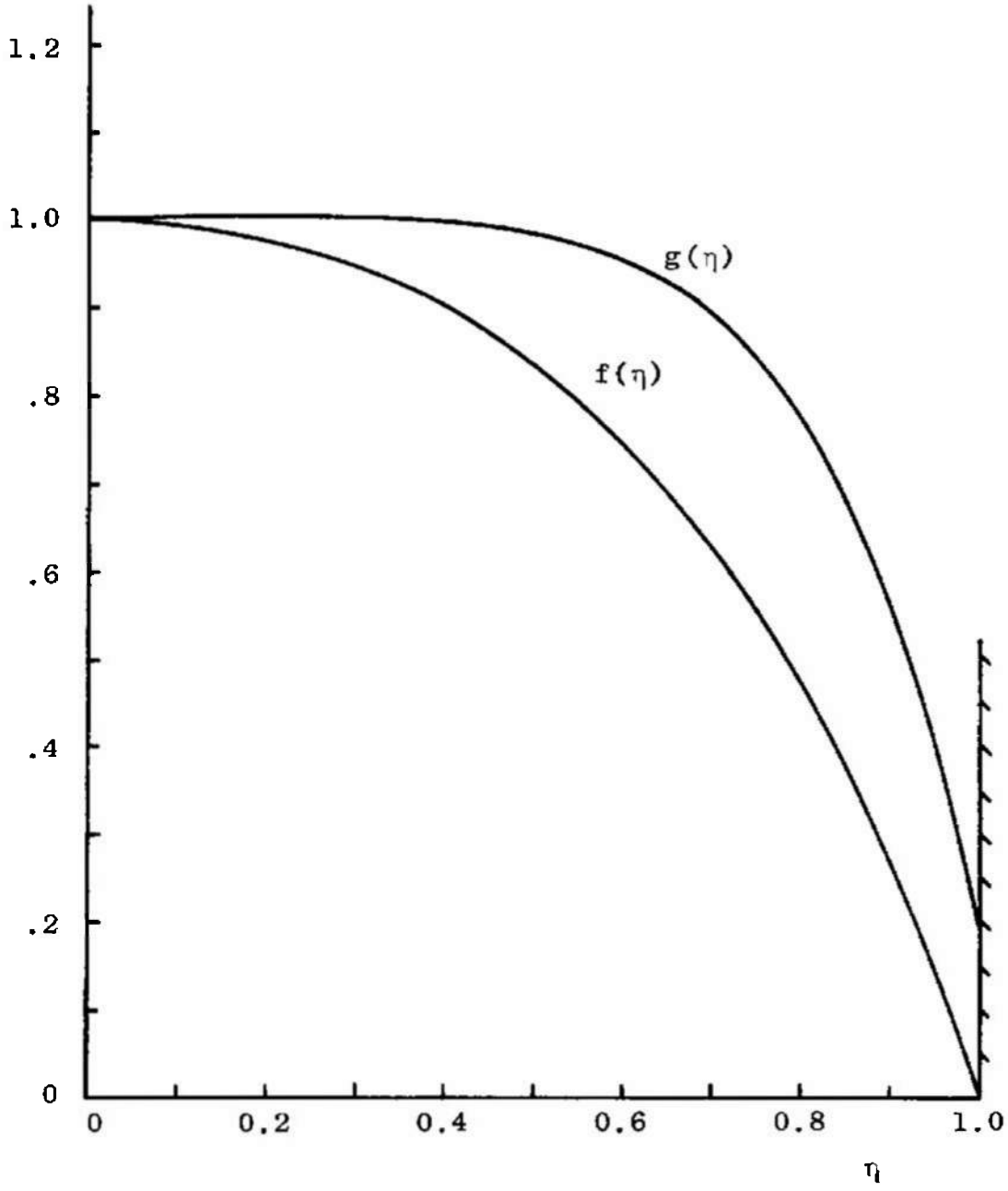

Fig. 6 Velocity and Temperature Profiles for Ha = 100, Φ = 1.2

Ha = 100 α = 1.503°
Φ = 1.6 g(α) = .209
M = 2.24
Re = 5150

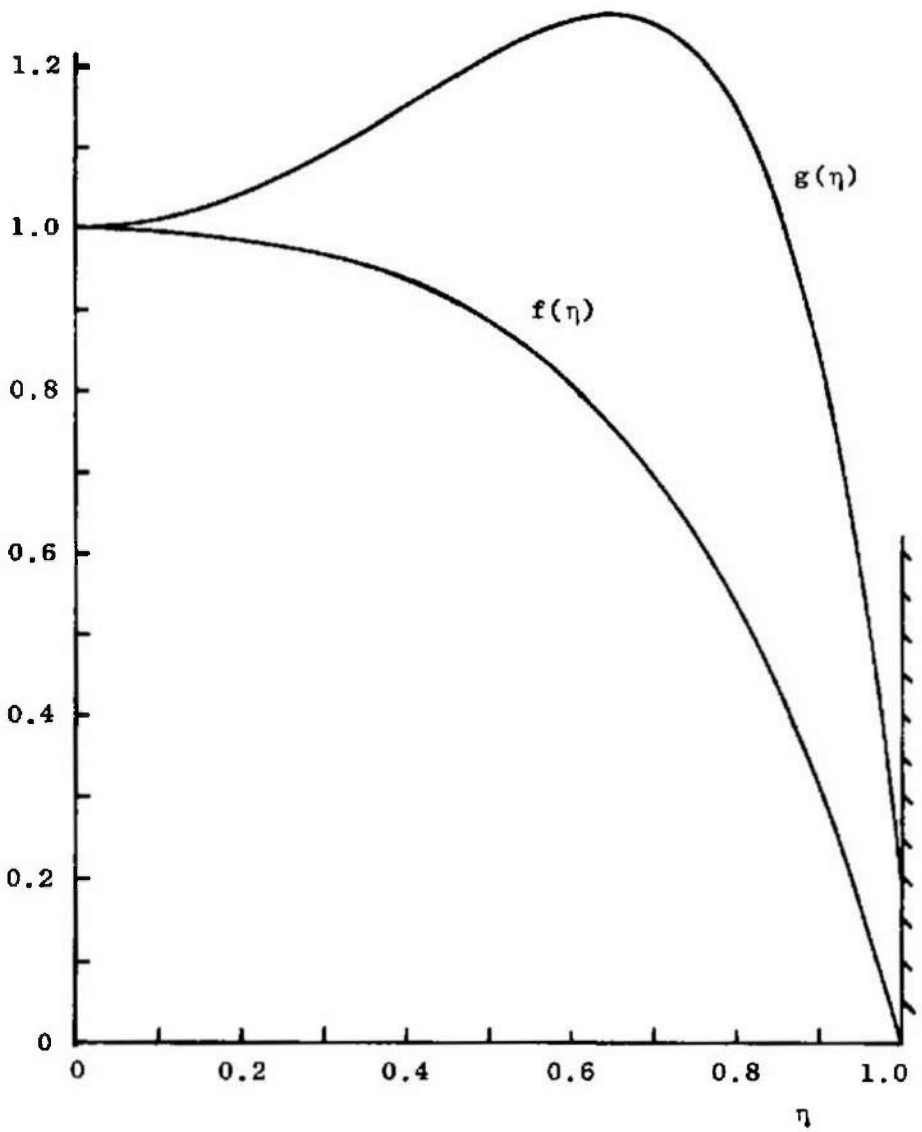

Fig. 7 Velocity and Temperature Profiles for Ha = 100, Φ = 1.6

Ha = 100 α = 1.502°
Φ = 2.0 g(α) = .202
M = 2.02
Re = 9700

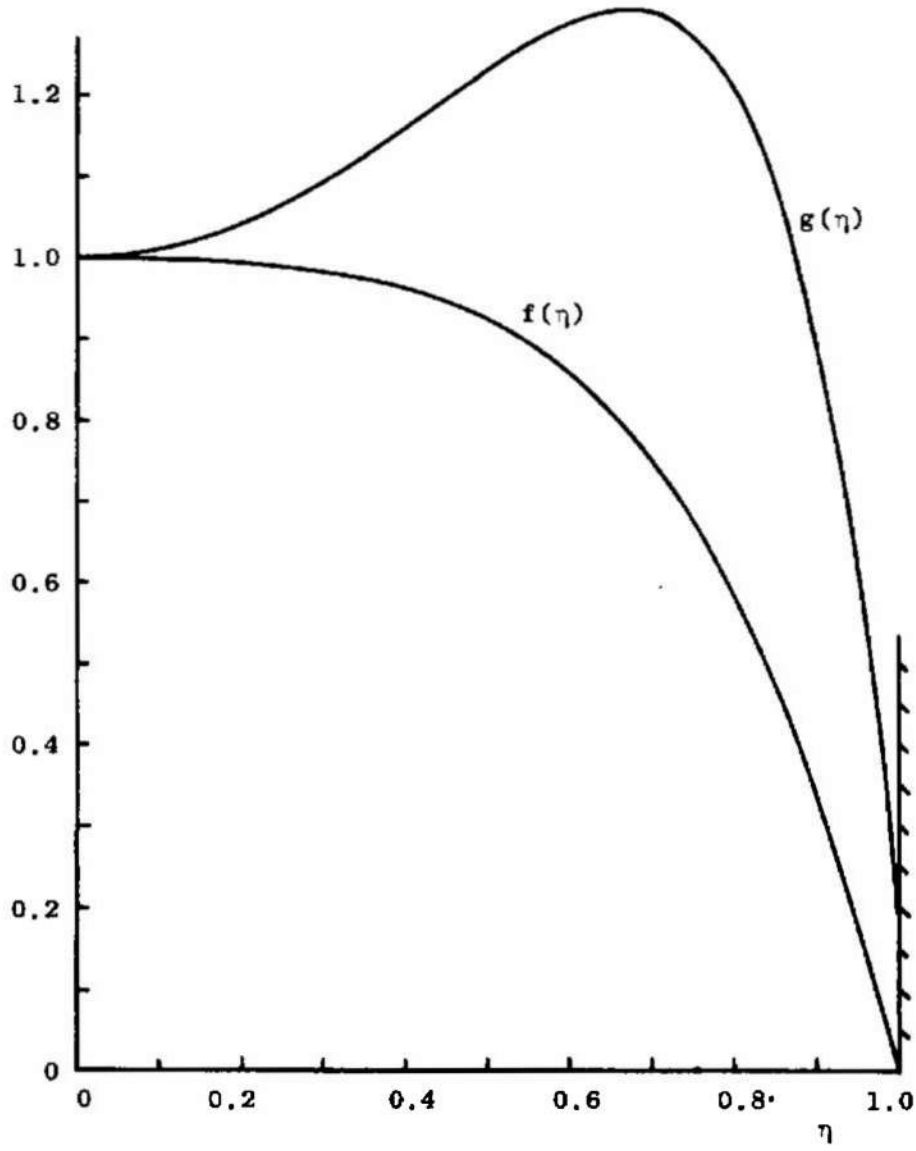

Fig. 8 Velocity and Temperature Profiles for Ha = 100, Φ = 2.0

Ha = 150 α = 1.500°
Φ = 1.2 g(α) = .207
M = 3.0
Re = 4100

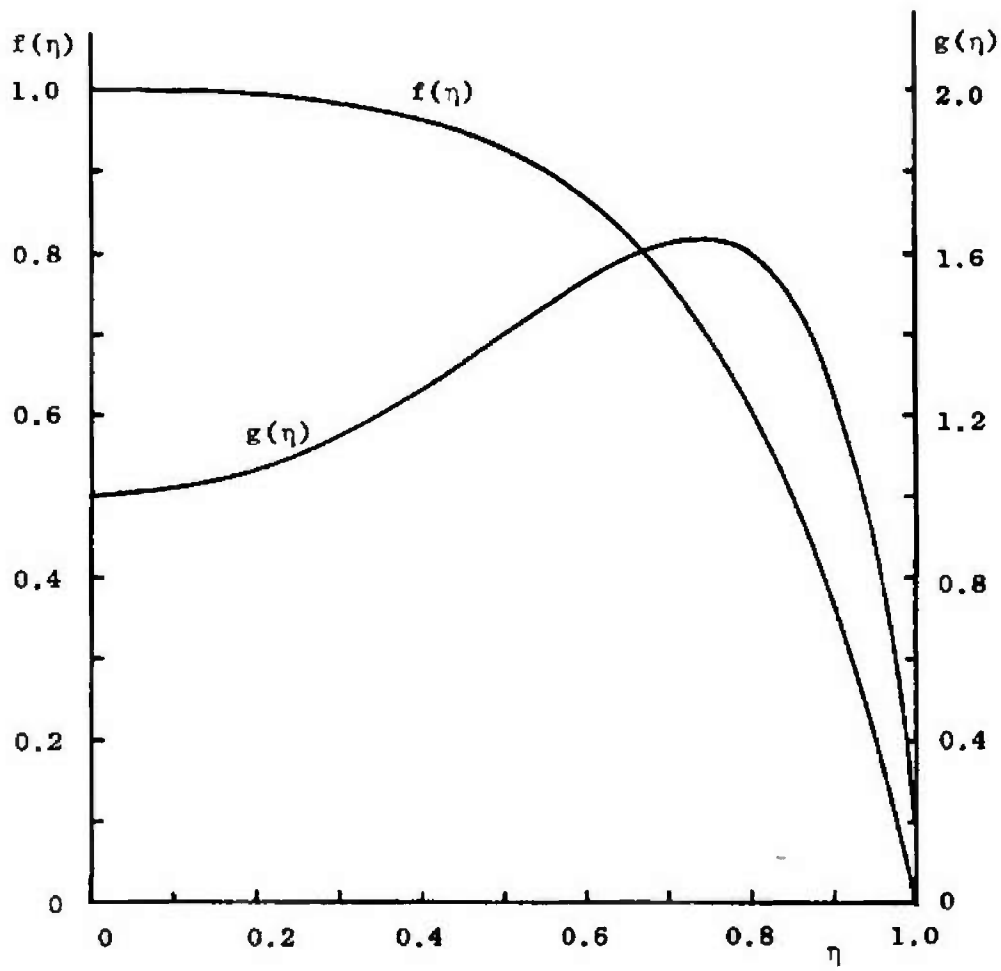

Fig. 9 Velocity and Temperature Profiles for Ha = 150, Φ = 1.2

Ha = 150 α = 1.502°
Φ = 1.6 g(α) = .202
M = 2.704
Re = 14010

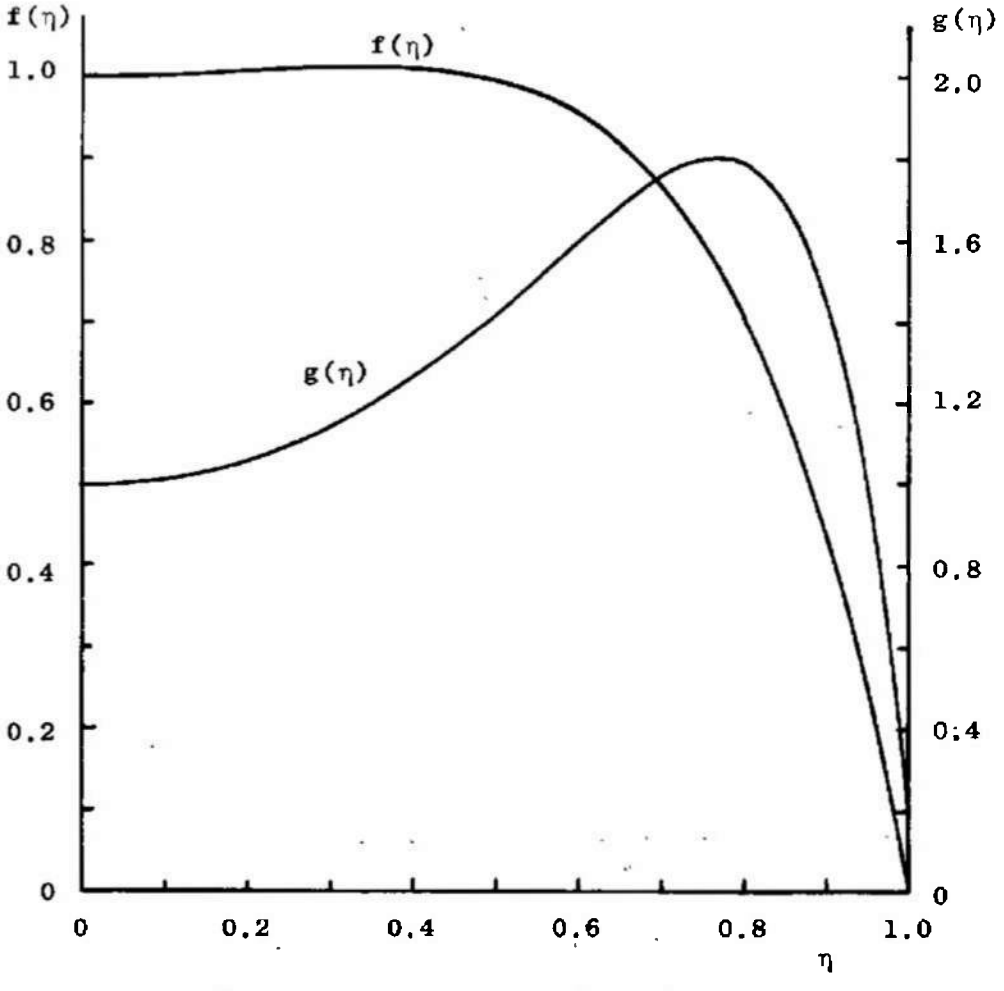

Fig. 10 Velocity and Temperature Profiles for Ha = 150, Φ = 1.6

Ha = 150 α = 1.500°
Φ = 2.0 g(α) = .202
M = 2.209
Re = 23045

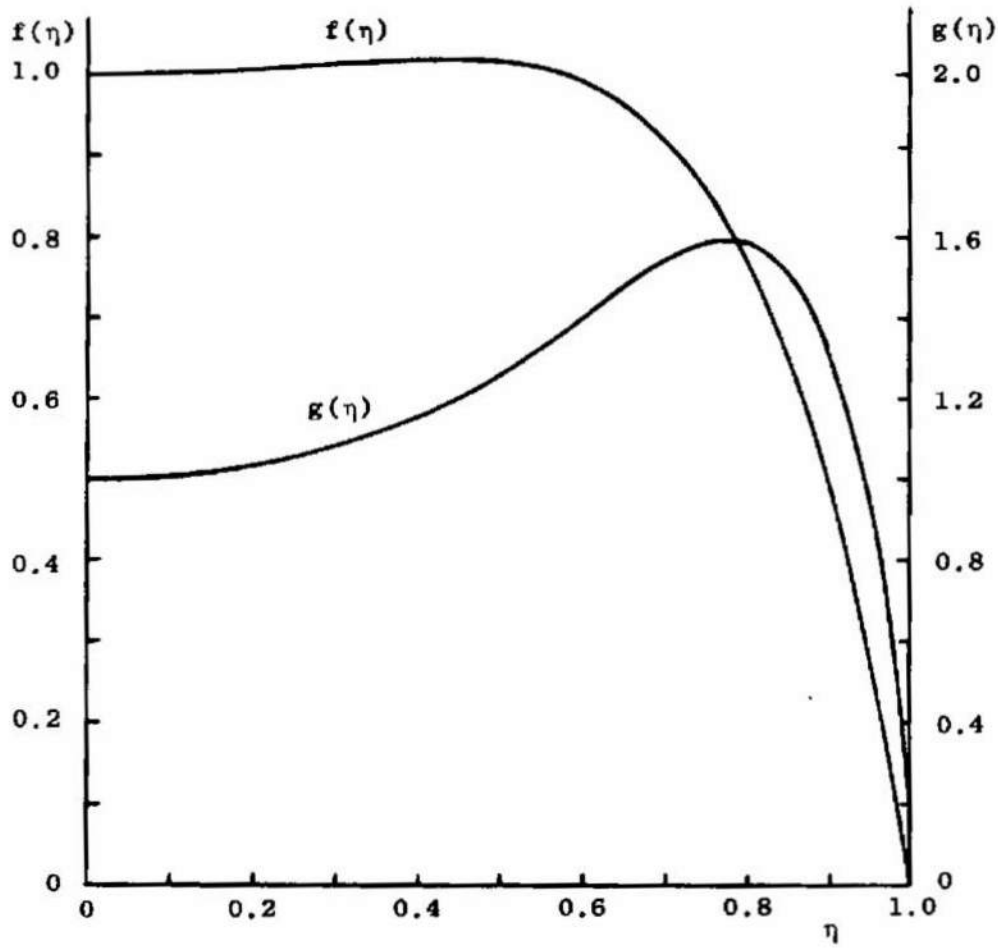

Fig. 11 Velocity and Temperature Profiles for Ha = 150, Φ = 2.0

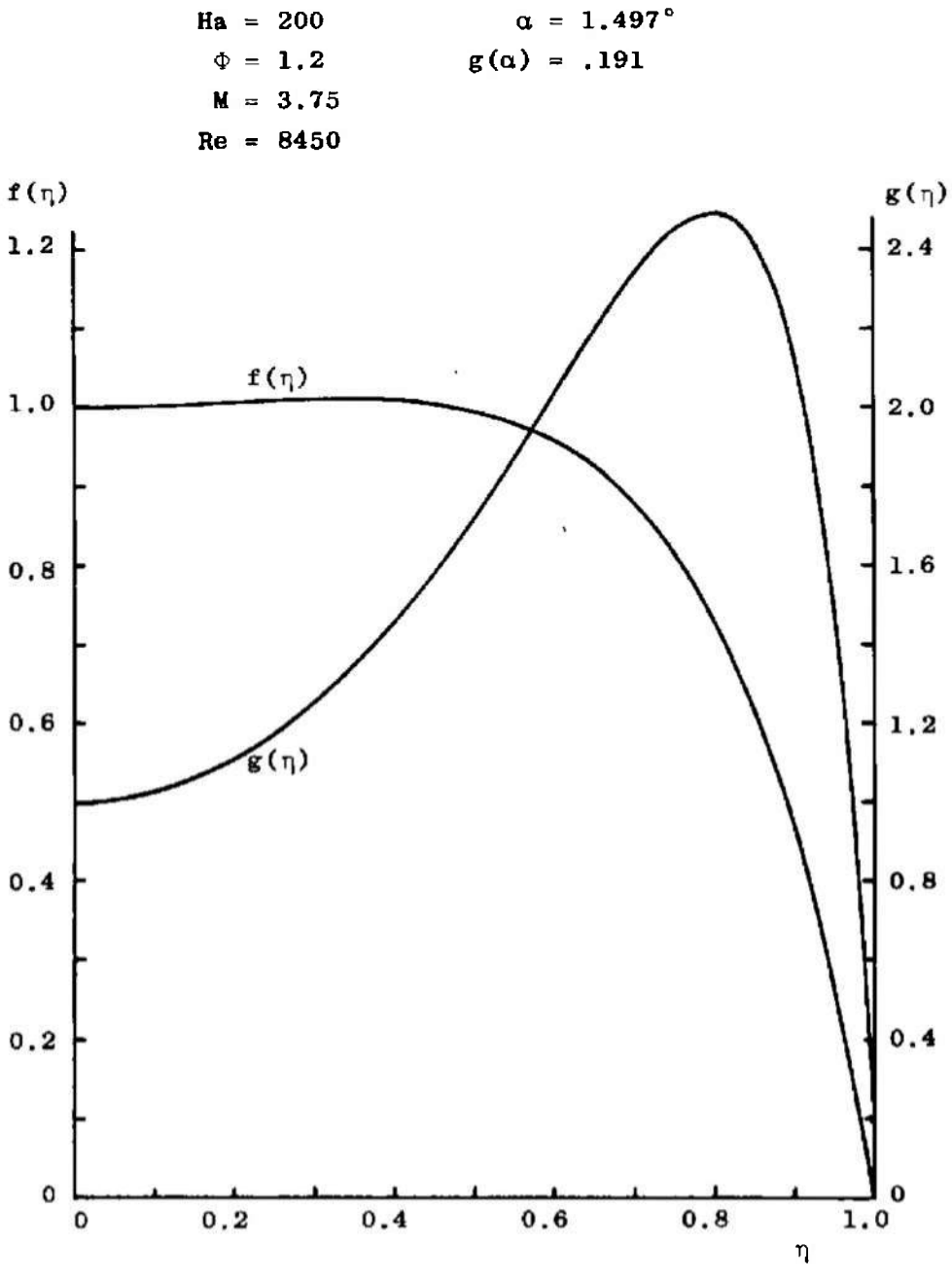

Fig. 12 Velocity and Temperature Profiles for Ha = 200, Φ = 1.2

Ha = 200 α = 1.501°
Φ = 1.6 g(α) = .190
M = 2.86
Re = 24600

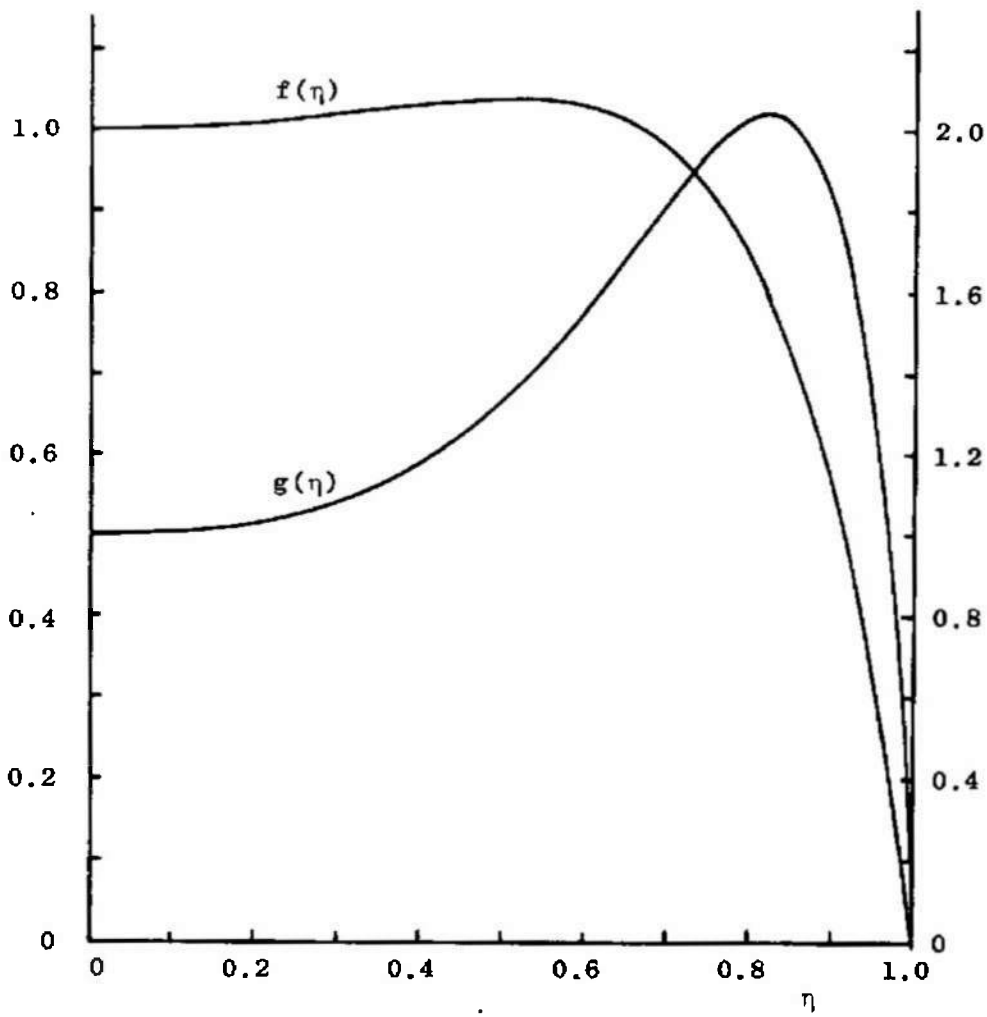

Fig. 13 Velocity and Temperature Profiles for Ha = 200, Φ = 1.6

Ha = 200 α = 1.504°
Φ = 2.0 g(α) = .202
M = 2.2376
Re = 40250

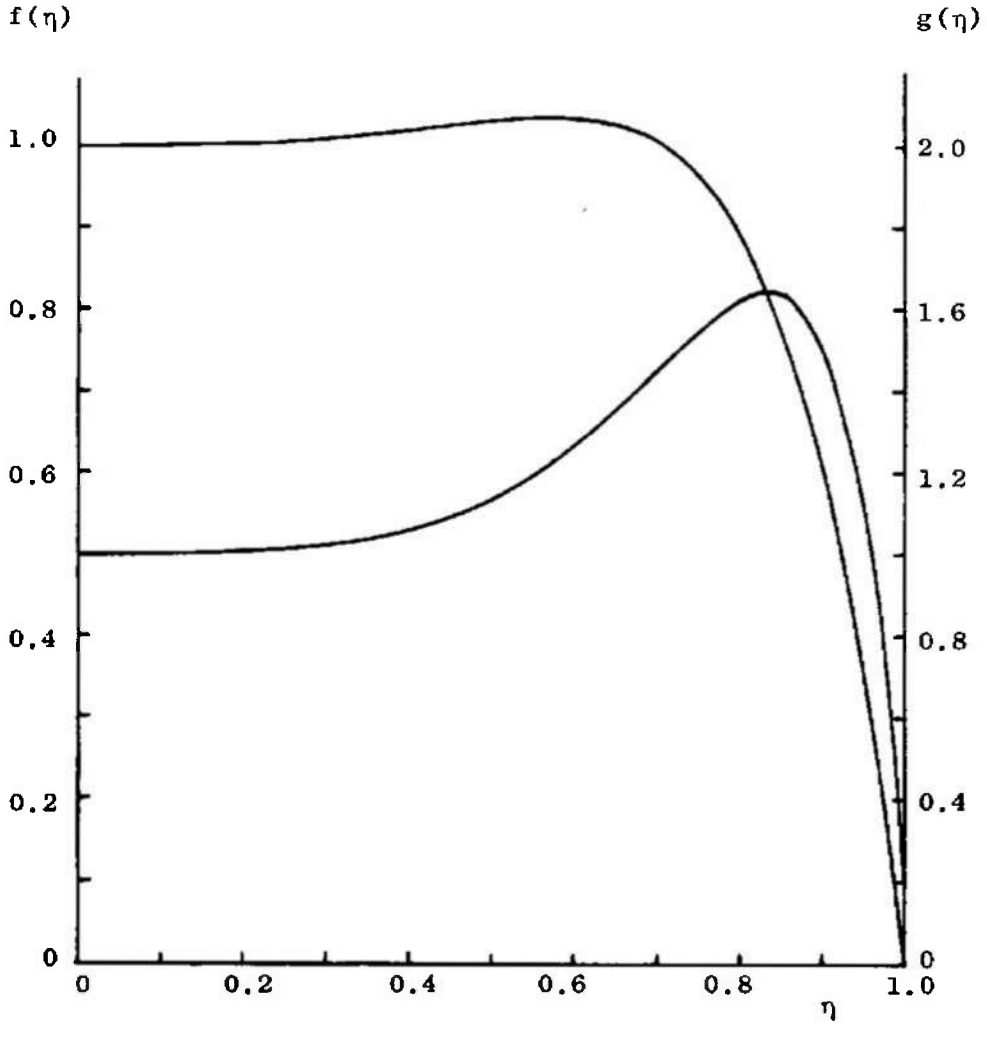

Fig. 14 Velocity and Temperature Profiles for Ha = 200, Φ = 2.0

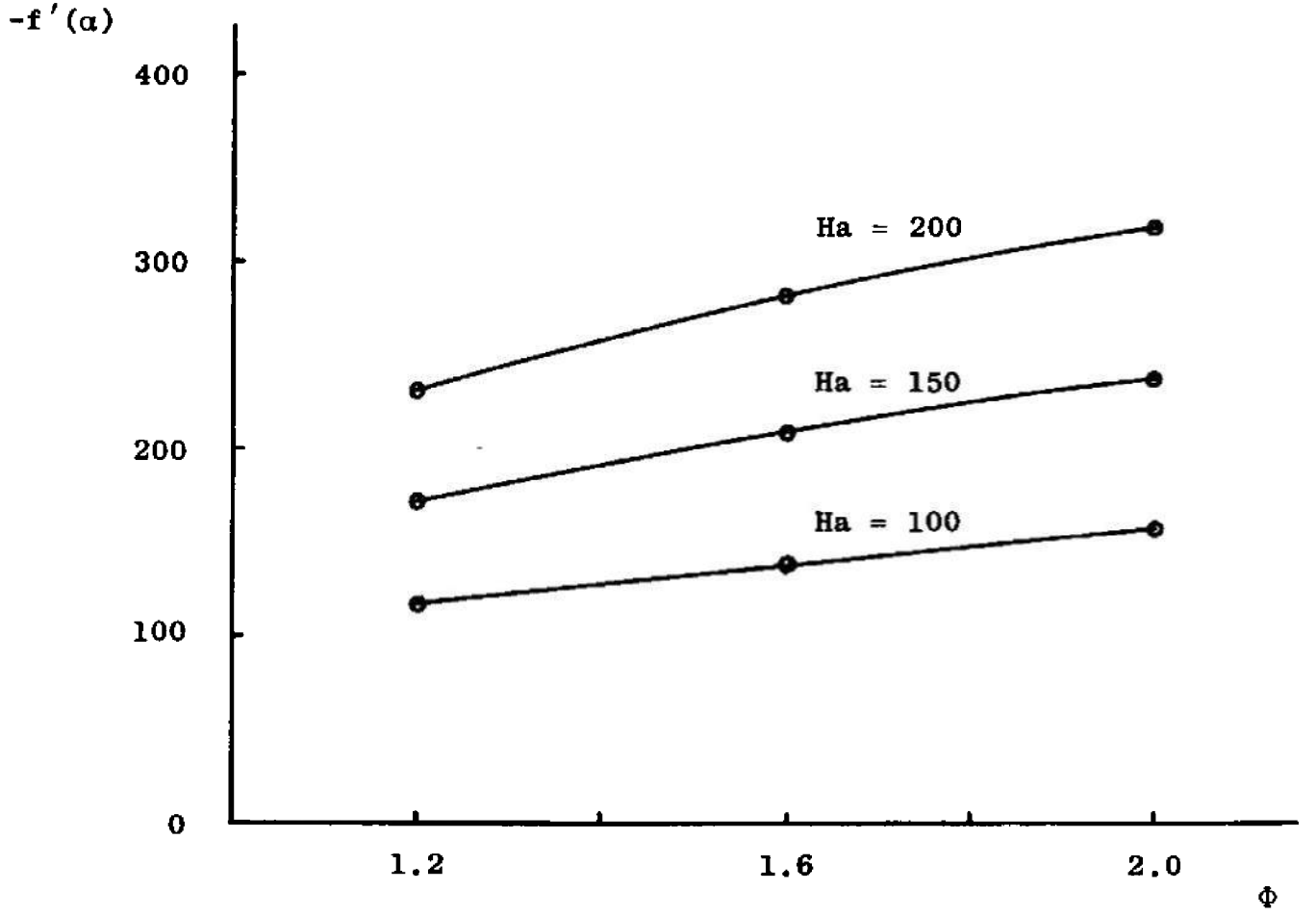

Fig. 15 Variation of the Velocity Gradient at the Wall for $\alpha = 1.5°$, $g(\alpha) = 2.0$

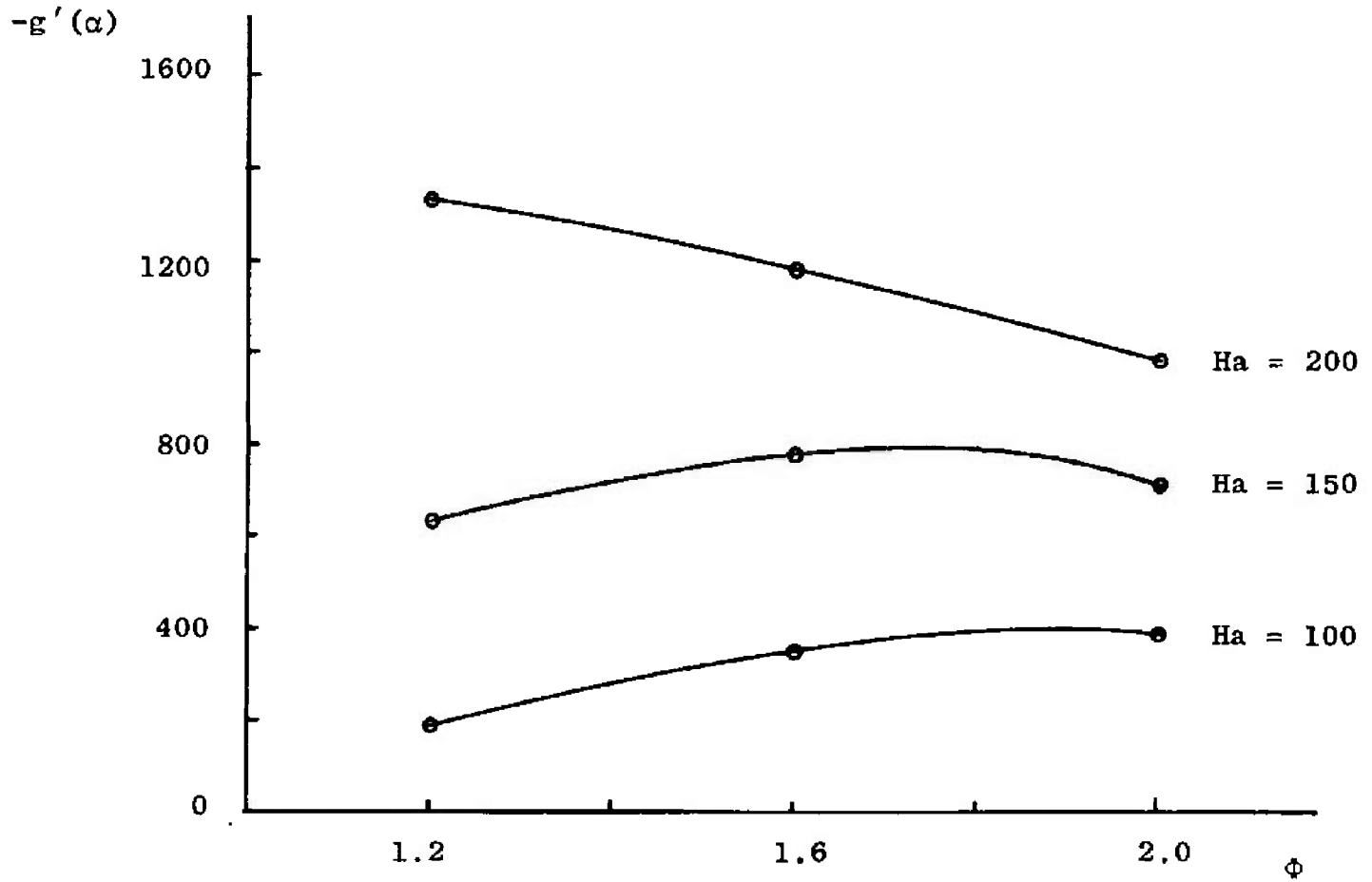

Fig. 16 Variation of the Temperature Gradient at the Wall for $\alpha = 1.5°$, $g(\alpha) = 0.2$

Ha = 100 α = 1.252°
Φ = 1.6 g(α) = .206
M = 1.95
Re = 3800

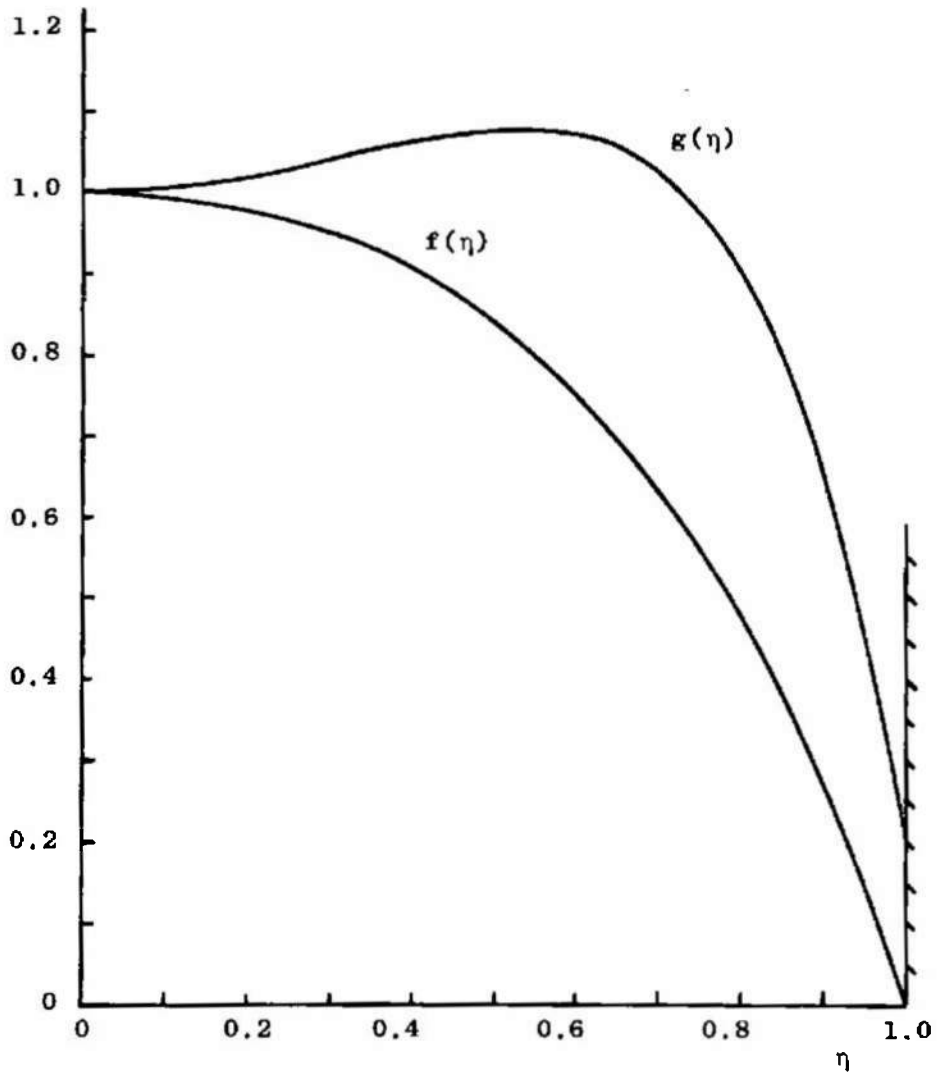

Fig. 17 Velocity and Temperature Profiles for Ha = 100, Φ = 1.6

Ha = 150 α = 1.250°
Φ = 1.2 g(α) = .197
M = 2.515
Re = 3075

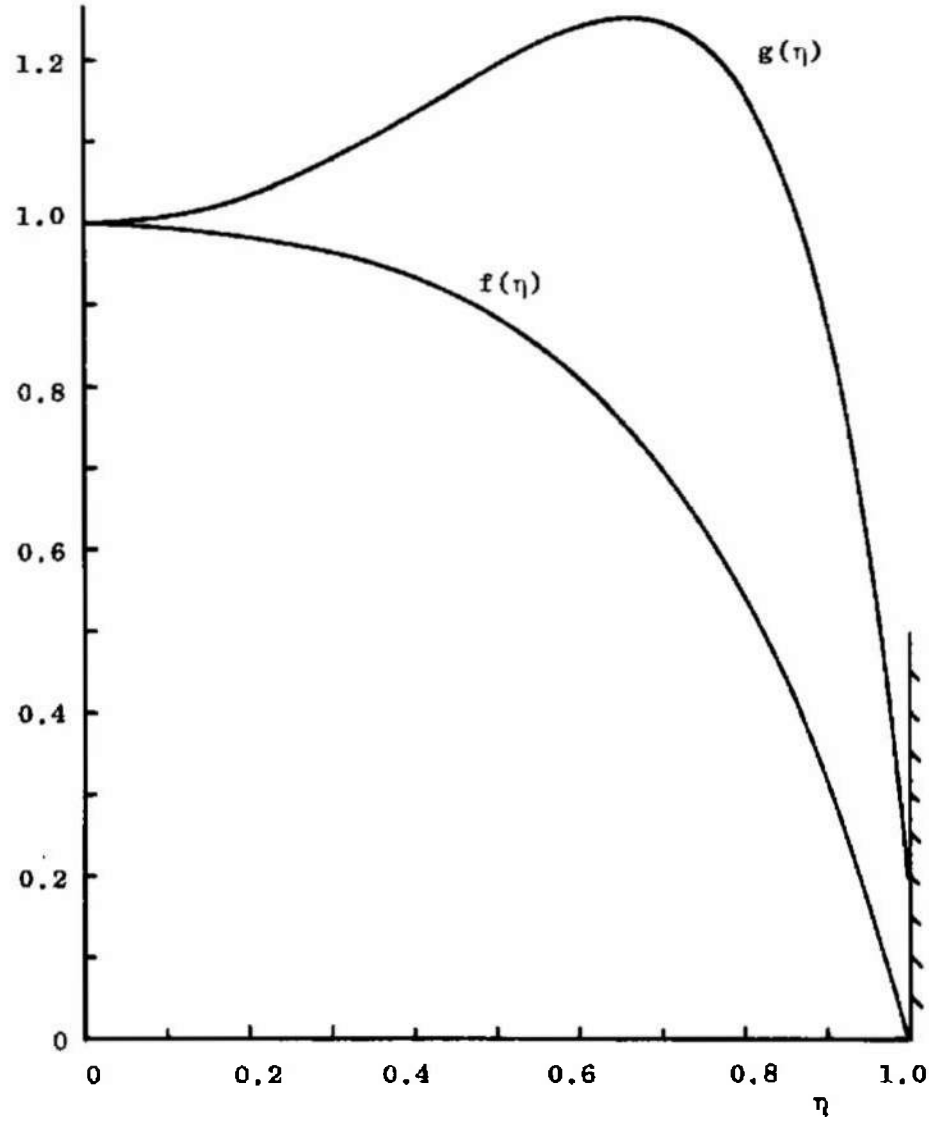

Fig. 18 Velocity and Temperature Profiles for Ha = 150, Φ = 1.2

Ha = 150 α = 1.249
Φ = 1.6 $g(\alpha)$ = .199
M = 2.525
Re = 13490

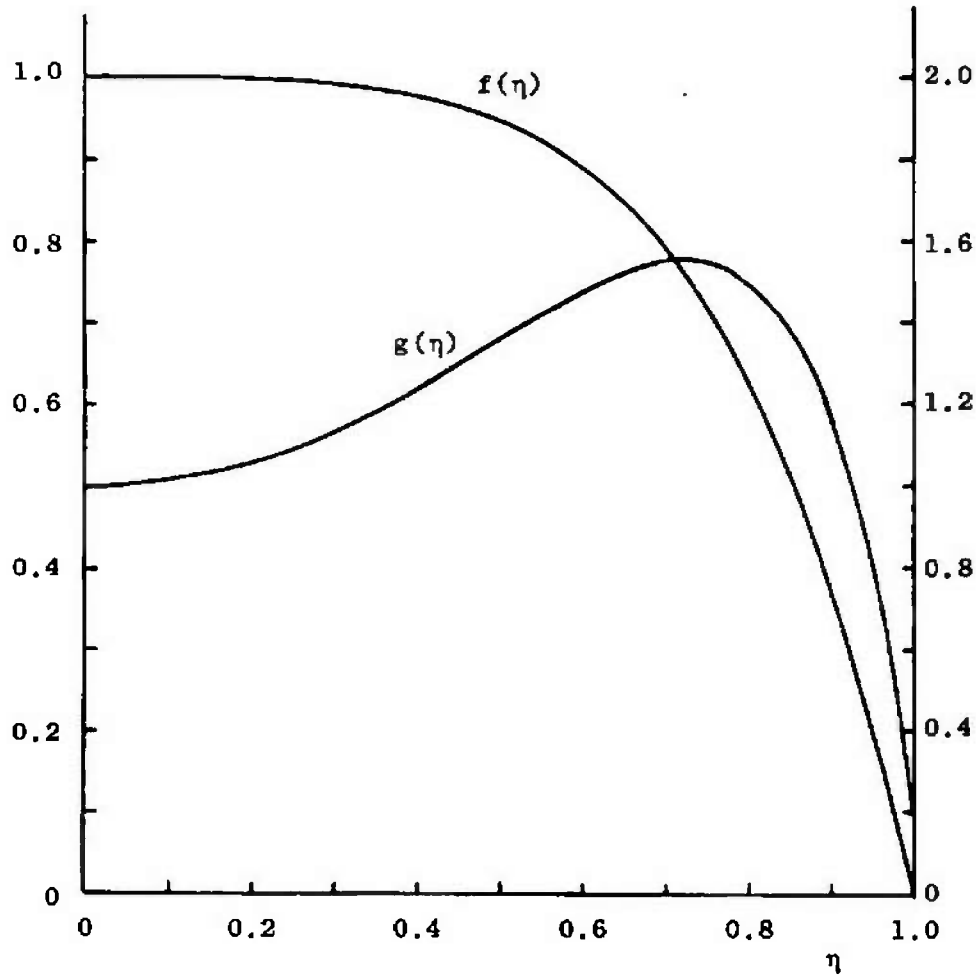

Fig. 19 Velocity and Temperature Profiles for Ha = 150, Φ = 1.6

Ha = 100 α = 1.249°
Φ = 1.6 g(α) = .200
M = 1.96
Re = 3925

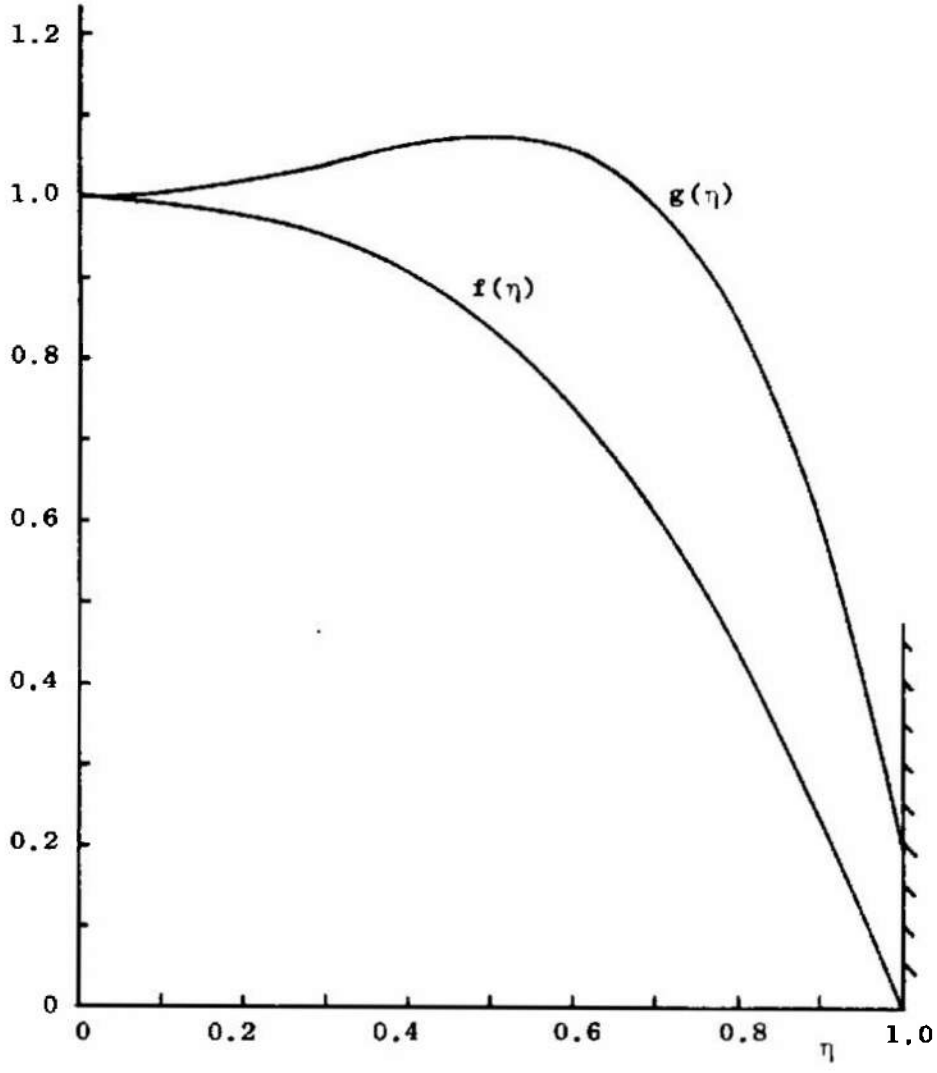

Fig. 20 Velocity and Temperature Profiles for Ha = 100, Φ = 1.6, $\sigma \approx T^{3/2}$

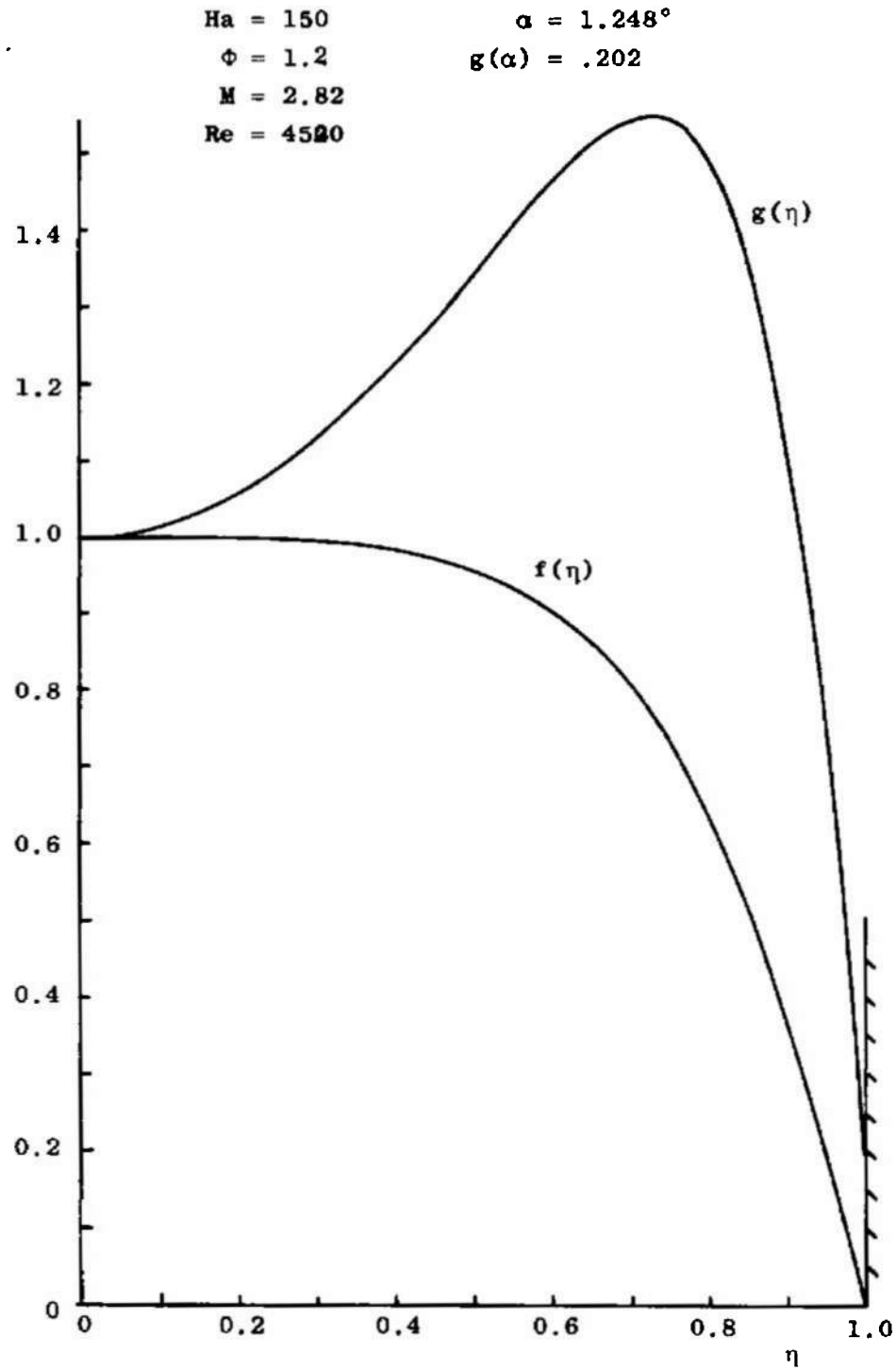

Fig. 21 Velocity and Temperature Profiles for Ha = 150, Φ = 1.2, $\sigma \sim T^{3/2}$

Ha = 150 α = 1.245°
Φ = 1.6 $g(\alpha)$ = .199
M = 2.815
Re ≐ 17500

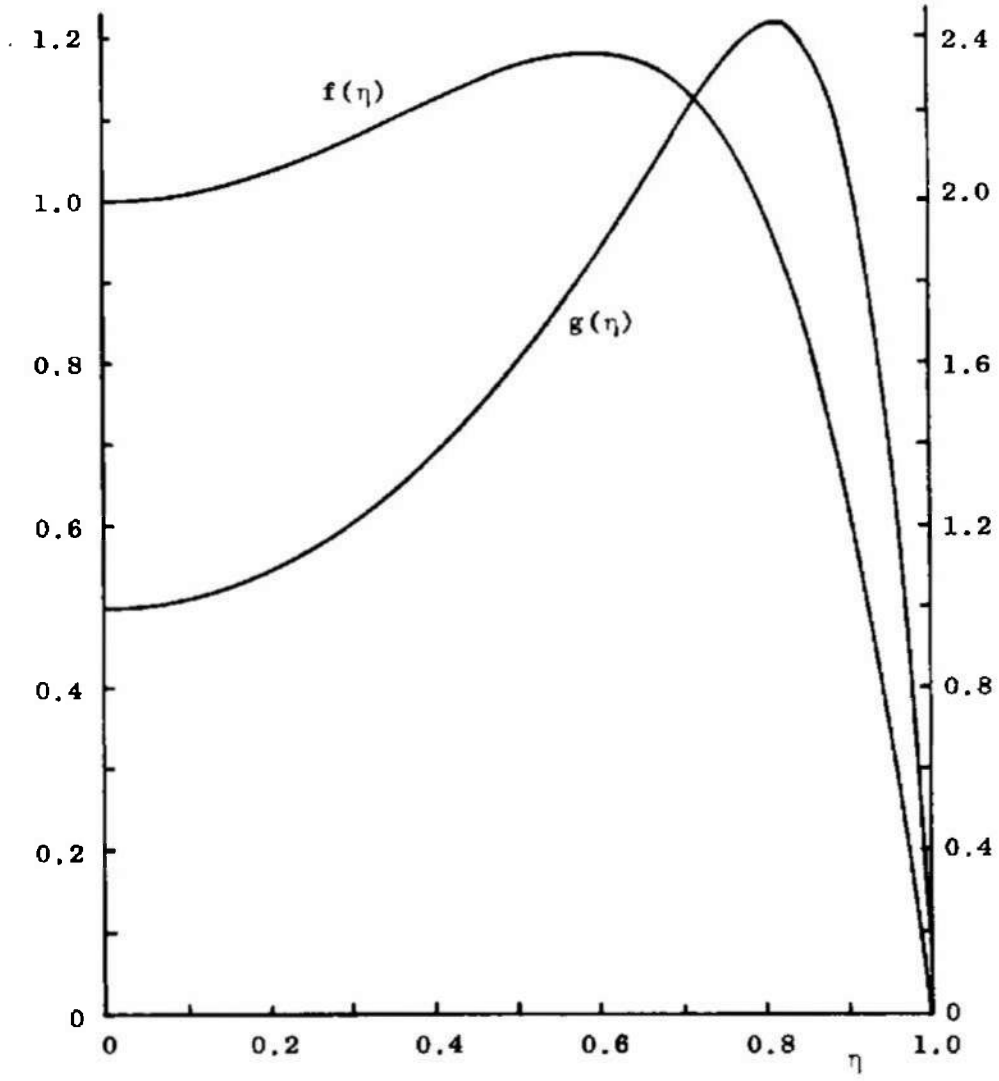

Fig. 22 Velocity and Temperature Profiles for Ha = 150, Φ = 1.6, $\sigma \sim T^{3/2}$

Ha = 100 α = 1.249°
Φ = 1.6 g(α) = 2.02
M = 2.05
Re = 4550

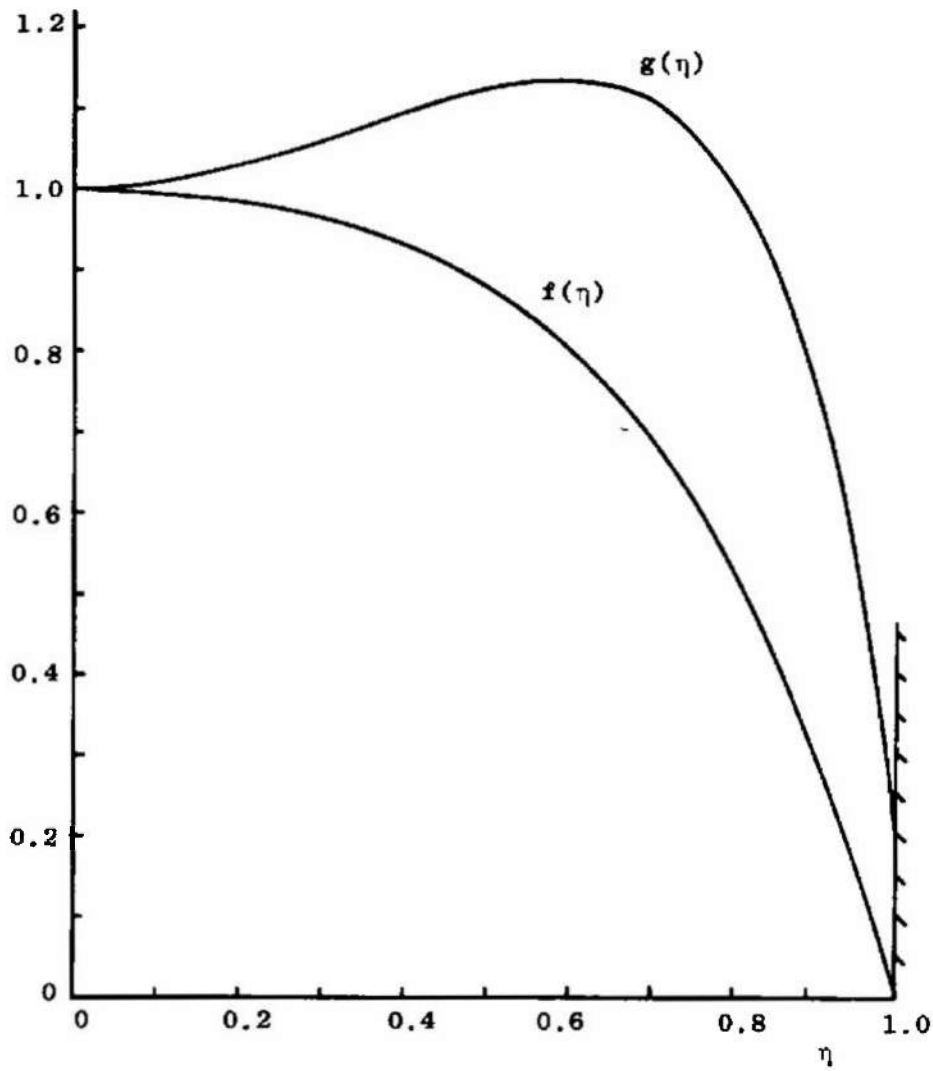

Fig. 23 Velocity and Temperature Profiles for Ha = 100, Φ = 1.6, $\sigma \sim T^{3/2}$, $\mu \sim \kappa \sim T^{1/2}$

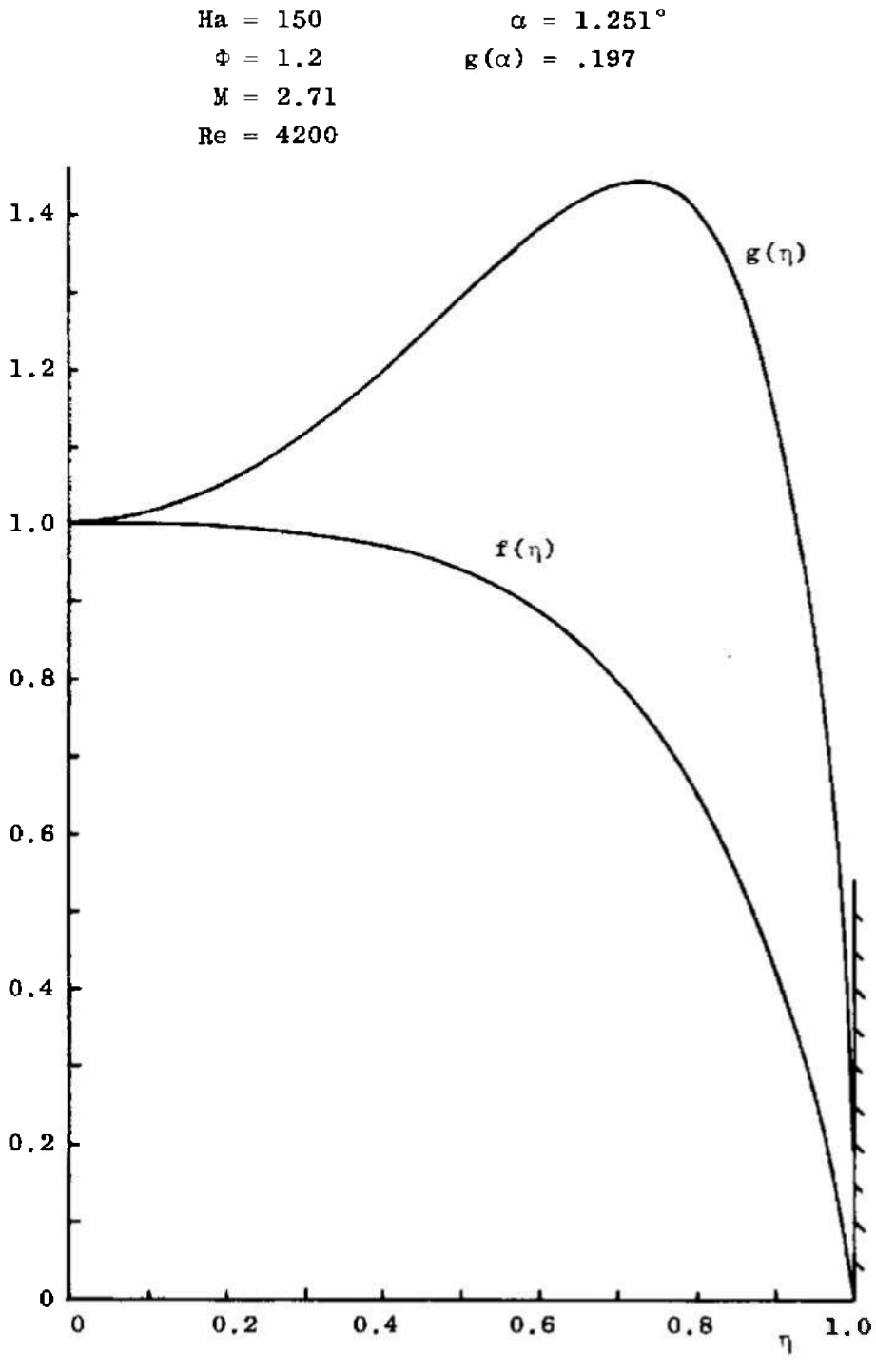

Fig. 24 Velocity and Temperature Profiles for Ha = 150, Φ = 1.2, $\sigma \sim T^{3/2}$, $\mu \sim \kappa \sim T^{1/2}$

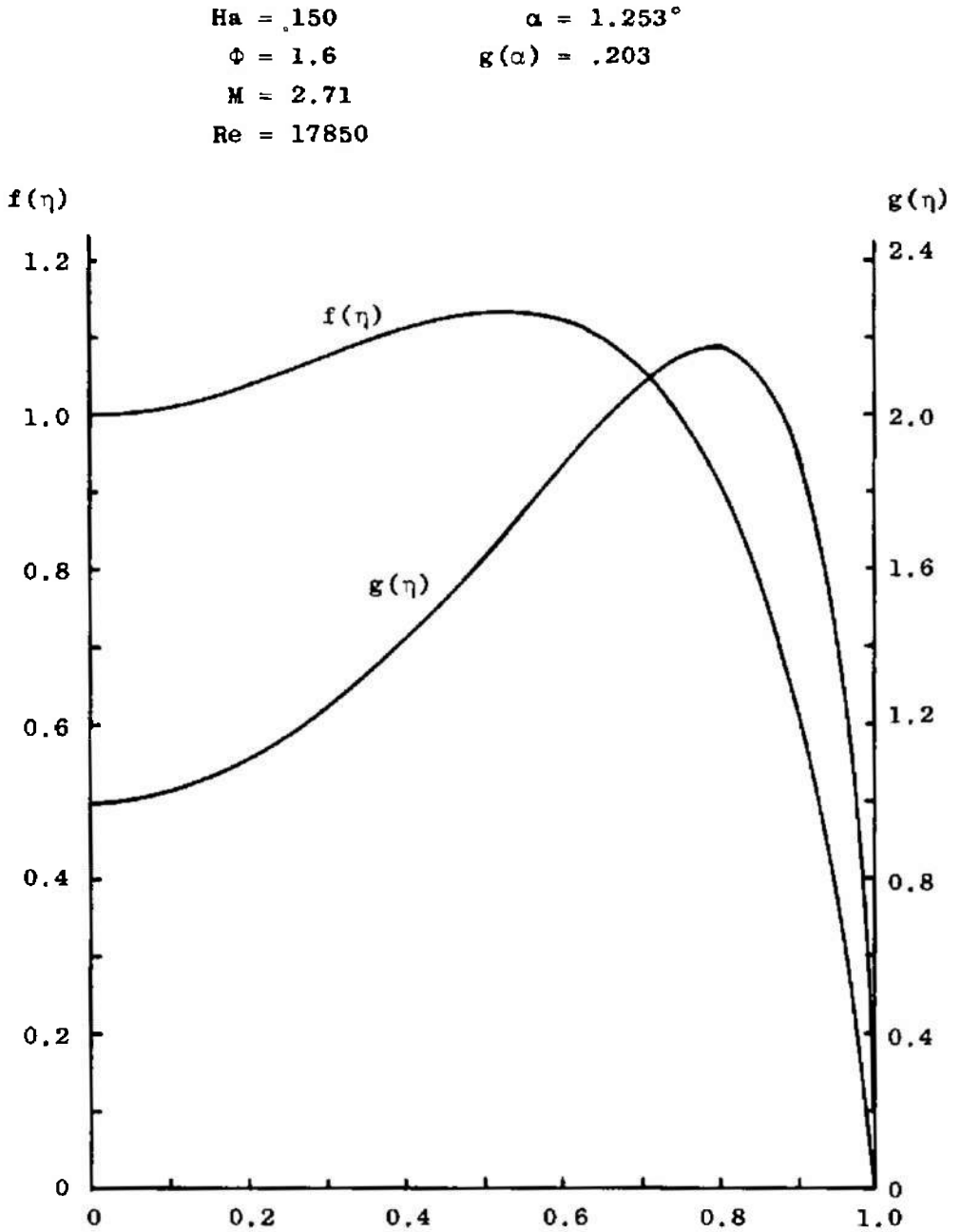

Fig. 25 Velocity and Temperature Profiles for Ha = 150, Φ = 1.6, $\sigma \sim T^{3/2}$, $\mu \sim \kappa \sim T^{1/2}$

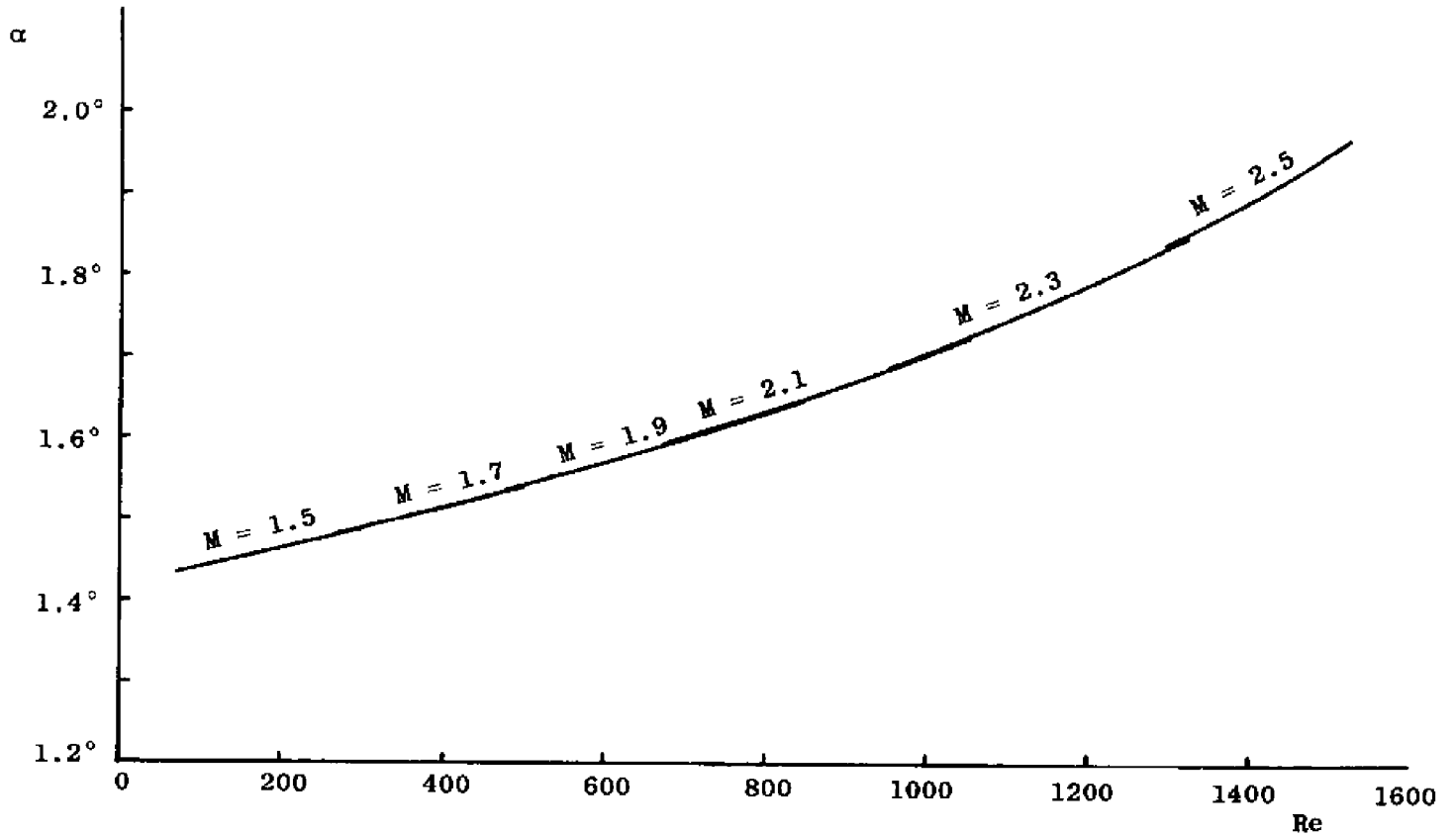

Fig. 26 Variation of α with Re and M for Ha = 100, Φ = 1.2

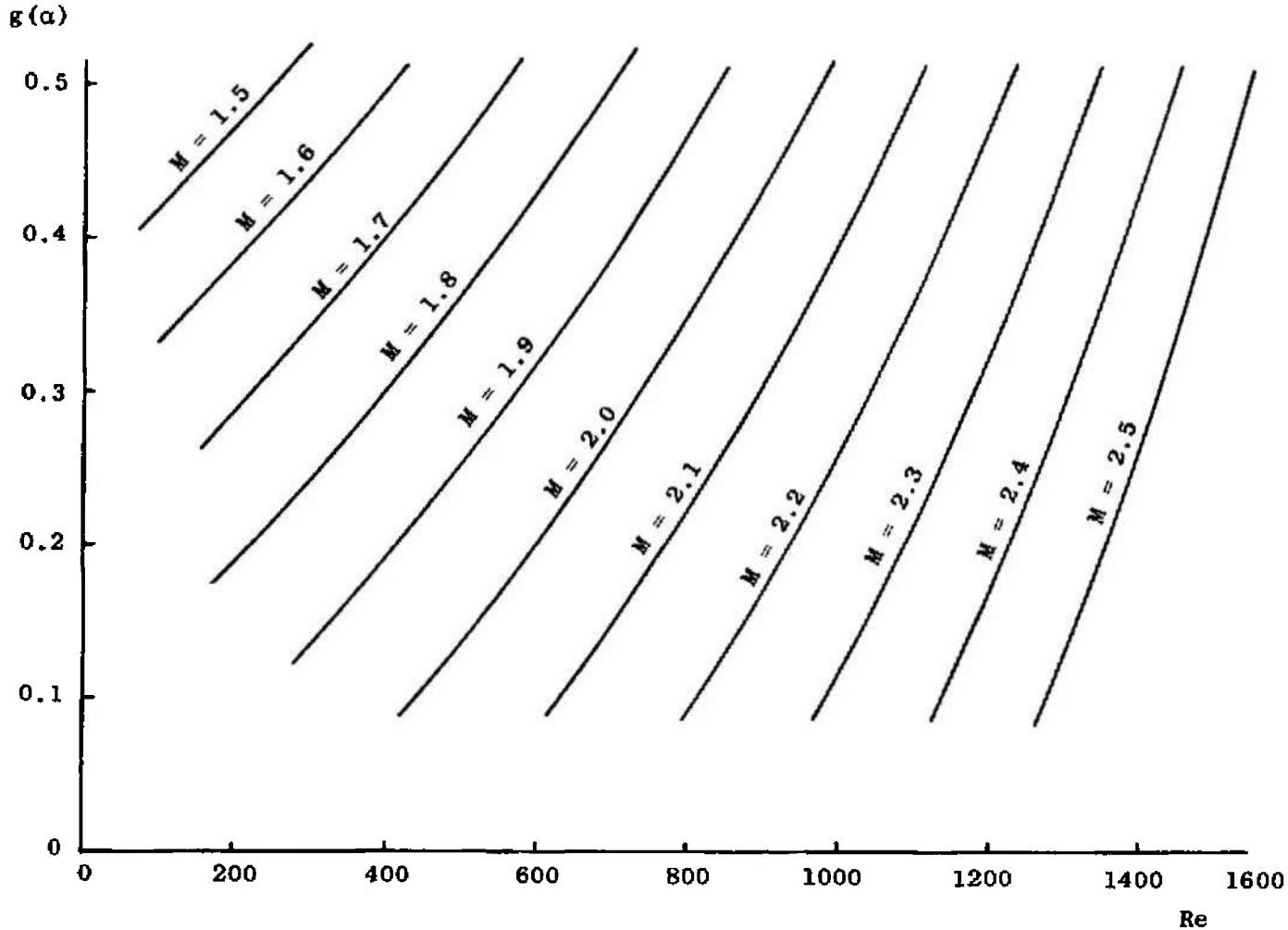

Fig. 27 Variation of $g(\alpha)$ with Re and M for Ha = 100, Φ = 1.2

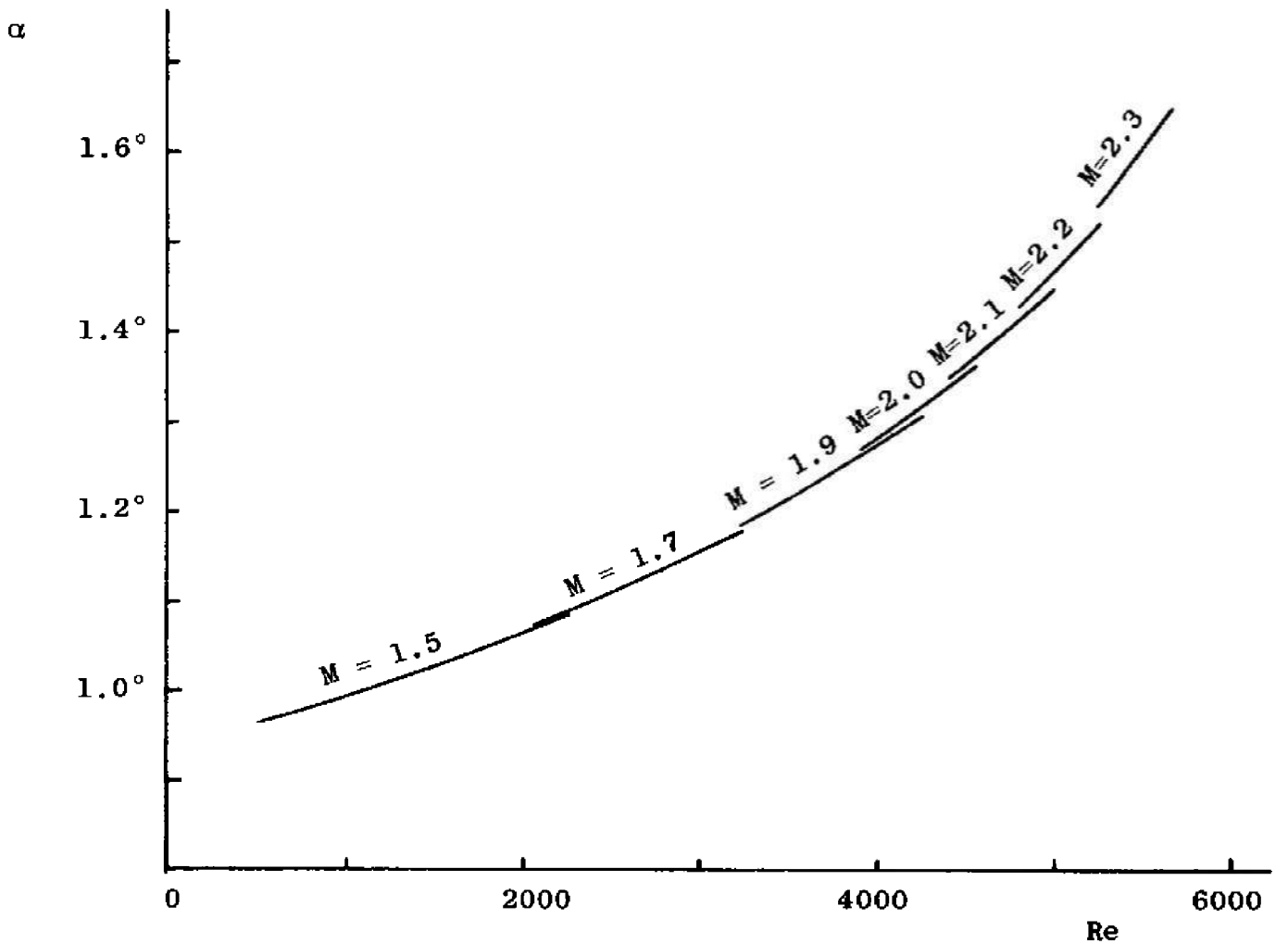

Fig. 28 Variation of α with Re and M for Ha = 100, Φ = 1.6

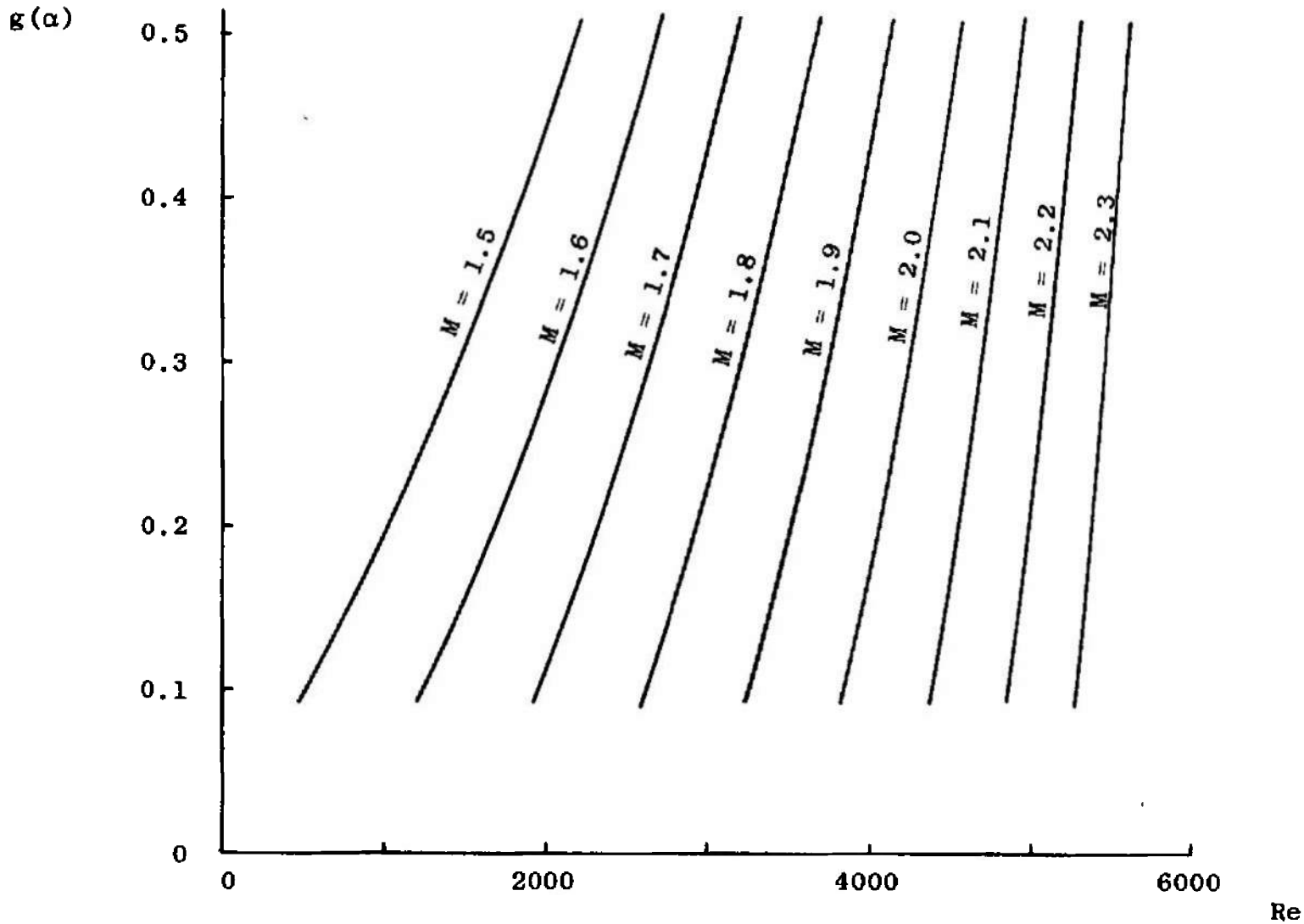

Fig. 29 Variation of $g(\alpha)$ with Re and M for Ha = 100, Φ = 1.6

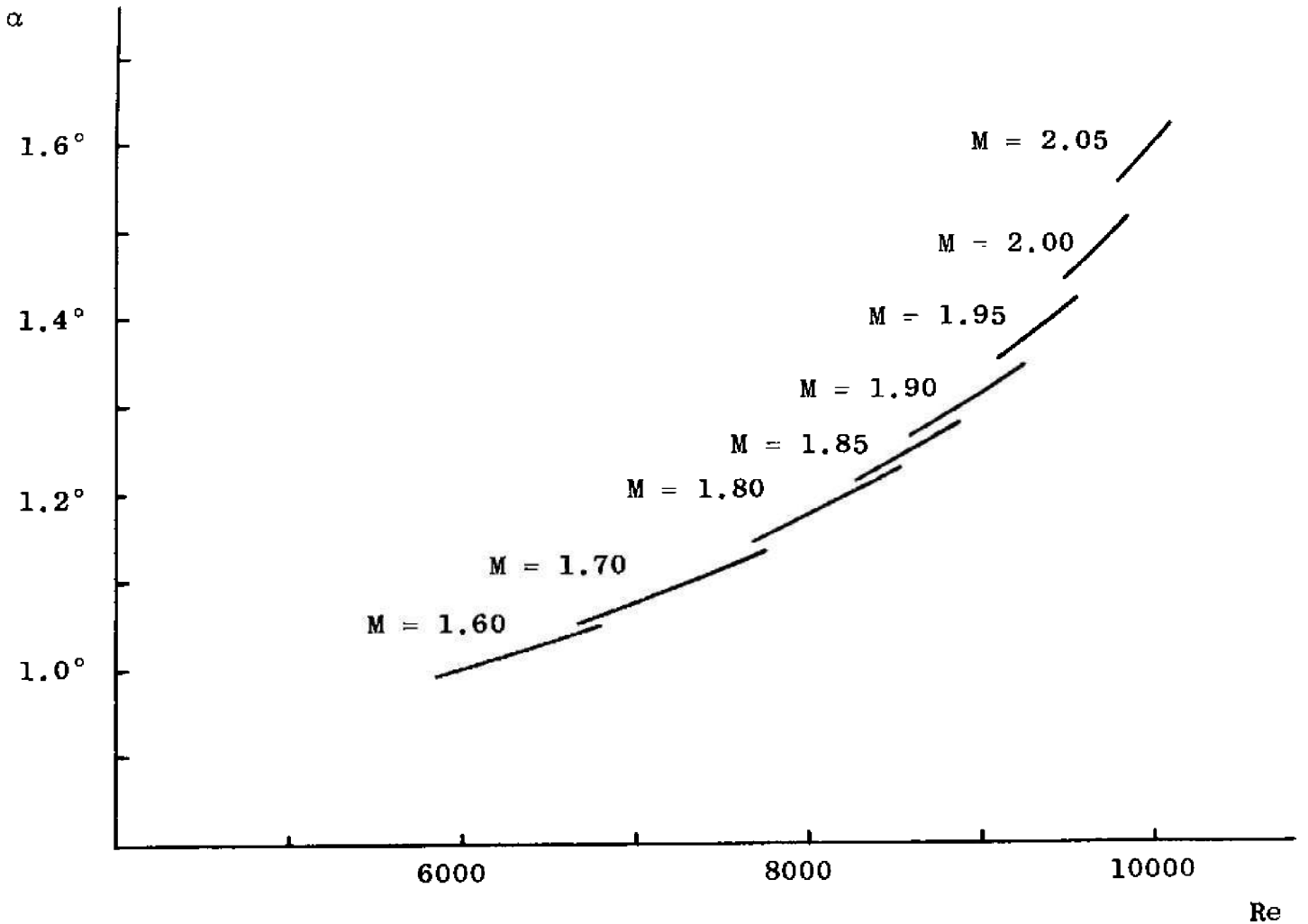

Fig. 30 Variation of α with Re and M for Ha = 100, Φ 2.0

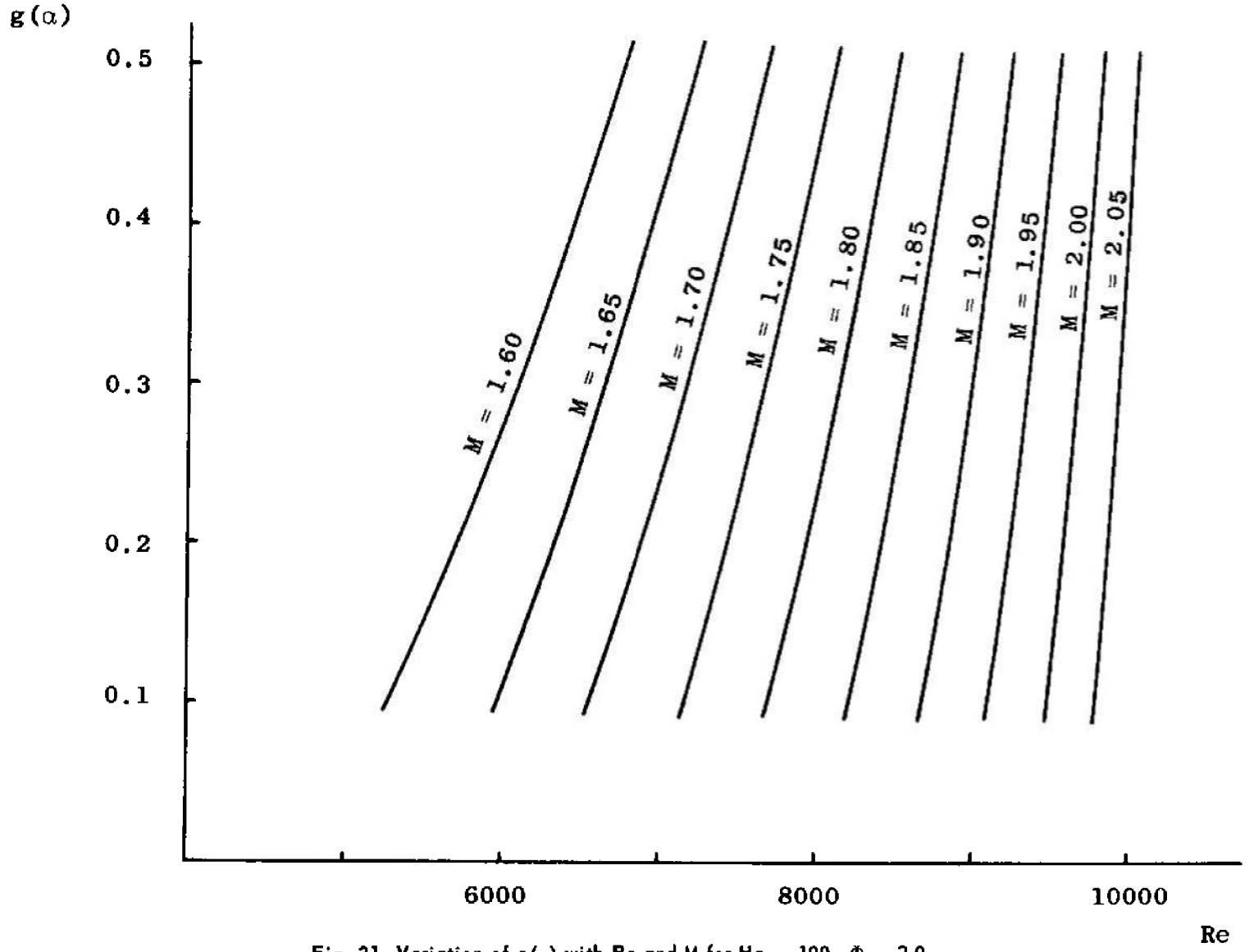

Fig. 31 Variation of $g(\alpha)$ with Re and M for Ha = 100, Φ = 2.0

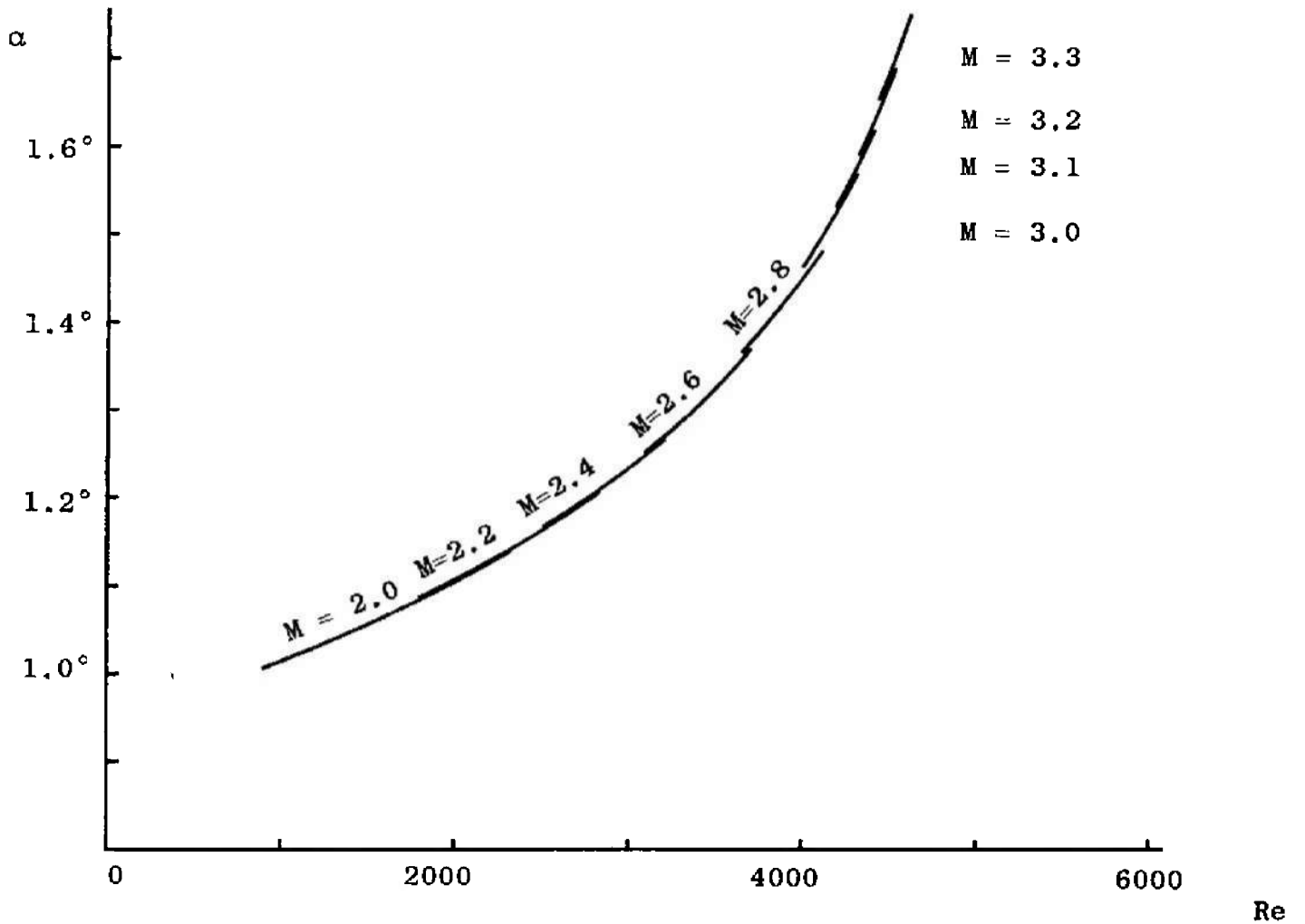

Fig. 32 Variation of α with Re and M for Ha = 150, Φ = 1.2

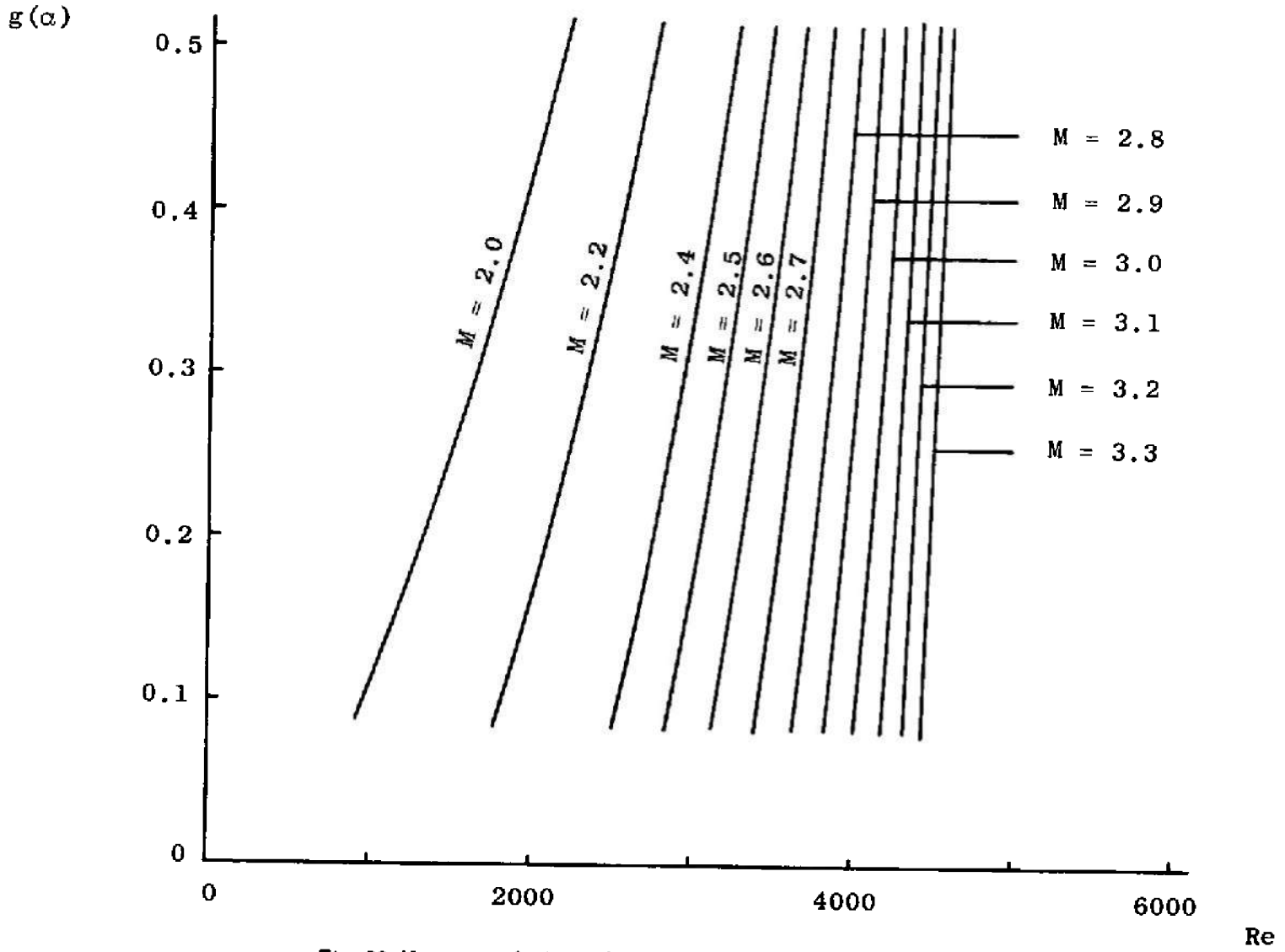

Fig. 33 Variation of g(α) with Re and M for Ha = 150, Φ = 1.2

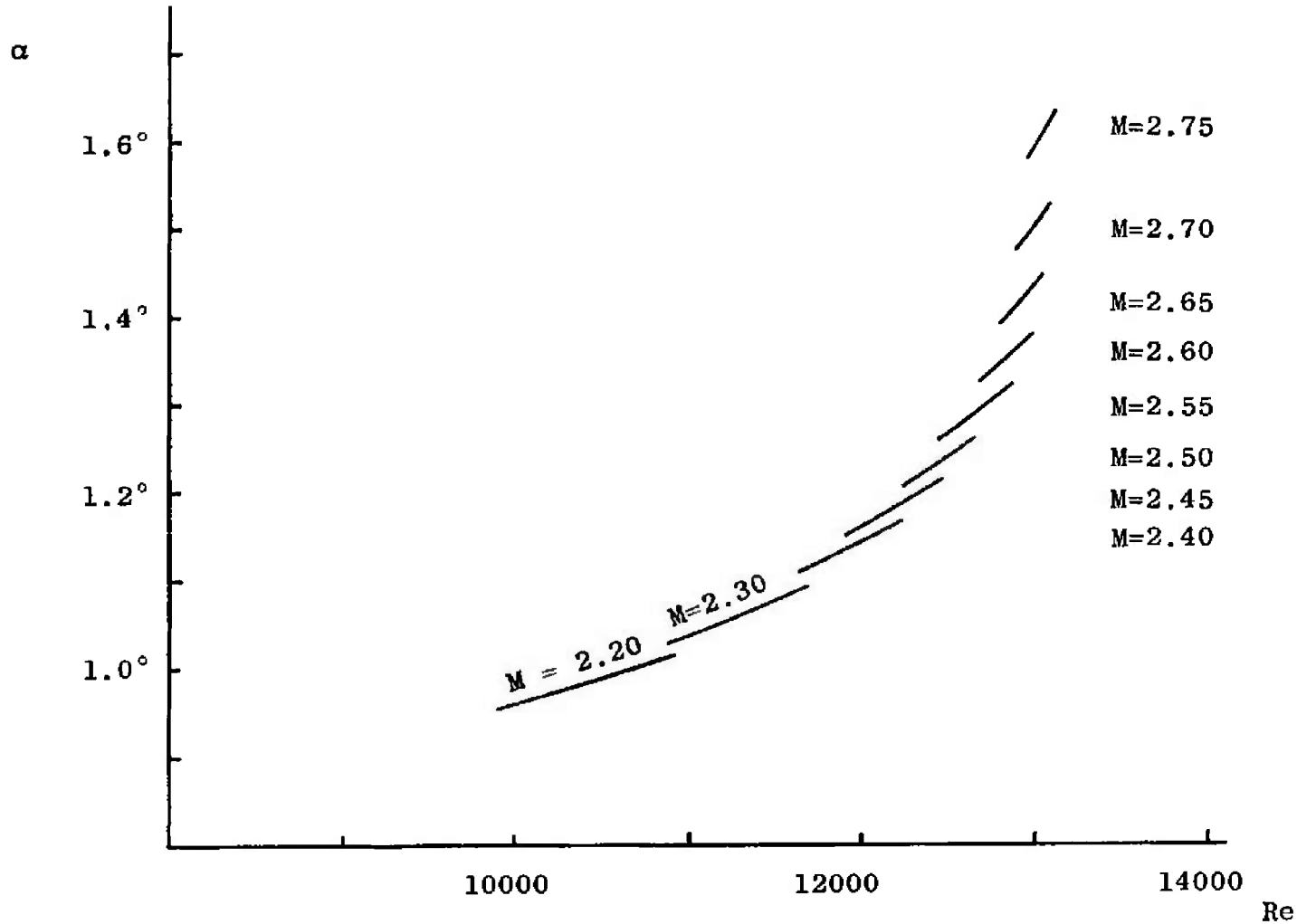

Fig. 34 Variation of α with Re and M for Ha = 150, Φ = 1.6

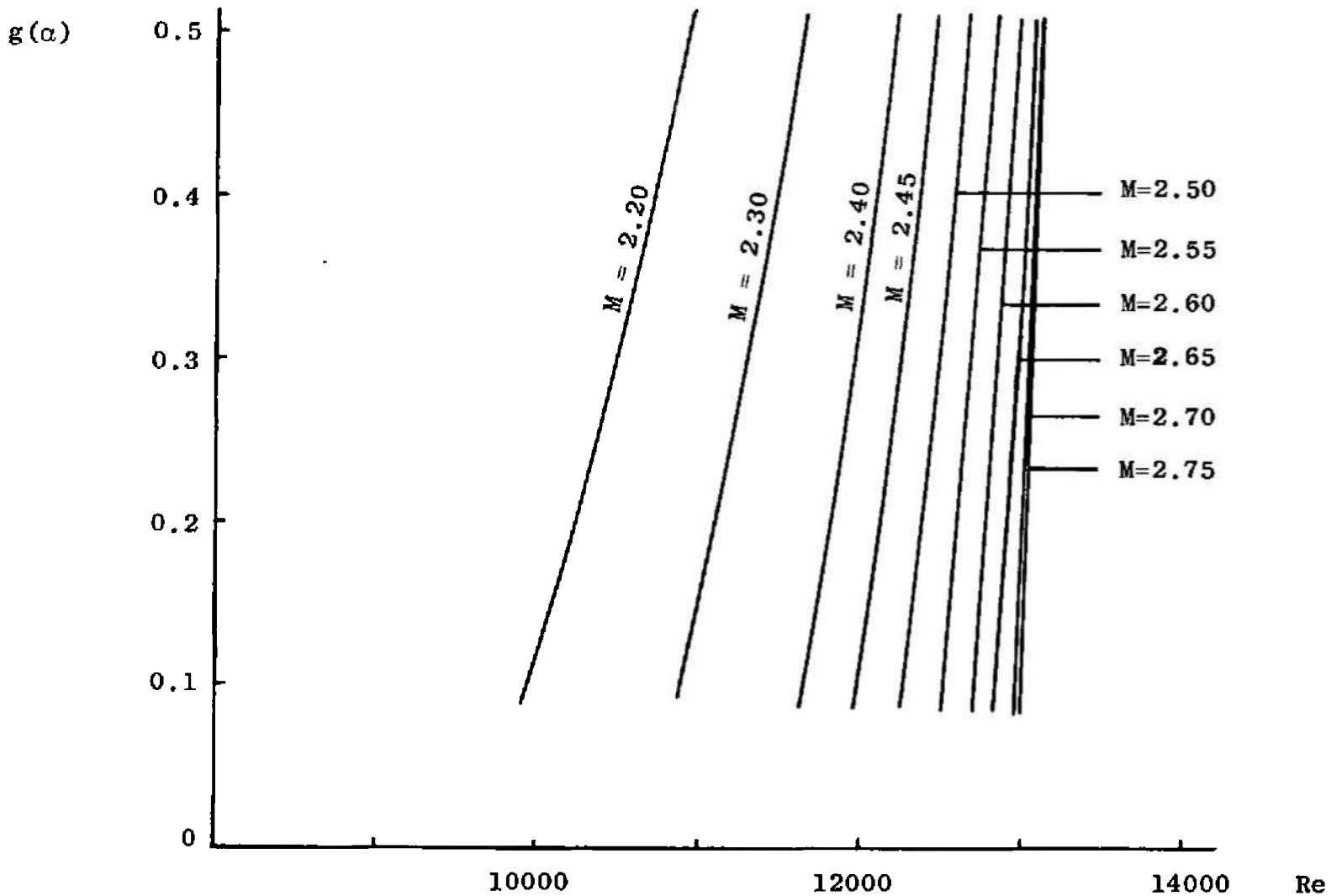

Fig. 35 Variation of g(α) with Re and M for Ha = 150, Φ = 1.6

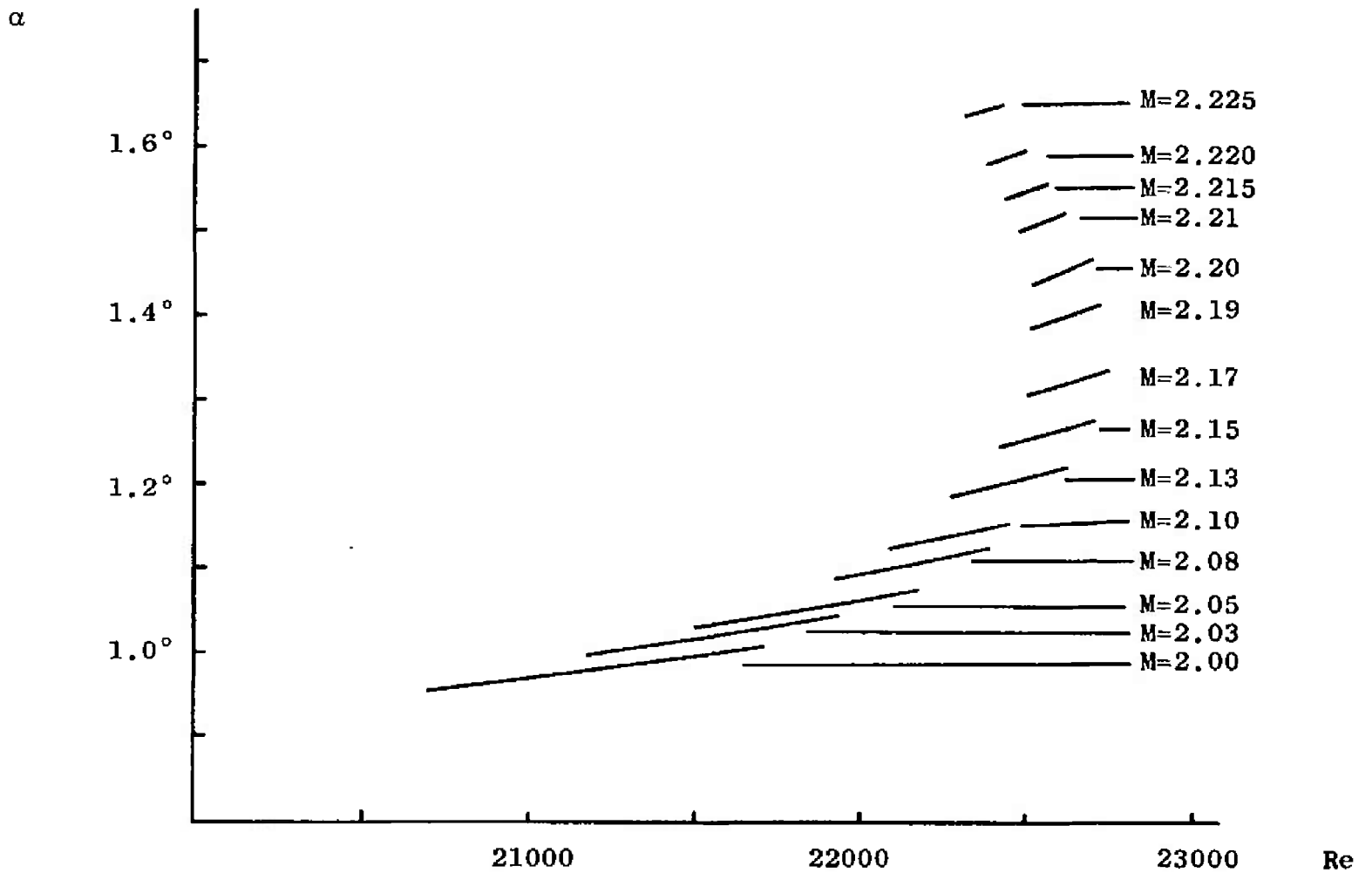

Fig. 36 Variation of α with Re and M for Ho = 150, Φ = 2.0

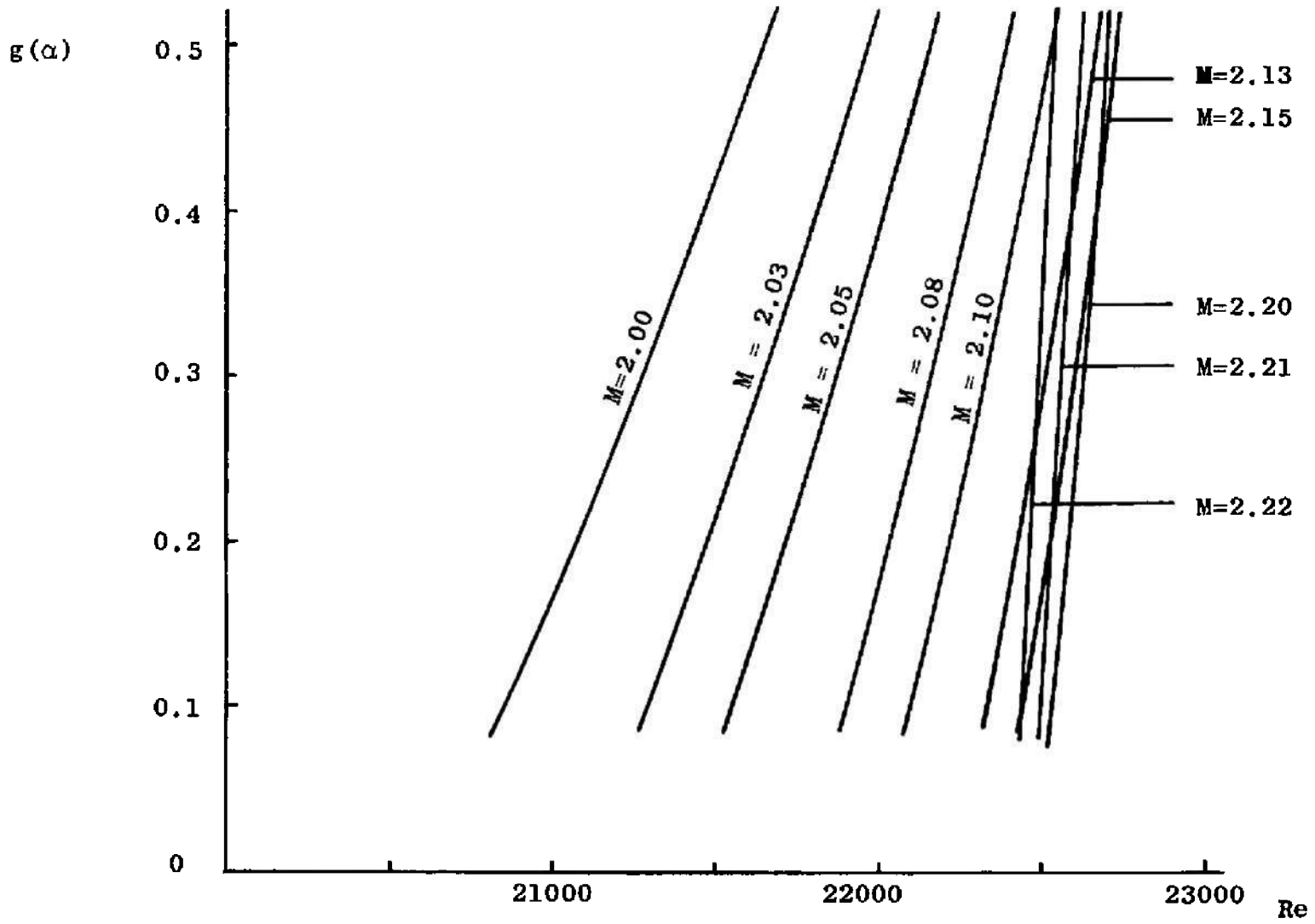

Fig. 37 Variation of $g(\alpha)$ with Re and M for Ha = 150, Φ = 2.0

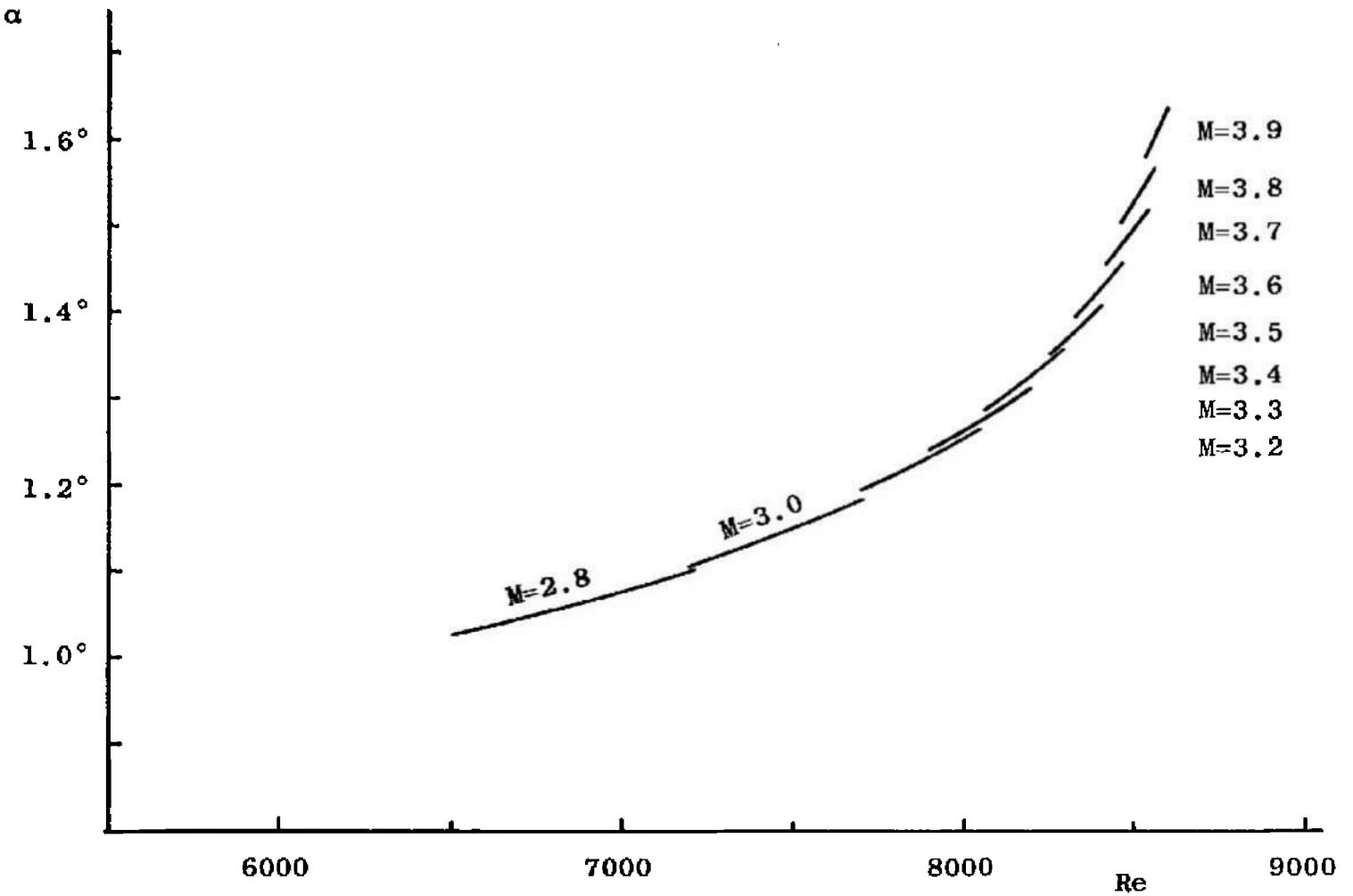

Fig. 38 Variation of α with Re and M for Ha = 200, Φ = 1.2

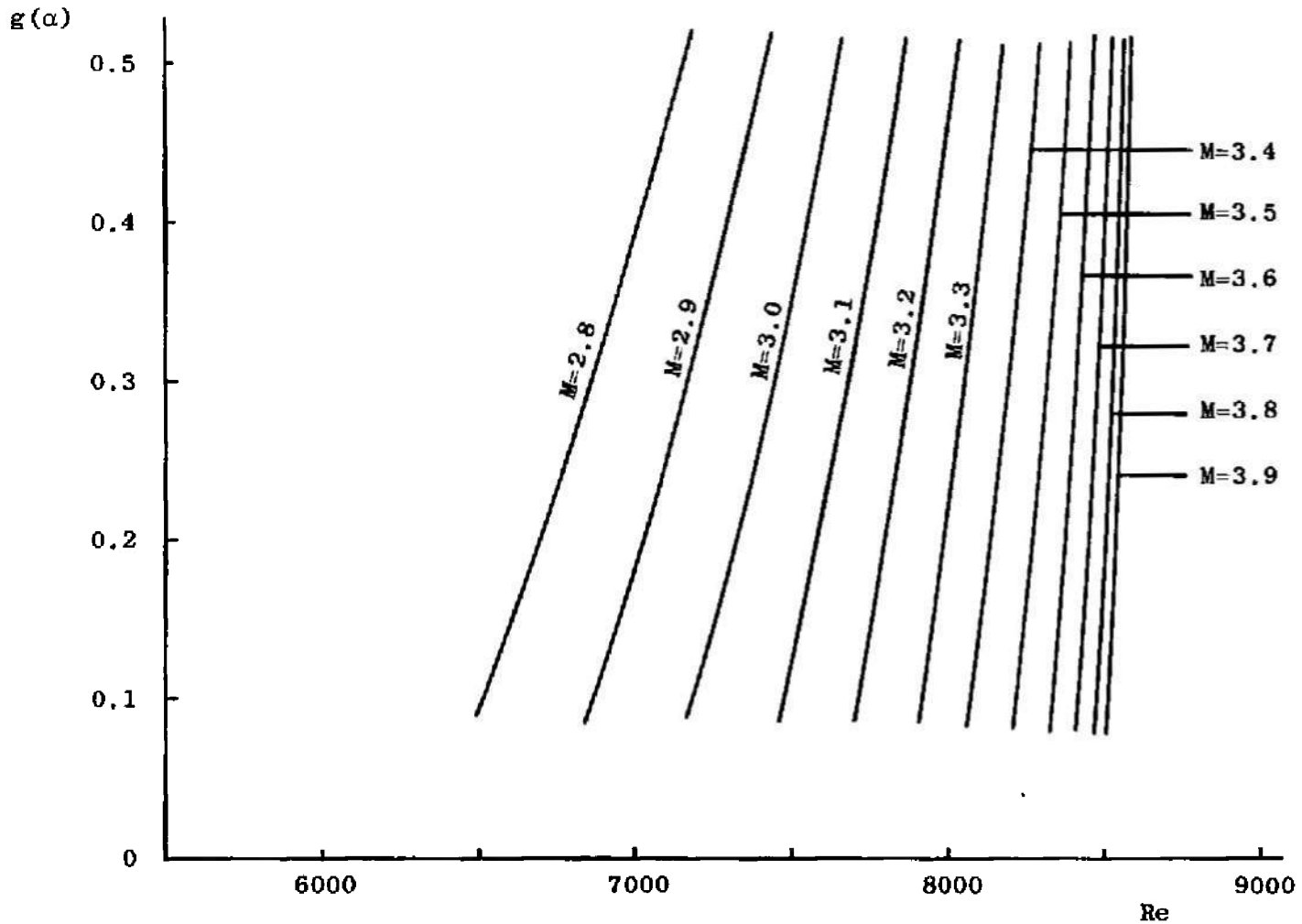

Fig. 39 Variation of $g(\alpha)$ with Re and M for Ha = 200, Φ = 1.2

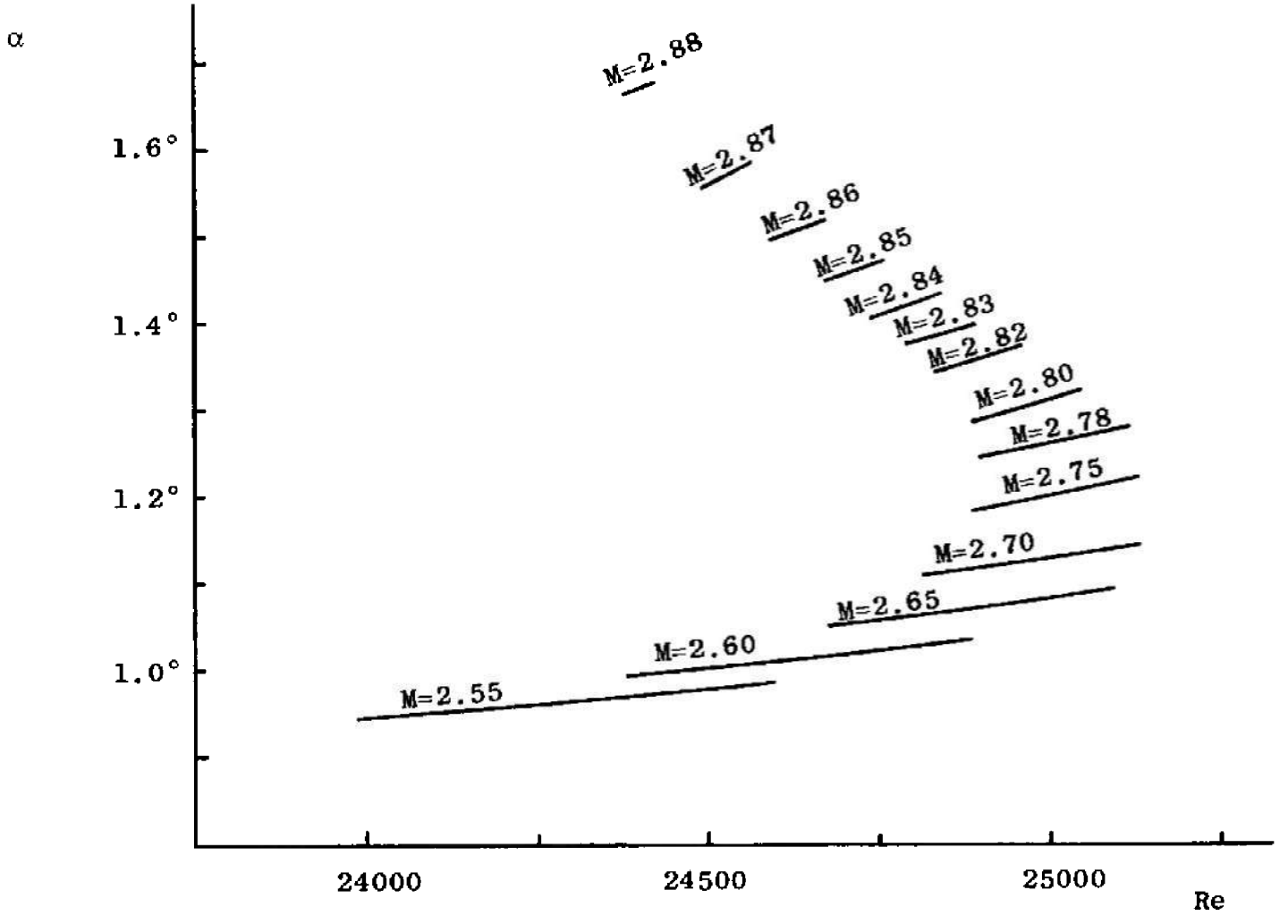

Fig. 40 Variation of α with Re and M for Ha = 200, Φ = 1.6

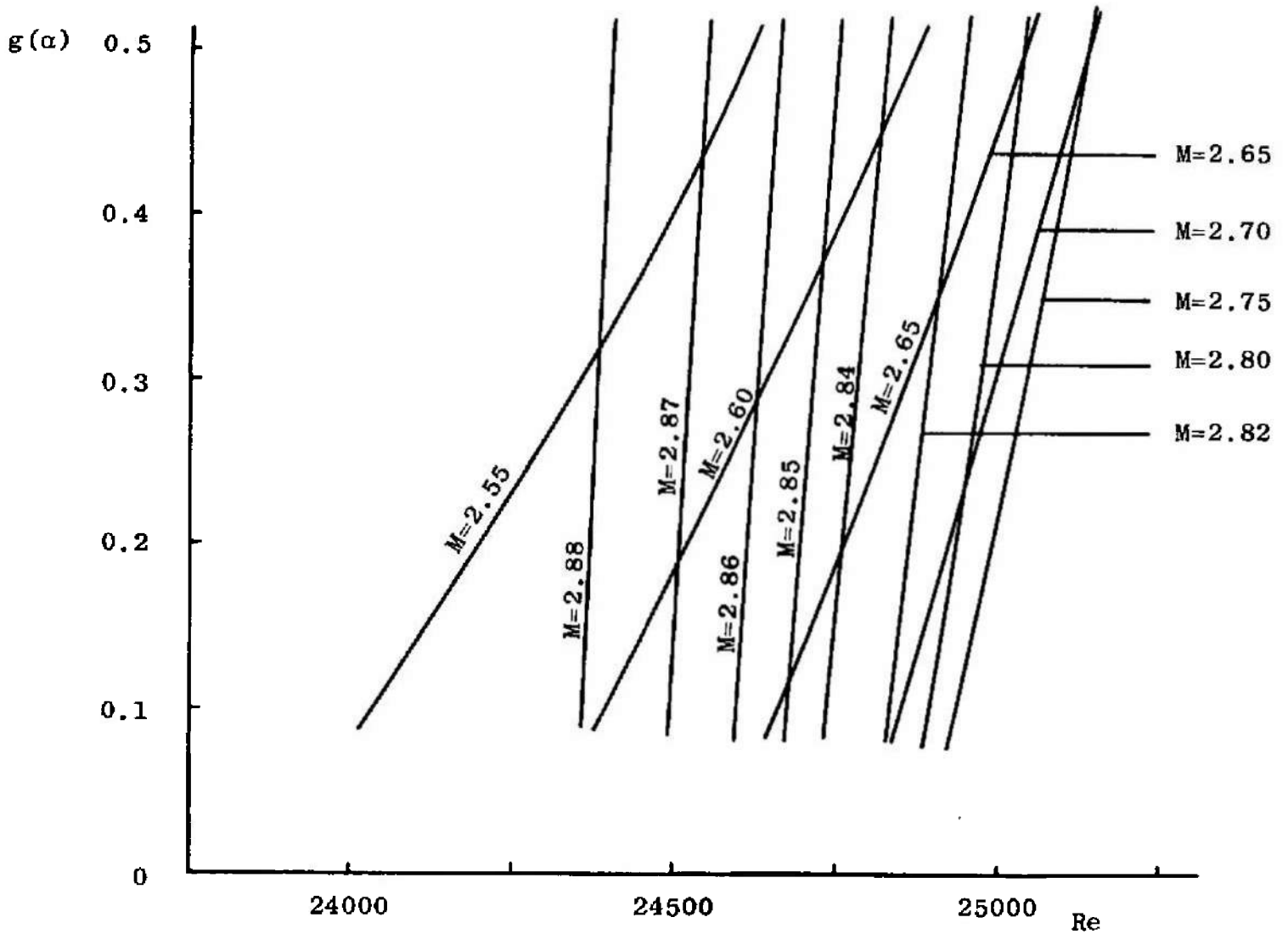

Fig. 41 Variation of g(α) with Re and M for Ha = 200, Φ = 1.6

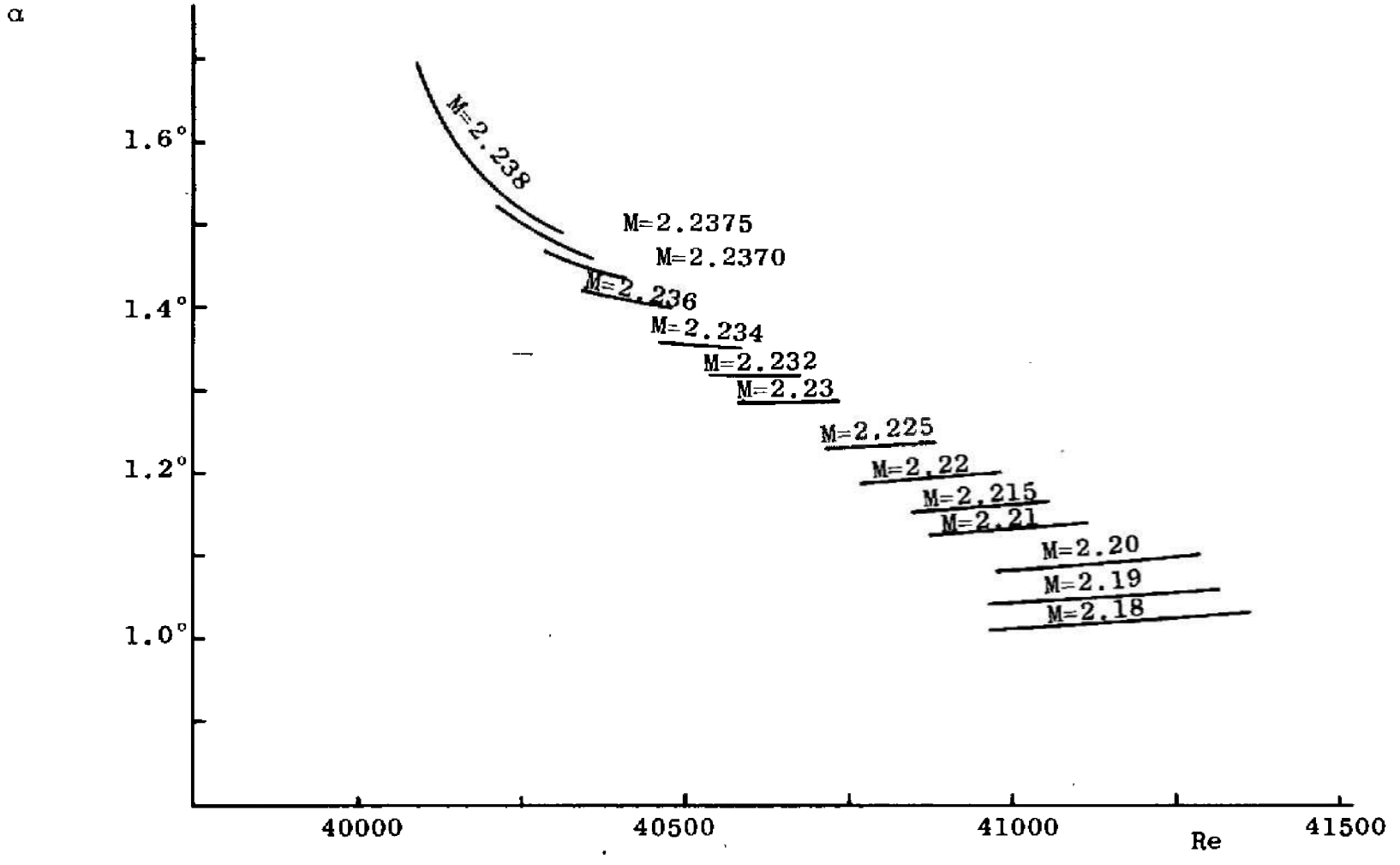

Fig. 42 Variation of α with Re and M for Ha = 200, Φ = 2.0

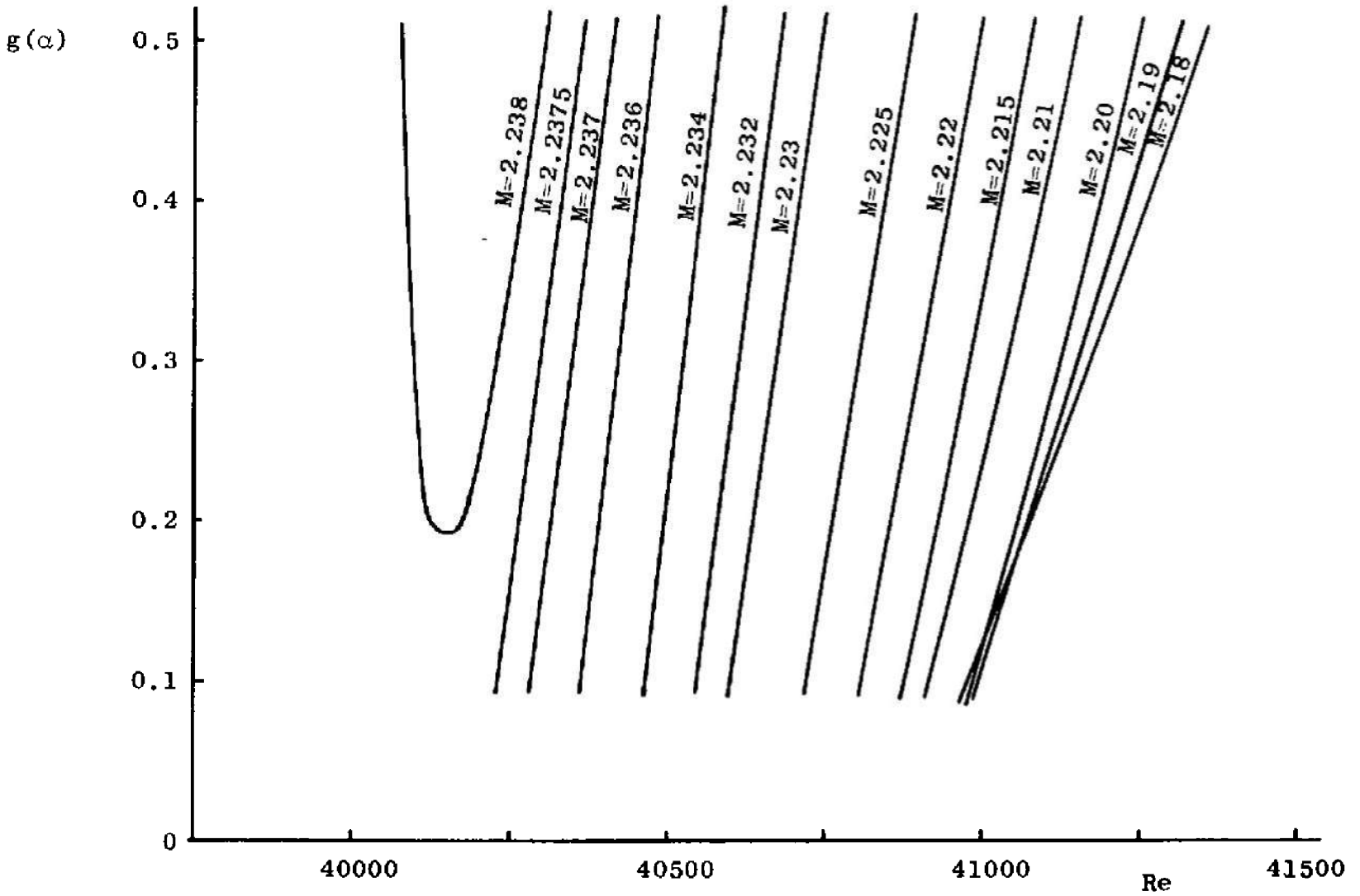

Fig. 43 Variation of $g(\alpha)$ with Re and M for Ha = 200, Φ = 2.0

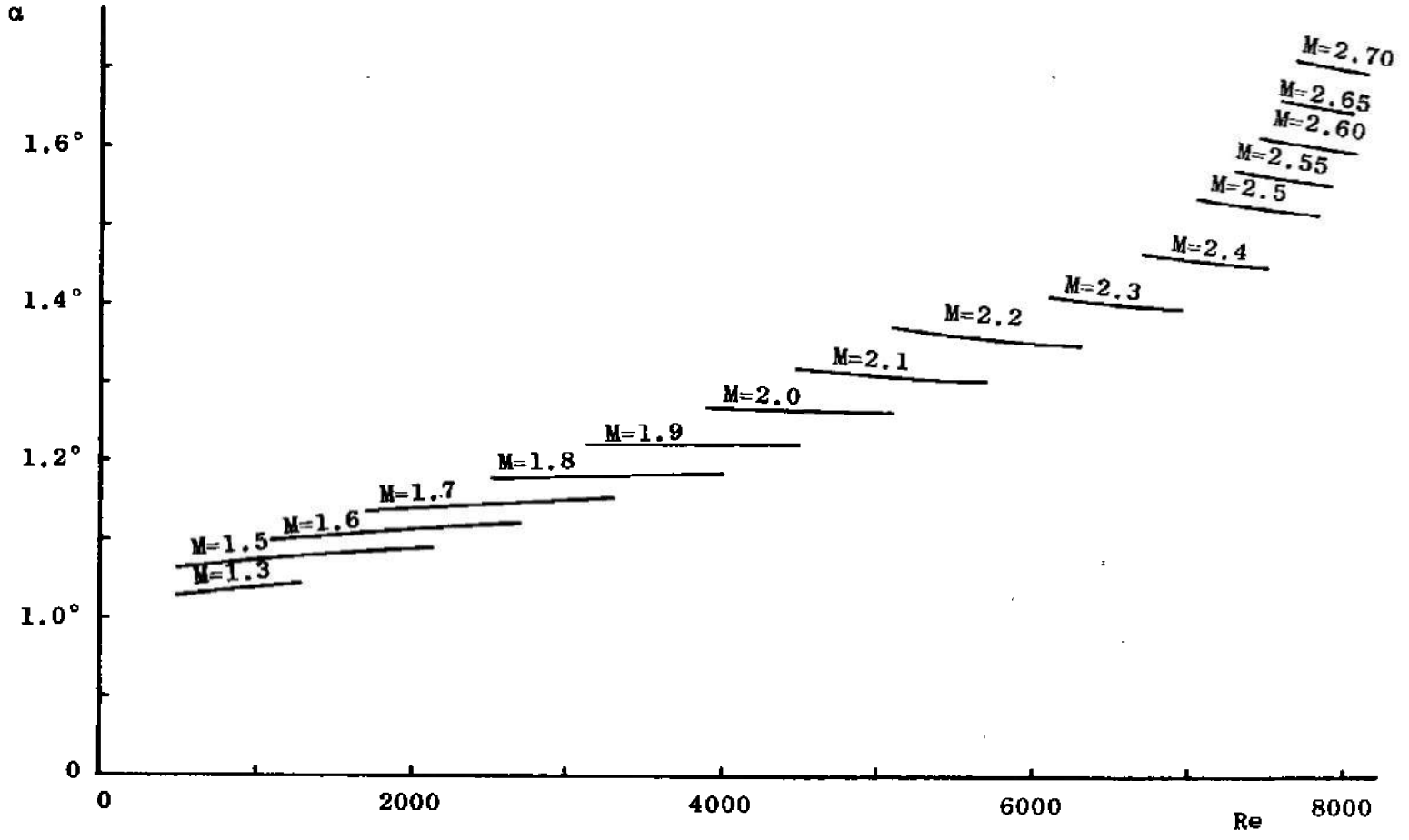

Fig. 44 Variation of α with Re and M for Ha = 100, Φ = 1.6, $\sigma \sim T^{3/2}$

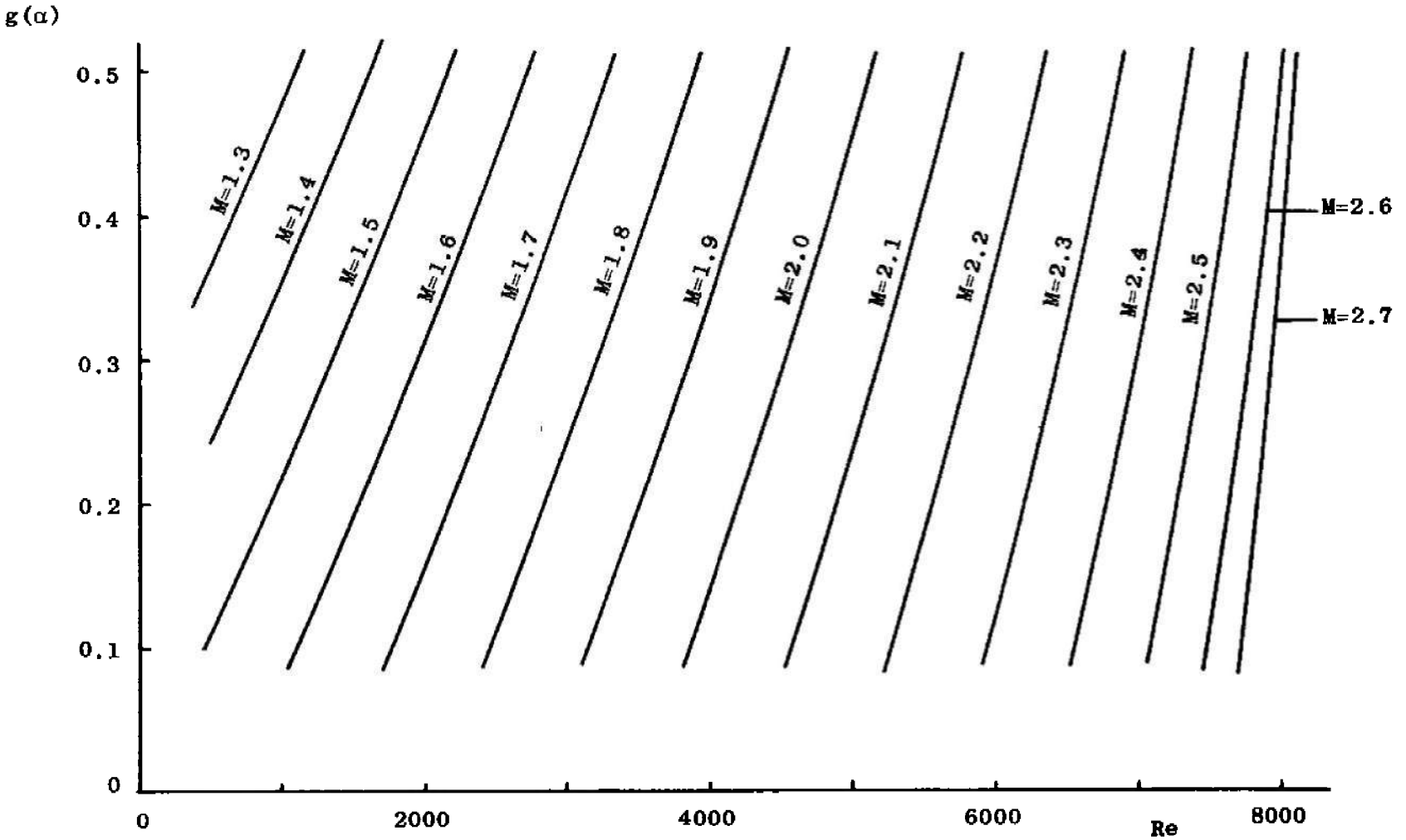

Fig. 45 Variation of $g(\alpha)$ with Re, M for Ha = 100, $\Phi = 1.6$, $\sigma \sim T^{3/2}$

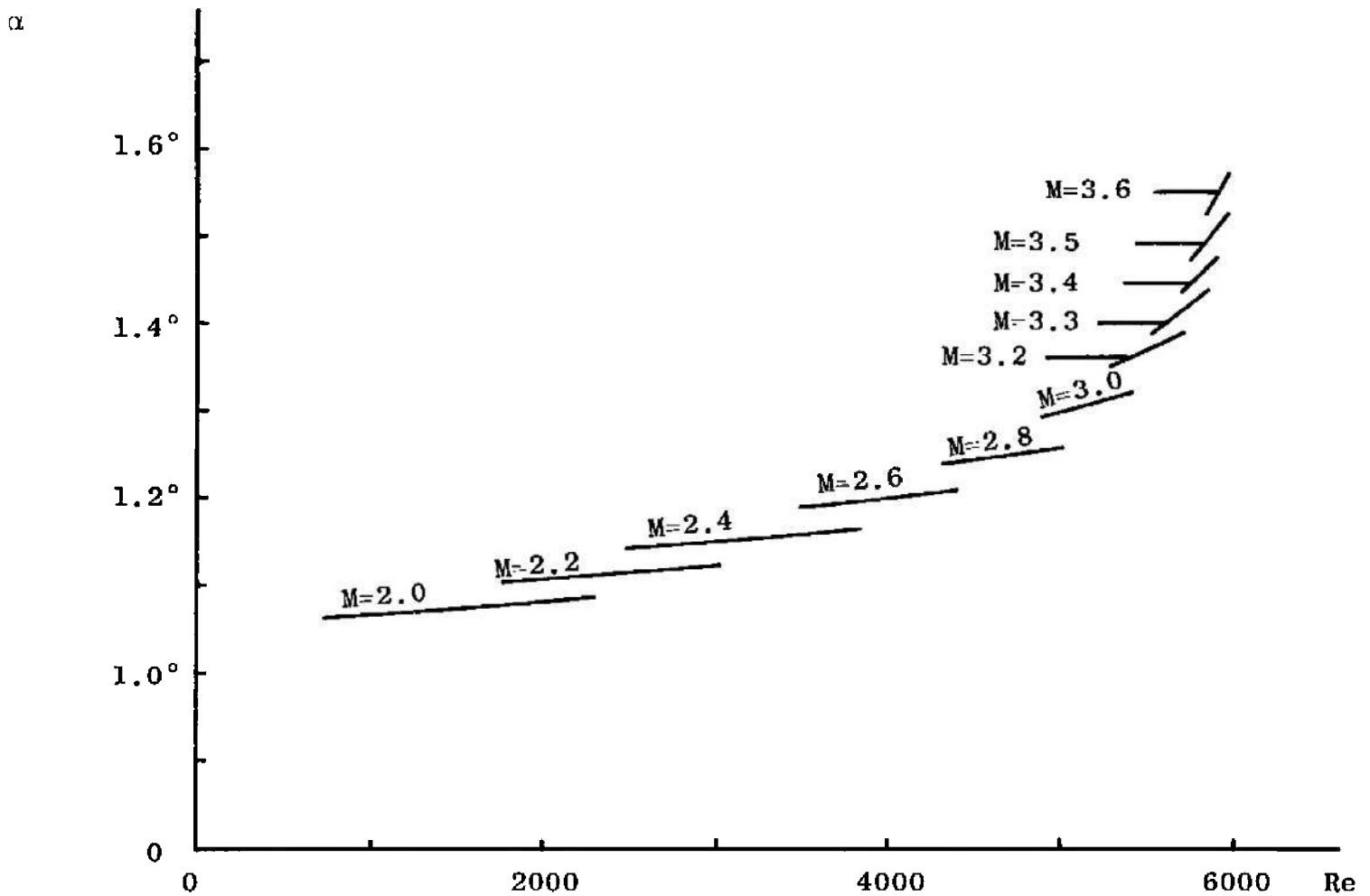

Fig. 46 Variation of α with Re and M for Ha = 150, Φ = 1.2. $\sigma \sim T^{3/2}$

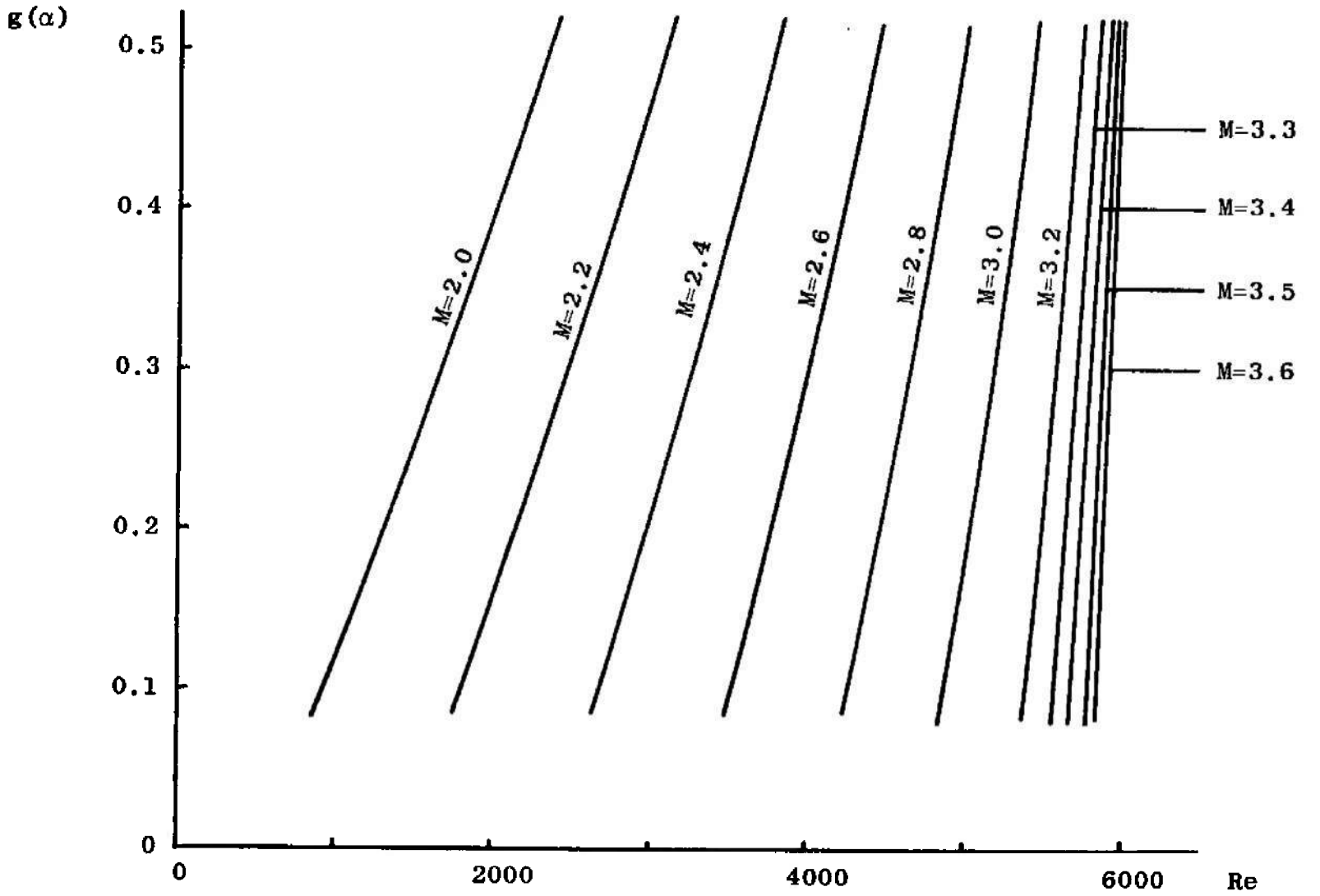

Fig. 47 Variation of $g(\alpha)$ with Re and M for Ha = 150, Φ = 1.2, $\sigma = T^{3/2}$

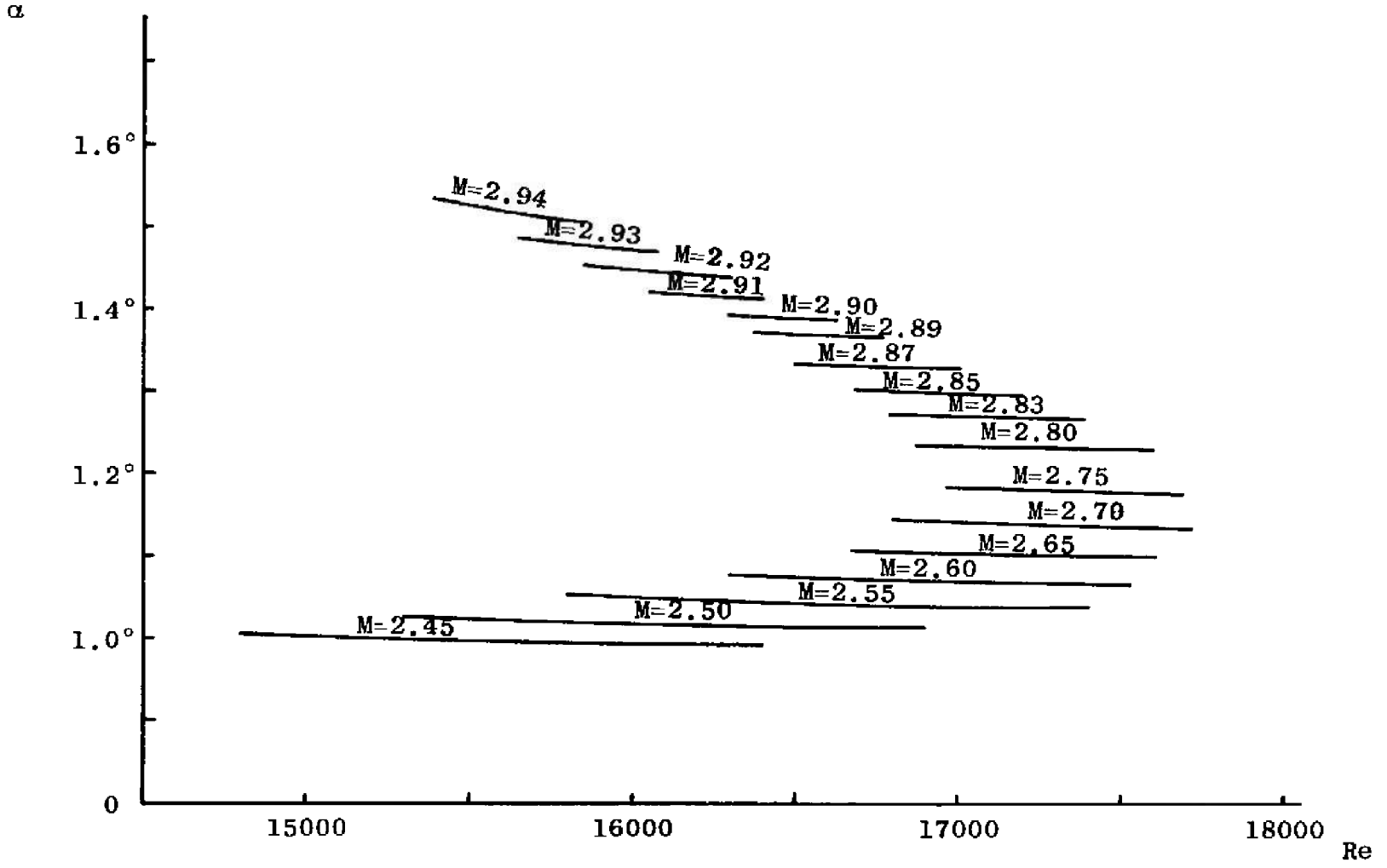

Fig. 48 Variation of α with Re and M for Ha = 150, Φ = 1.6, $\sigma \sim T^{3/2}$

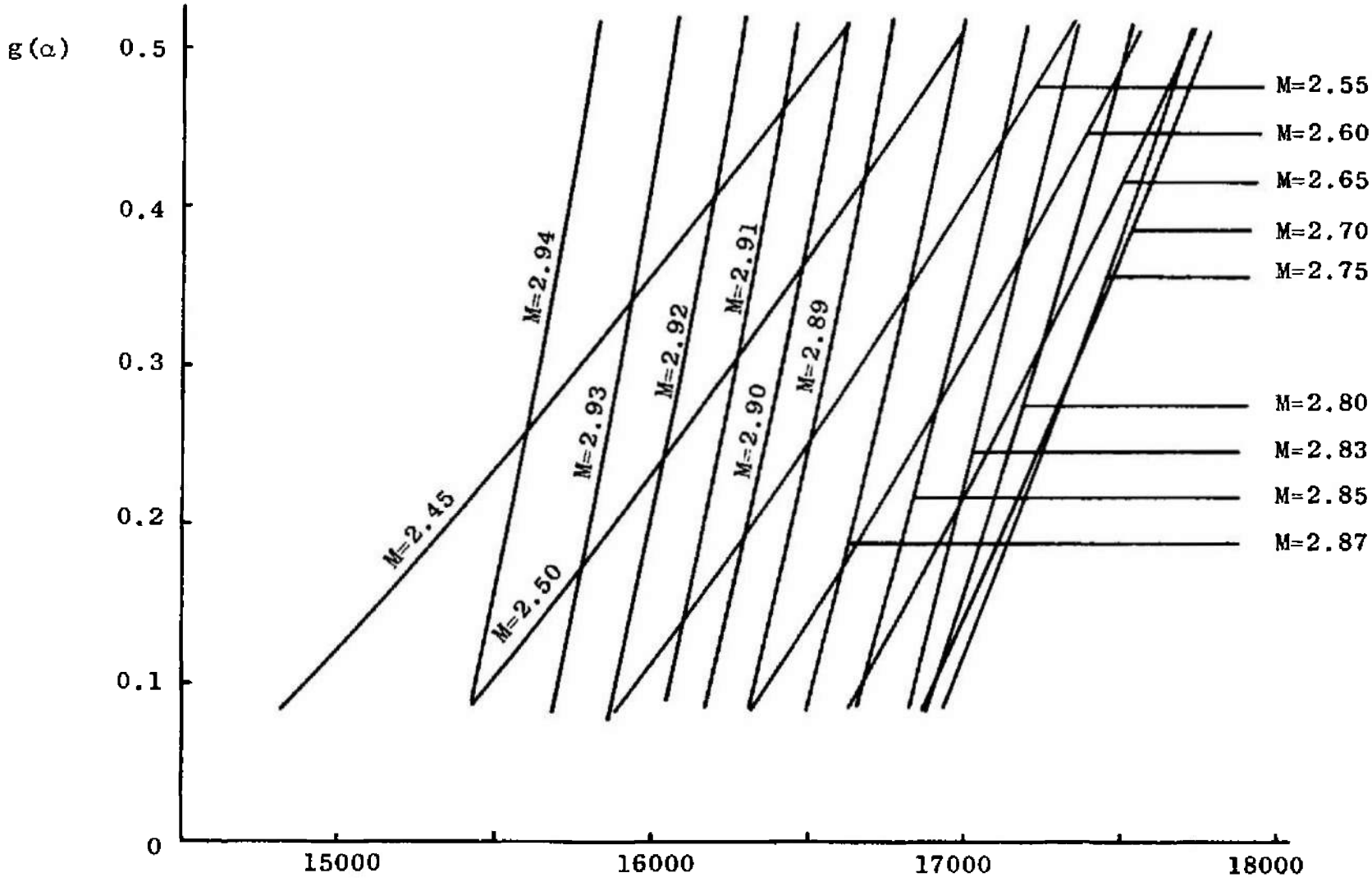

Fig. 49 Variation of $g(\alpha)$ with Re and M for Ha = 150, Φ = 1.6, $\sigma \sim T^{3/2}$

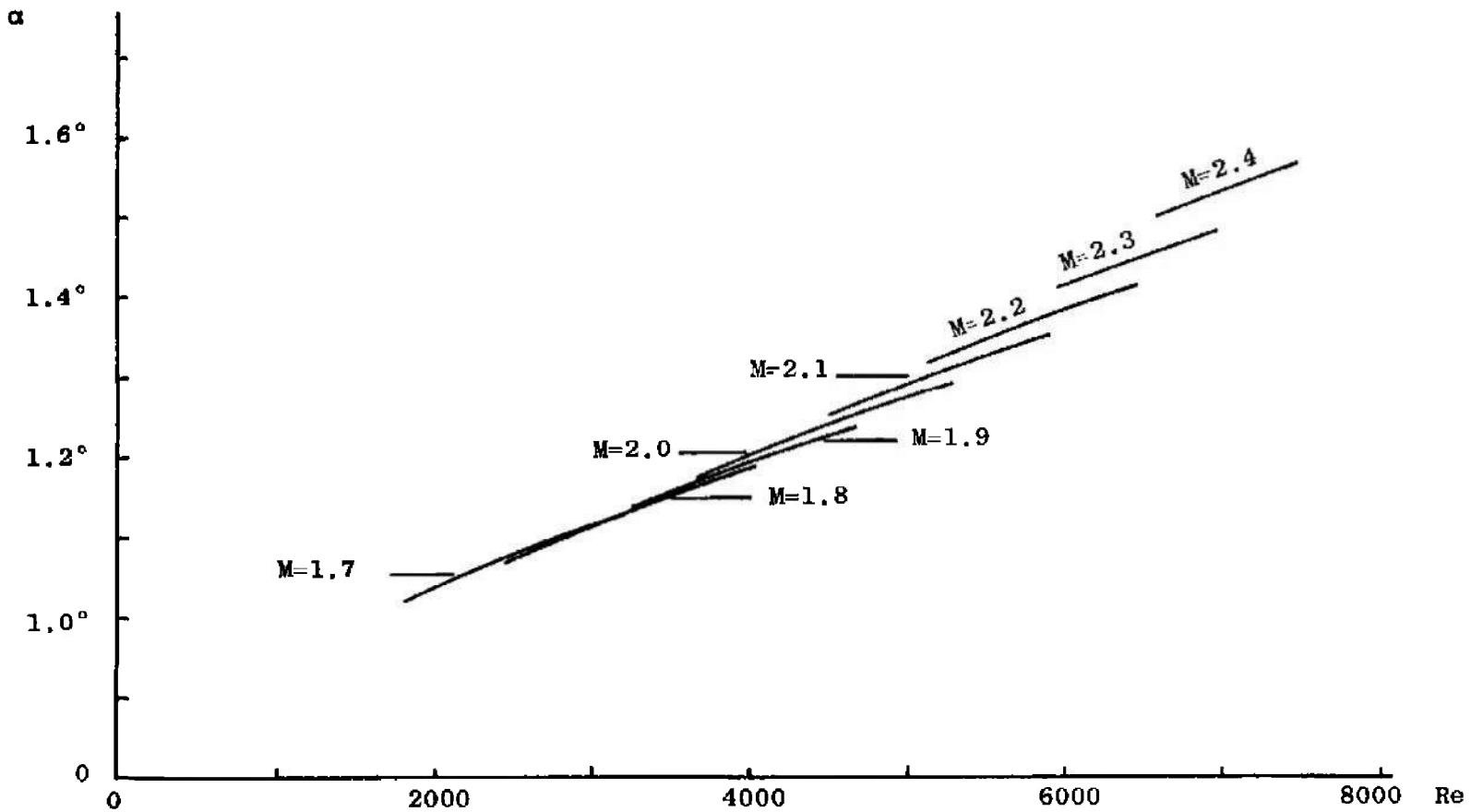

Fig. 50 Variation of α with Re and M for Ha = 100, Φ = 1.6, $\sigma \sim T^{1/2}$, $\mu \sim \kappa \sim T^{1/2}$

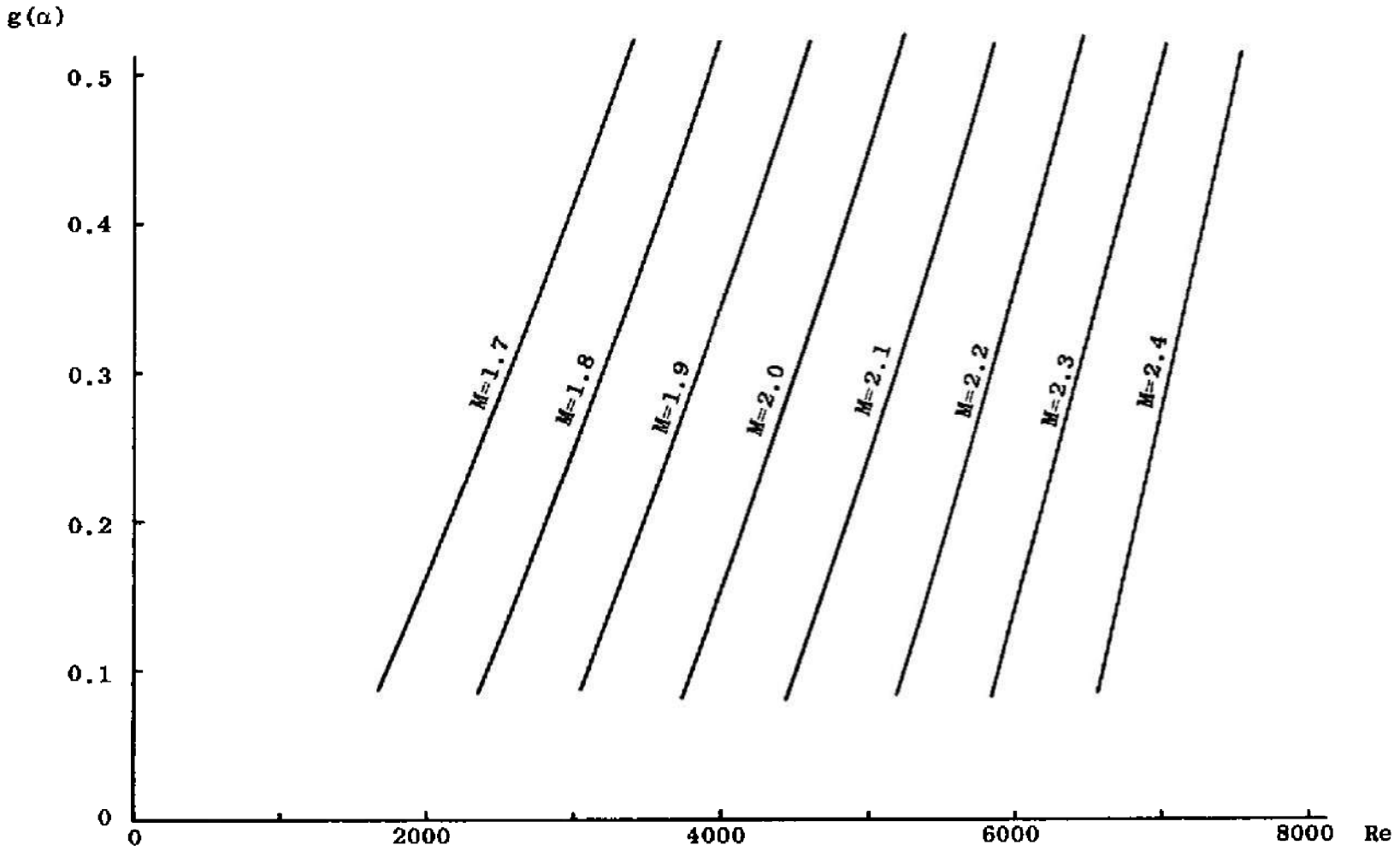

Fig. 51 Variation of $g(\alpha)$ with Re and M for Ha = 100, $\Phi = 1.6$, $\sigma \sim T^{3/2}$, $\mu \sim \kappa \sim T^{1/2}$

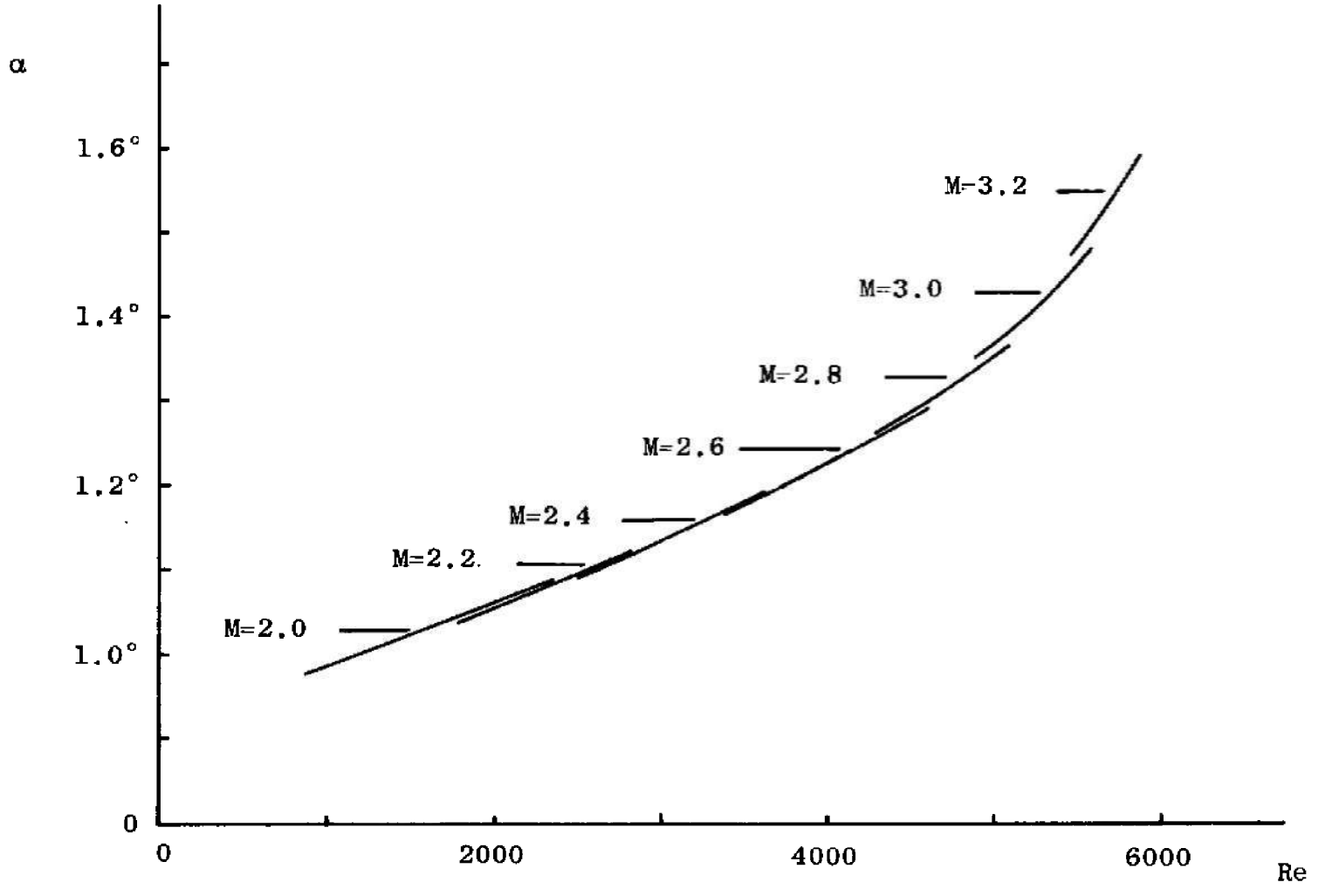

Fig. 52 Variation of α with Re and M for Ha = 150, Φ = 1.2, $\sigma \sim T^{3/2}$, $\mu \sim \kappa \sim T^{1/2}$

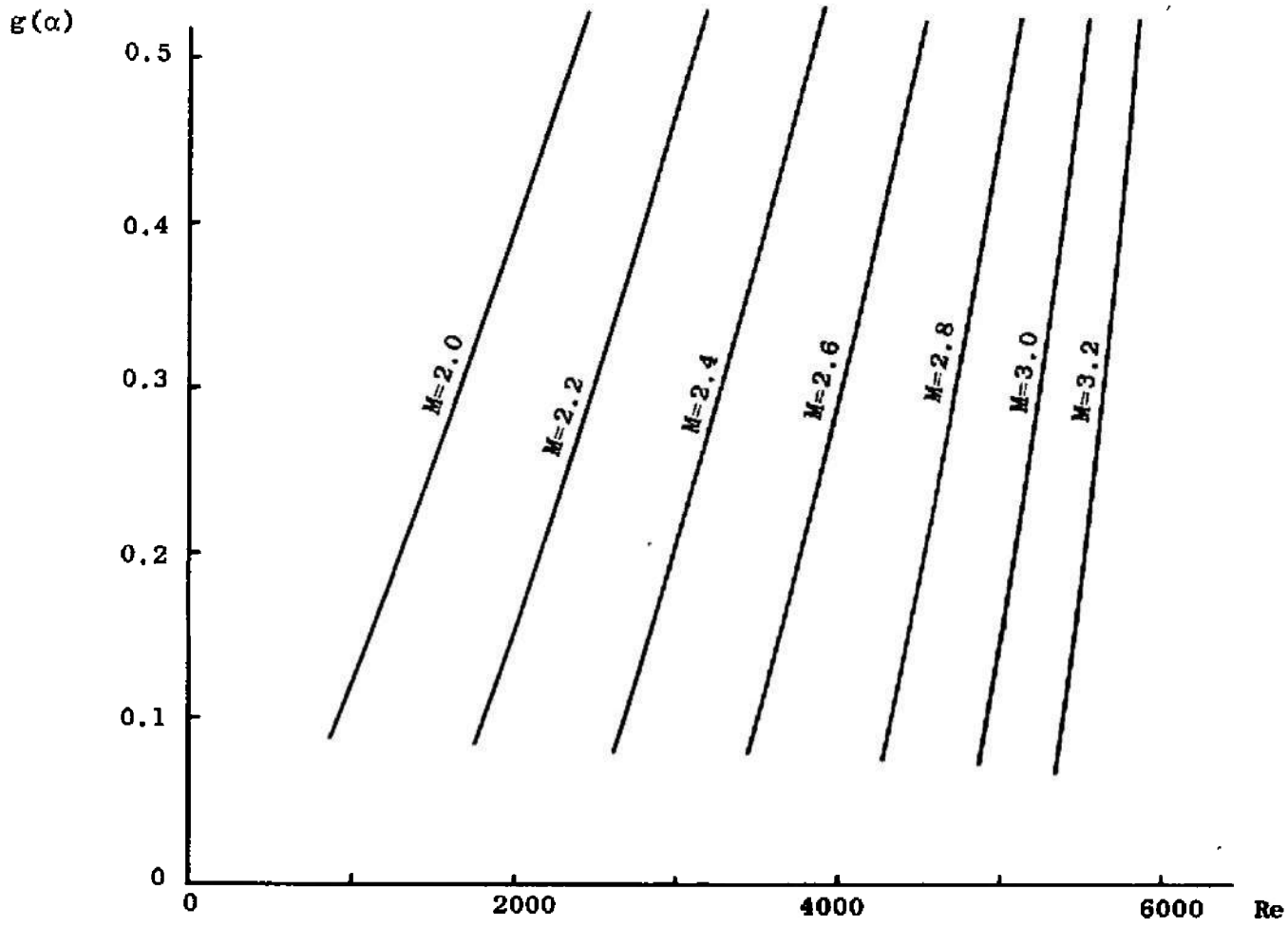

Fig. 53 Variation of $g(\alpha)$ with Re and M for Ha = 150, Φ = 1.2, $\sigma \sim T^{3/2}$, $\mu \sim \kappa \sim T^{1/2}$

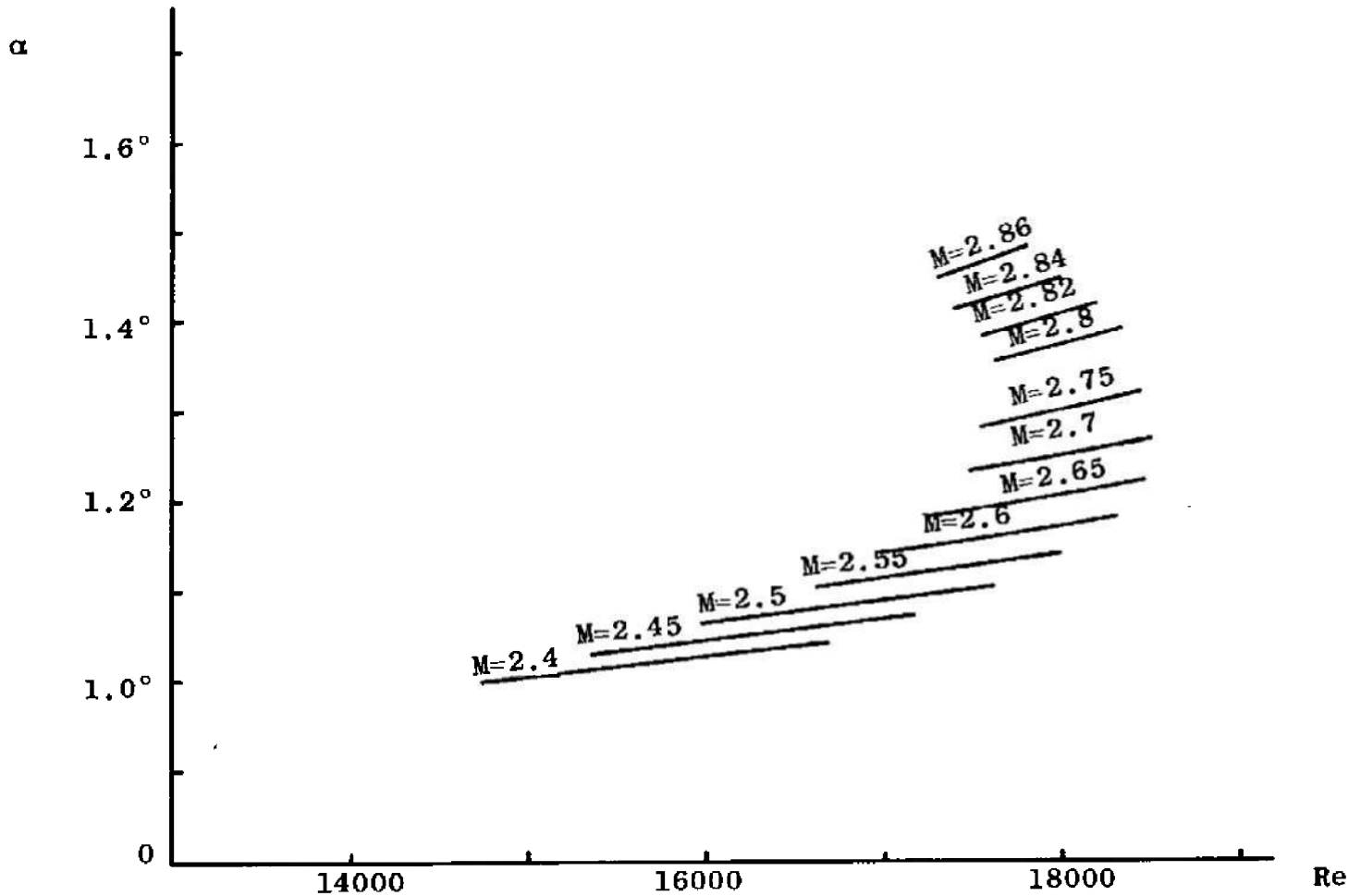

Fig. 54 Variation of α with Re and M for Ha = 150, Φ = 1.6, $\sigma \sim T^{3/2}$, $\mu \sim \kappa \sim T^{1/2}$

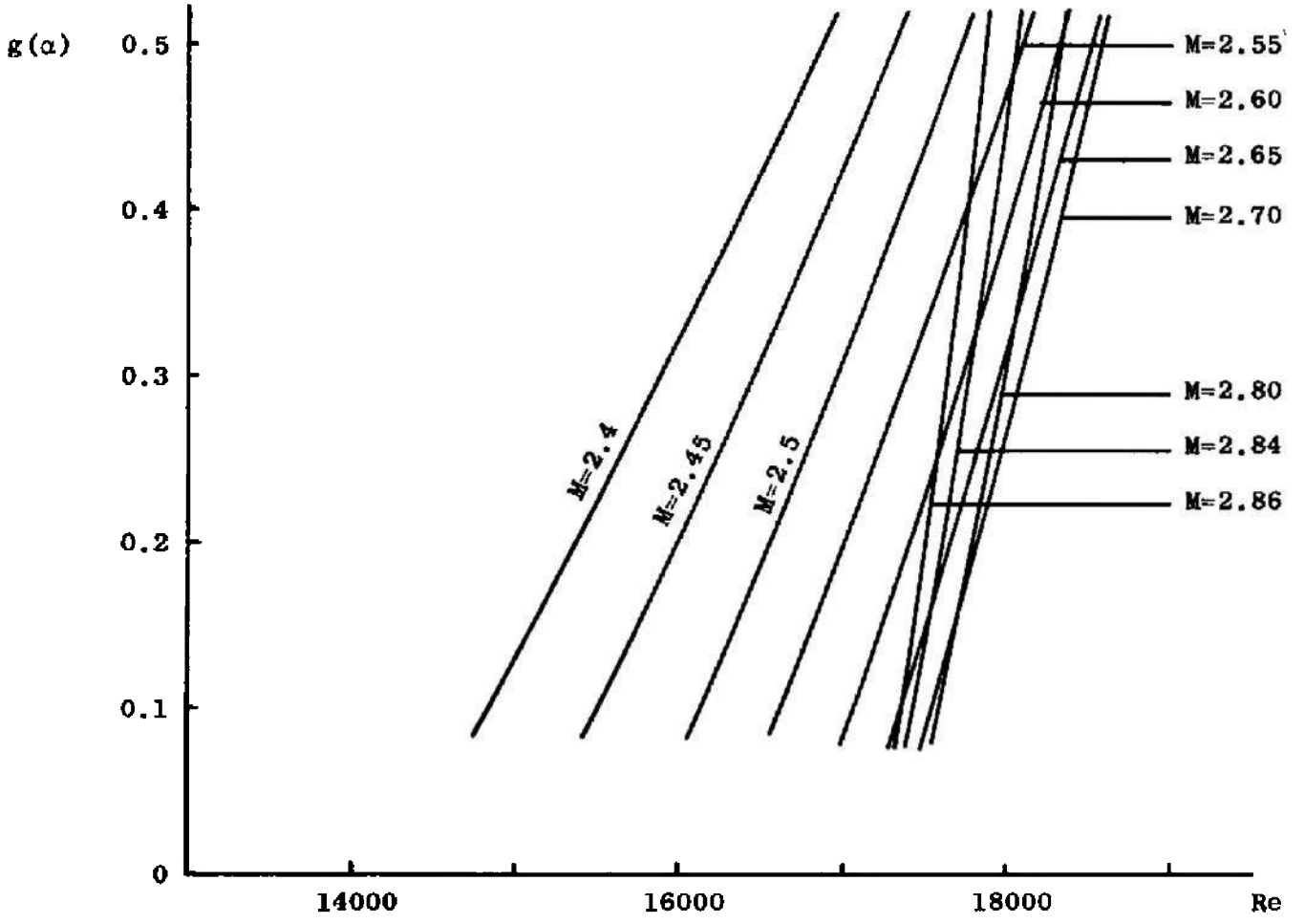

Fig. 55 Variation of $g(\alpha)$ with Re and M for Ha = 150, $\Phi = 1.6$, $\sigma \sim T^{3/2}$, $\mu \sim \kappa \sim T^{1/2}$

TABLE I
LIMITING VALUES OF α, M AND Re

Ha	Φ	α_{min}	M_{limit}	Re_{limit}
100	1.2	1.420°	4.9894	1906.6
100	1.6	.938°	2.8857	5968.9
100	2.0	.756°	2.2357	9981.4
150	1.2	.946°	4.9961	4406.6
150	1.6	.625°	2.8863	8068.9
150	2.0	.504°	2.2359	22481.4
200	1.2	.710°	4.9973	7906.6
200	1.6	.469°	2.8865	23968.9
200	2.0	.378°	2.2360	39981.4

TABLE II
SUMMARY OF RESULTS FOR CONSTANT PROPERTIES

Ha	Φ	Re	M	$f'(\alpha)$	$g'(\alpha)$	$p^*(0)$
100	1.2	350	1.87	- 117	- 186	.0372
100	1.6	5150	2.24	- 138	- 347	.00361
100	2.0	9700	2.02	- 156	- 386	.00157
150	1.2	4100	3.00	- 172	- 629	.00819
150	1.6	14010	2.704	- 209	- 776	.00194
150	2.0	23045	2.209	- 238	- 711	.00079
200	1.2	8450	3.750	- 231	- 1333	.00621
200	1.6	24600	2.860	- 281	- 1180	.00124
200	2.0	40250	2.2376	- 318	- 980	.00046

TABLE III
COMPARISON OF $f'(\alpha)$ AND $g'(\alpha)$ FOR CONSTANT AND VARIABLE PROPERTIES

		Constant Properties		$\sigma \sim T^{3/2}$		$\sigma \sim T^{3/2}$ $\mu \sim \kappa \sim T^{3/2}$	
Ha	Φ	$f'(\alpha)$	$g'(\alpha)$	$f'(\alpha)$	$g'(\alpha)$	$f'(\alpha)$	$g'(\alpha)$
100	1.6	- 139	- 272	- 110	- 204	- 251	- 499
150	1.2	- 172	- 449	- 181	- 576	- 392	- 1141
150	1.6	- 207	- 666	- 322	- 1322	- 662	- 2434

Security Classification

DOCUMENT CONTROL DATA - R&D

(Security classification of title, body of abstract and indexing annotation must be entered when the overall report is classified)

1 ORIGINATING ACTIVITY *(Corporate author)*
The University of Tennessee Space Institute
Tullahoma, Tennessee

2a REPORT SECURITY CLASSIFICATION
UNCLASSIFIED

2b GROUP
N/A

3 REPORT TITLE
FULLY DEVELOPED MAGNETOGASDYNAMIC FLOW BETWEEN DIVERGING PLANE WALLS

4 DESCRIPTIVE NOTES *(Type of report and inclusive dates)*
Final Report

5 AUTHOR(S) *(Last name, first name, initial)*
Snyder, William T. and Maus, James R.

6 REPORT DATE
April 1967

7a TOTAL NO OF PAGES
120

7b NO. OF REFS
20

8a CONTRACT OR GRANT NO.
AF 40(600)-1113

b. PROJECT NO. 8950

c Program Element 62405334

d Task 895001

9a ORIGINATOR'S REPORT NUMBER(S)
AEDC-TR-67-80

9b OTHER REPORT NO(S) *(Any other numbers that may be assigned this report)*
N/A

10 AVAILABILITY/LIMITATION NOTICES
Distribution of this document is unlimited.

11 SUPPLEMENTARY NOTES
Available in DDC

12 SPONSORING MILITARY ACTIVITY
Arnold Engineering Development Center
Air Force Systems Command
Arnold Air Force Station, Tennessee

13 ABSTRACT

A solution has been obtained to the magnetogasdynamic equations of motion including the effects of compressibility, viscosity, thermal conductivity and crossed electric and magnetic fields. The solution obtained is valid for an acceleration flow in which a separation of variable form of solution is utilized. The constraints under which a separable solution is valid are clearly delineated. The solution is an exact solution in the sense that no terms have been dropped from the governing equations and boundary layer approximations have not been employed. (U)

The results of the investigation were presented in the form of velocity and temperature profiles for several values of the electromagnetic parameters Ha and Φ. Although the mathematical model used in the present investigation is too crude to be utilized for detailed design of a practical MHD accelerator, it is believed, nevertheless, that the model displays certain qualitative features of the flow which are likely to be encountered in a practical device. (U)

DD FORM 1 JAN 64 1473

Security Classification

Security Classification

14 KEY WORDS	LINK A ROLE	LINK A WT	LINK B ROLE	LINK B WT	LINK C ROLE	LINK C WT
2 MHD flow						
velocity						
1 Hall effect						
fluids						
density						
3 potassium chloride						
15-20						
4. MHD accelerators.						
5 Diverging walls						

INSTRUCTIONS

1. ORIGINATING ACTIVITY: Enter the name and address of the contractor, subcontractor, grantee, Department of Defense activity or other organization *(corporate author)* issuing the report.

2a. REPORT SECURITY CLASSIFICATION: Enter the overall security classification of the report. Indicate whether "Restricted Data" is included. Marking is to be in accordance with appropriate security regulations.

2b. GROUP: Automatic downgrading is specified in DoD Directive 5200.10 and Armed Forces Industrial Manual. Enter the group number. Also, when applicable, show that optional markings have been used for Group 3 and Group 4 as authorized.

3. REPORT TITLE: Enter the complete report title in all capital letters. Titles in all cases should be unclassified. If a meaningful title cannot be selected without classification, show title classification in all capitals in parenthesis immediately following the title.

4. DESCRIPTIVE NOTES: If appropriate, enter the type of report, e.g., interim, progress, summary, annual, or final. Give the inclusive dates when a specific reporting period is covered.

5. AUTHOR(S): Enter the name(s) of author(s) as shown on or in the report. Enter last name, first name, middle initial. If military, show rank and branch of service. The name of the principal author is an absolute minimum requirement.

6. REPORT DATE: Enter the date of the report as day, month, year; or month, year. If more than one date appears on the report, use date of publication.

7a. TOTAL NUMBER OF PAGES: The total page count should follow normal pagination procedures, i.e., enter the number of pages containing information.

7b. NUMBER OF REFERENCES: Enter the total number of references cited in the report.

8a. CONTRACT OR GRANT NUMBER: If appropriate, enter the applicable number of the contract or grant under which the report was written.

8b, 8c, & 8d. PROJECT NUMBER: Enter the appropriate military department identification, such as project number, subproject number, system numbers, task number, etc.

9a. ORIGINATOR'S REPORT NUMBER(S): Enter the official report number by which the document will be identified and controlled by the originating activity. This number must be unique to this report.

9b. OTHER REPORT NUMBER(S): If the report has been assigned any other report numbers *(either by the originator or by the sponsor)*, also enter this number(s).

10. AVAILABILITY/LIMITATION NOTICES: Enter any limitations on further dissemination of the report, other than those imposed by security classification, using standard statements such as:

(1) "Qualified requesters may obtain copies of this report from DDC."

(2) "Foreign announcement and dissemination of this report by DDC is not authorized."

(3) "U. S. Government agencies may obtain copies of this report directly from DDC. Other qualified DDC users shall request through _____."

(4) "U. S. military agencies may obtain copies of this report directly from DDC. Other qualified users shall request through _____."

(5) "All distribution of this report is controlled. Qualified DDC users shall request through _____."

If the report has been furnished to the Office of Technical Services, Department of Commerce, for sale to the public, indicate this fact and enter the price, if known.

11. SUPPLEMENTARY NOTES: Use for additional explanatory notes.

12. SPONSORING MILITARY ACTIVITY: Enter the name of the departmental project office or laboratory sponsoring *(paying for)* the research and development. Include address.

13. ABSTRACT: Enter an abstract giving a brief and factual summary of the document indicative of the report, even though it may also appear elsewhere in the body of the technical report. If additional space is required, a continuation sheet shall be attached.

It is highly desirable that the abstract of classified reports be unclassified. Each paragraph of the abstract shall end with an indication of the military security classification of the information in the paragraph, represented as *(TS)*, *(S)*, *(C)*, or *(U)*.

There is no limitation on the length of the abstract. However, the suggested length is from 150 to 225 words.

14. KEY WORDS: Key words are technically meaningful terms or short phrases that characterize a report and may be used as index entries for cataloging the report. Key words must be selected so that no security classification is required. Identifiers, such as equipment model designation, trade name, military project code name, geographic location, may be used as key words but will be followed by an indication of technical context. The assignment of links, rules, and weights is optional.

Security Classification